NASA/TM–2020–220574

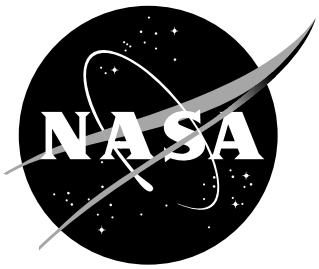

Entropy Stable Nonconforming Discretizations with the Summation-By-Parts Property for Curvilinear Coordinates.

David C. Del Rey Fernández
National Institute of Aerospace and NASA Langley Research Center, Hampton, Virginia, United States,
Mark H. Carpenter
NASA Langley Research Center, Hampton, Virginia, United States,
Lisandro Dalcin
King Abdullah University of Science and Technology, Thuwal, Saudi Arabia,
Lucas Fredrich
University of Cologne, North Rhine-Westphalia, Germany,
Diego Rojas
King Abdullah University of Science and Technology, Thuwal, Saudi Arabia,
Andrew R. Winters
Linköping University, Linköping, Östergötland, Sweden,
Gregor J. Gassner
University of Cologne, Cologne, North Rhine-Westphalia, Germany,
Stefano Zampini and Matteo Parsani
King Abdullah University of Science and Technology, Thuwal, Saudi Arabia,

March 2020

NASA STI Program ... in Profile

Since its founding, NASA has been dedicated to the advancement of aeronautics and space science. The NASA scientific and technical information (STI) program plays a key part in helping NASA maintain this important role.

The NASA STI Program operates under the auspices of the Agency Chief Information Officer. It collects, organizes, provides for archiving, and disseminates NASA's STI. The NASA STI Program provides access to the NASA Aeronautics and Space Database and its public interface, the NASA Technical Report Server, thus providing one of the largest collection of aeronautical and space science STI in the world. Results are published in both non-NASA channels and by NASA in the NASA STI Report Series, which includes the following report types:

- TECHNICAL PUBLICATION. Reports of completed research or a major significant phase of research that present the results of NASA programs and include extensive data or theoretical analysis. Includes compilations of significant scientific and technical data and information deemed to be of continuing reference value. NASA counterpart of peer-reviewed formal professional papers, but having less stringent limitations on manuscript length and extent of graphic presentations.
- TECHNICAL MEMORANDUM. Scientific and technical findings that are preliminary or of specialized interest, e.g., quick release reports, working papers, and bibliographies that contain minimal annotation. Does not contain extensive analysis.
- CONTRACTOR REPORT. Scientific and technical findings by NASA-sponsored contractors and grantees.
- CONFERENCE PUBLICATION. Collected papers from scientific and technical conferences, symposia, seminars, or other meetings sponsored or co-sponsored by NASA.
- SPECIAL PUBLICATION. Scientific, technical, or historical information from NASA programs, projects, and missions, often concerned with subjects having substantial public interest.
- TECHNICAL TRANSLATION. English-language translations of foreign scientific and technical material pertinent to NASA's mission.

Specialized services also include creating custom thesauri, building customized databases, and organizing and publishing research results.

For more information about the NASA STI Program, see the following:

- Access the NASA STI program home page at ***http://www.sti.nasa.gov***
- E-mail your question via the Internet to help@sti.nasa.gov
- Fax your question to the NASA STI Help Desk at (757) 864-9658
- Phone the NASA STI Help Desk at (757) 864-9658
- Write to:
  NASA STI Help Desk
  NASA Center for AeroSpace Information
  7115 Standard Drive
  Hanover, MD 21076–1320

NASA/TM–2020–220574

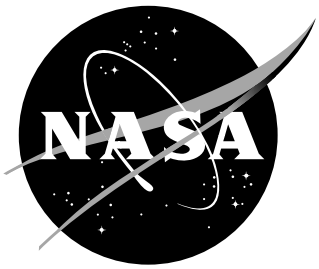

Entropy Stable Nonconforming Discretizations with the Summation-By-Parts Property for Curvilinear Coordinates.

David C. Del Rey Fernández
National Institute of Aerospace and NASA Langley Research Center, Hampton, Virginia, United States,
Mark H. Carpenter
NASA Langley Research Center, Hampton, Virginia, United States,
Lisandro Dalcin
King Abdullah University of Science and Technology, Thuwal, Saudi Arabia,
Lucas Fredrich
University of Cologne, North Rhine-Westphalia, Germany,
Diego Rojas
King Abdullah University of Science and Technology, Thuwal, Saudi Arabia,
Andrew R. Winters
Linköping University, Linköping, Östergötland, Sweden,
Gregor J. Gassner
University of Cologne, Cologne, North Rhine-Westphalia, Germany,
Stefano Zampini and Matteo Parsani
King Abdullah University of Science and Technology, Thuwal, Saudi Arabia,

National Aeronautics and
Space Administration

NASA Langley Research Center
Hampton, Virginia 23681-2199

March 2020

Acknowledgments

Special thanks are extended to Dr. Mujeeb R. Malik for partially funding this work as part of the NASA's "Transformational Tools and Technologies" (T^3) project. The research reported in this publication was also supported by funding from King Abdullah University of Science and Technology (KAUST). We are thankful for the computing resources of the Supercomputing Laboratory and the Extreme Computing Research Center at KAUST. Gregor Gassner and Lucas Friedrich have been supported by the European Research Council (ERC) under the European Unions Eights Framework Program Horizon 2020 with the research project Extreme, ERC grant agreement no. 714487.

Available from:

NASA Center for AeroSpace Information
7115 Standard Drive
Hanover, MD 21076-1320
443-757-5802

Abstract

The entropy conservative/stable algorithm of Friedrich *et al.* (2018) for hyperbolic conservation laws on nonconforming p-refined/coarsened Cartesian grids, is extended to curvilinear grids for the compressible Euler equations. The primary focus is on constructing appropriate coupling procedures across the curvilinear nonconforming interfaces. A simple and flexible approach is proposed that uses interpolation operators from one element to the other. On the element faces, the analytic metrics are used to construct coupling terms, while metric terms in the volume are approximated to satisfy a discretization of the geometric conservation laws. The resulting scheme is entropy conservative/stable, elementwise conservative, and freestream preserving. The accuracy and stability properties of the resulting numerical algorithm are shown to be comparable to those of the original conforming scheme ($\sim p+1$ convergence) in the context of the isentropic Euler vortex and the inviscid Taylor–Green vortex problems on manufactured high order grids.

Contents

1 Introduction

High-order accurate finite-element methods (FEM) provide an efficient approach to achieve high solution accuracy. Their computational kernels are arithmetically dense making them compatible with the current and future highly concurrent hardware. In addition, they are amenable to h-, p-, and r-refinement algorithms, thus facilitating the redistribution of the degrees of freedom to better resolve multiscale physics.

High-order accurate methods are known to be more efficient than low-order methods for linear wave propagation [32, 55]. Although high-order discretizations have a long history of development, their application to nonlinear partial differential equations (PDEs) for practical applications has been limited by robustness issues. Thus, nominally second-order accurate discretization operators are typically used in commercial and industrial software.

The summation-by-parts (SBP) framework provides a systematic and discretization-agnostic methodology for constructing arbitrarily high-order accurate and provably stable numerical methods for linear and variable coefficient linear problems (see, for instance, the survey papers [18, 54]). SBP operators can be viewed as matrix difference operators that are mimetic of integration by parts in that they have a telescoping property. Discrete stability over the whole domain is achieved by combining the SBP mechanics with suitable interelement coupling procedures and boundary conditions (e.g., the simultaneous approximation terms (SATs) [7, 40]).

For nonlinear problems, progress towards provably stable algorithms applicable to practical problems has been much slower. However, a certain class of nonlinear conservation laws come endowed with a complementary inequality statement (equality for smooth solutions) on the mathematical entropy (see, for instance, Refs. [14]). Therefore, it is desirable for the numerical method to satisfy a corresponding discrete analogue. This can then be used to prove nonlinear stability of the numerical scheme [56, 57]. Along these lines, a productive trajectory was initiated by Tadmor [56] who constructed entropy conservative low-order finite-volume schemes that achieve entropy conservation by using two-point flux functions that when contracted with the entropy variables result in a telescoping entropy flux. Entropy stability was ensured by adding appropriate dissipation. Through the telescoping property, the continuous L^2 entropy stability analysis is mimicked by the semidiscrete stability analysis (for a review of these ideas see Tadmor [57]). Tadmor's basic idea has led to the construction of a number of high-order and low-order entropy stable schemes (see, for instance, Refs. [23, 46]). An alternative approach, developed by Olsson and Oliger [41], Gerritsen and Olsson [26] and Yee *et al.* [65] (see also Refs. [47, 49]), relies on choosing entropy functions that result in a homogeneity property on the Euler fluxes. By using this property, splittings of the Euler fluxes are constructed such that when contracted with the entropy variables result in stability estimates analogous in form to energy estimates obtained for linear PDEs. Thus, discretizing the resulting split form using SBP operators, the nonlinear stability analysis performed at the continuous level is mimicked at the semidiscrete level.

A complementary extension of Tadmor's ideas to finite domains was initiated by Fisher and coworkers who combined the SBP framework, using classical finite-difference SBP operators, with Tadmor's two-point flux [20–22]. The resulting schemes follow the continuous entropy analysis and can be shown to be entropy conservative and be made entropy stable by adding appropriate interface dissipation. This nonlinearly stable approach inherits all the mechanics of linear SBP schemes for the imposition of boundary conditions and interelement coupling and therefore gives a systematic methodology for discretizing problems on complex geometries [5, 43, 44].

Moreover, by constructing schemes that are discretely mimetic of the continuous stability analysis, the need to assume exact integration in the stability proofs is eliminated (see for example the work of Hughes *et al.* [27]). These ideas have been extended to include collocated spectral elements [5], fully- and semistaggered spectral elements [9, 42], Cartesian, semistaggered, nonconforming p-refinement [9], WENO spectral collocation [64], multidimensional SBP operators [12, 13], multidimensional staggered SBP operators [17], modal decoupled SBP operators [10], and fully discrete explicit entropy-stable schemes [24, 45], as well as to a number of PDEs besides the compressible Euler and Navier–Stokes equations (for example the magnetohydrodynamics [62] and the shallow water [63] equations).

A necessary constraint for entropy stability on curvilinear meshes is satisfaction of discrete geometric conservation law (GCL) conditions [5, 20, 22, 42]. Well documented procedures exist for generating discrete transformation metrics on conforming meshes that satisfy the GCL conditions [58, 59]. These procedures extend immediately to the nonconforming case provided that the polynomial order of the method is sufficient to analytically resolve the element surface transformation metrics; a condition that is naturally satisfied if the polynomial orders of the geometry, p_g and discretization, p, are related by the inequality $p_g \leq \frac{p+1}{2}$. While it is possible to generate body fitted meshes with full geometric surface order ($p_g = p$) and reduced off body order $p_g \leq \frac{p+1}{2}$, this forces undue complexity on the already complex task of grid generation. Enforcing the $p_g = p$ grid constraint on near-body elements, while avoiding grid line crossover or negative Jacobians, increases in complexity with mesh aspect ratio, and is virtually impossible to achieve in the high Reynolds number limit of realistic aerodynamic configurations.

Herein, the primary objective is to construct entropy-stable discretizations suitable for the mechanics of high-order FEM p-adaptivity, applicable for general meshes containing hexahedral polynomial elements of full geometric order (i.e., $p_g \leq p$). Initial nonconforming efforts focused on Cartesian, semistaggered spectral collocation operators [9], but identifying a curvilinear extension has proven difficult. Thus, this work extends to curvilinear coordinates, the Cartesian grid work previously reported by Friedrich *et al.* [25], and primarily focuses on constructing appropriate coupling procedures across curvilinear nonconforming interfaces. We note that there has been substantial previous work in the SBP community to deal with the nonconforming interface problem, e.g., see Refs. [2, 3, 31, 36, 38, 39, 60, 61].

Many novel contributions are included in this work. They are summarized as follows:

- A general, yet simple entropy-stable nonconforming algorithm is proposed in curvilinear coordinates for the compressible Euler equations that
  - Encapsulates and generalizes several approaches for coupling curvilinear nonconforming interfaces
  - Formalizes necessary conditions for entropy conservation at curvilinear nonconforming interfaces
  - Elegantly handles various mesh generation strategies including elements of full geometric order ($p_g \leq p$)
  - Extends the metric approximation approach of Crean *et al.* [13] to curvilinear nonconforming interfaces
  - Satisfies the discrete GCL conditions, therefore ensuring freestream preservation

  - Exploits the generality of distinct surface and volume metrics that couple through the GCL constraint

- Numerical evidence is provided that supports the assertion that the conforming [5, 42] and nonconforming algorithms exhibit similar 1) nonlinear robustness properties and 2) L^2-norm convergence rates, (i.e., nominally $p+1$ for polynomials of degree p).

The paper is organized as follows: Section 2 delineates the notation used herein. The nonconforming algorithm is presented in the simple context of the convection equation in Section 3. This is followed by an introduction to the construction of nonlinearly stable schemes by examining the discretization of the Burgers' equation (Section 4). The nonconforming algorithm presented in Section 3 and the mechanics presented in Section 4 are combined in Section 5 to construct an entropy conservative/stable nonconforming discretization for the compressible Euler equations. Numerical experiments are are given in Section (7), while conclusions are drawn in Section 8.

2 Notation

PDEs are discretized on hexahedra having Cartesian computational coordinates denoted by the triple (ξ_1, ξ_2, ξ_3), where the physical coordinates are denoted by the triple (x_1, x_2, x_3). Vectors are represented by lowercase bold font, for example $\boldsymbol{u}$, while matrices are represented using sans-serif font, for example, B. Continuous functions on a space-time domain are denoted by capital letters in script font. For example,

$$\mathcal{U}(\xi_1, \xi_2, \xi_3, t) \in L^2([\alpha_1, \beta_1] \times [\alpha_2, \beta_2] \times [\alpha_3, \beta_3] \times [0, T])$$

represents a square integrable function, where t is the temporal coordinate. The restriction of such functions onto a set of mesh nodes is denoted by lower case bold font. For example, the restriction of $\mathcal{U}$ onto a grid of $N_1 \times N_2 \times N_3$ nodes is given by the vector

$$\boldsymbol{u} = \left[\mathcal{U}\left(\boldsymbol{\xi}^{(1)}, t\right), \ldots, \mathcal{U}\left(\boldsymbol{\xi}^{(N)}, t\right)\right]^{\mathrm{T}},$$

where, N is the total number of nodes ($N \equiv N_1 N_2 N_3$) square brackets ([]) are used to delineate vectors and matrices as well as ranges for variables (the context will make clear which meaning is being used). Moreover, $\boldsymbol{\xi}$ is a vector of vectors constructed from the three vectors $\boldsymbol{\xi}_1$, $\boldsymbol{\xi}_2$, and $\boldsymbol{\xi}_3$, which are vectors of size N_1, N_2, and N_3 and contain the coordinates of the mesh in the three computational directions, respectively. Finally, $\boldsymbol{\xi}$ is constructed as

$$\boldsymbol{\xi}(3(i-1)+1:3i) \equiv \boldsymbol{\xi}^{(i)} \equiv [\boldsymbol{\xi}_1(i), \boldsymbol{\xi}_2(i), \boldsymbol{\xi}_3(i)]^{\mathrm{T}},$$

where the notation $\boldsymbol{u}(i)$ means the i^{th} entry of the vector $\boldsymbol{u}$ and $\boldsymbol{u}(i:j)$ is the subvector constructed from $\boldsymbol{u}$ using the i^{th} through j^{th} entries (i.e., Matlab notation is used).

Oftentimes, monomials are discussed and the following notation is used:

$$\boldsymbol{\xi}_l^j \equiv \left[(\boldsymbol{\xi}_l(1))^j, \ldots, (\boldsymbol{\xi}_l(N_l))^j\right]^{\mathrm{T}},$$

and the convention that $\boldsymbol{\xi}_l^j = \mathbf{0}$ for $j < 0$ is used.

Herein, one-dimensional SBP operators are used to discretize derivatives. The definition of a one-dimensional SBP operator in the ξ_l direction, $l = 1, 2, 3$, is [16, 18, 54]

Definition 1. ***Summation-by-parts operator for the first derivative****: A matrix operator with constant coefficients, $\mathsf{D}_{\xi_l}^{(1D)} \in \mathbb{R}^{N_l \times N_l}$, is a linear SBP operator of degree p approximating the derivative $\frac{\partial}{\partial \xi_l}$ on the domain $\xi_l \in [\alpha_l, \beta_l]$ with nodal distribution $\boldsymbol{\xi}_l$ having N_l nodes, if*

1. $\mathsf{D}_{\xi_l}^{(1D)} \boldsymbol{\xi}_l^j = j \boldsymbol{\xi}_l^{j-1}$, $j = 0, 1, \ldots, p$;
2. $\mathsf{D}_{\xi_l}^{(1D)} \equiv \left(\mathsf{P}_{\xi_l}^{(1D)}\right)^{-1} \mathsf{Q}_{\xi_l}^{(1D)}$, *where the norm matrix,* $\mathsf{P}_{\xi_l}^{(1D)}$, *is symmetric positive definite;*
3. $\mathsf{Q}_{\xi_l}^{(1D)} \equiv \left(\mathsf{S}_{\xi_l}^{(1D)} + \frac{1}{2}\mathsf{E}_{\xi_l}^{(1D)}\right)$, $\mathsf{S}_{\xi_l}^{(1D)} = -\left(\mathsf{S}_{\xi_l}^{(1D)}\right)^{\mathrm{T}}$, $\mathsf{E}_{\xi_l}^{(1D)} = \left(\mathsf{E}_{\xi_l}^{(1D)}\right)^{\mathrm{T}}$, $\mathsf{E}_{\xi_l}^{(1D)} = \mathrm{diag}\left(-1, 0, \ldots, 0, 1\right) = \boldsymbol{e}_{N_l}\boldsymbol{e}_{N_l}^{\mathrm{T}} - \boldsymbol{e}_{1_l}\boldsymbol{e}_{1_l}^{\mathrm{T}}$, $\boldsymbol{e}_{1_l} \equiv [1, 0, \ldots, 0]^{\mathrm{T}}$, *and* $\boldsymbol{e}_{N_l} \equiv [0, 0, \ldots, 1]^{\mathrm{T}}$.

Thus, a degree p SBP operator is one that differentiates exactly monomials up to degree p.

In this work, one-dimensional SBP operators are extended to multiple dimensions using tensor products ($\otimes$). The tensor product between the matrices A and B is given as $\mathsf{A}\otimes\mathsf{B}$. When referencing individual entries in a matrix the notation $\mathsf{A}(i,j)$ is used, which means the ij^{th} entry in the matrix A. The Hadamard product is also used in the construction of entropy conservative/stable discretizations, where, the Hadamard product between the matrices A and B is denoted by $\mathsf{A} \circ \mathsf{B}$.

The focus in this paper is exclusively on diagonal-norm SBP operators. Moreover, the same one-dimensional SBP operator is used in each direction, each operating on N nodes. Specifically, diagonal-norm SBP operators constructed on the Legendre–Gauss–Lobatto (LGL) nodes are used, i.e., a discontinuous Galerkin collocated spectral element approach is utilized.

The physical domain $\Omega \subset \mathbb{R}^3$, with boundary $\Gamma \equiv \partial\Omega$ is partitioned into K nonoverlapping hexahedral elements. The domain of the κ^{th} element is denoted by Ω_κ and has boundary $\partial\Omega_\kappa$. Numerically, PDEs are solved in computational coordinates, where each Ω_κ is locally transformed to $\hat{\Omega}_\kappa$, with boundary $\hat{\Gamma} \equiv \partial\hat{\Omega}_\kappa$, under the following assumption:

Assumption 1. *Each element in physical space is transformed using a local and invertible curvilinear coordinate transformation that is compatible at shared interfaces, meaning that points in computational space on either side of a shared interface mapped to the same physical location, and therefore, map back to the analogous location in computational space; this is the standard assumption that the curvilinear coordinate transformation is water tight.*

3 A p-nonconforming algorithm: Linear convection

The focus herein is on nonconformity arising from curvilinearly mapped elements that have conforming interfaces but nonconforming nodal distributions, as would result from p-refinement interfaces (see Fig. 1). The construction of entropy conservative/stable discretizations for the compressible Euler equations on Cartesian grids is detailed in Friedrich *et al.* [25]. Extending the Cartesian work involves developing a p-refinement, curvilinear, interface coupling technique that maintains 1) accuracy, 2) discrete entropy conservation/stability, and 3) elementwise conservation.

3.1 Scalar convection: continuous and semidiscrete analysis

Many of the salient difficulties encountered while constructing stable and conservative nonconforming discretizations of the Euler equations, are also present in discretization of linear convection.

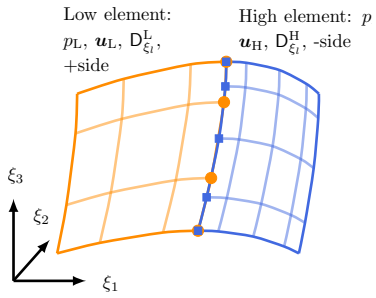

Figure 1. Nonconforming elements.

Consider the constant coefficient linear convection in Cartesian coordinates.

$$\frac{\partial \mathcal{U}}{\partial t} + \sum_{m=1}^{3} \frac{\partial \left(a_m \mathcal{U}\right)}{\partial x_m} = 0, \tag{1}$$

where $(a_m \mathcal{U})$ are the fluxes and a_m are the (constant) components of the convection speed. The stability of (1) can be determined using the energy method which proceeds by multiplying (1) by the solution $(\mathcal{U})$, and after using the chain rule results in

$$\frac{1}{2}\frac{\partial \mathcal{U}^2}{\partial t} + \frac{1}{2}\sum_{m=1}^{3} \frac{\partial \left(a_m \mathcal{U}^2\right)}{\partial x_m} = 0. \tag{2}$$

Integrating over the domain, Ω, using integration by parts, and Leibniz rule gives

$$\frac{\mathrm{d}}{\mathrm{d}t}\int_{\Omega} \frac{\mathcal{U}^2}{2}\mathrm{d}\Omega + \frac{1}{2}\sum_{m=1}^{3} \oint_{\Gamma} \left(a_m \mathcal{U}^2\right) n_{x_m}\mathrm{d}\Gamma = 0, \tag{3}$$

where n_{x_m} is the m^{th} component of the outward facing unit normal. What Eq. (3) demonstrates is that the time rate of change of the norm of the solution, $\|\mathcal{U}\|^2 \equiv \int_{\Omega} \mathcal{U}^2 \mathrm{d}\Omega$, depends solely on surface flux integrals. Imposing appropriate boundary conditions in Eq. (3) leads to an energy estimate on the solution, and therefore, a proof of stability. The discretizations that are developed in this paper mimic the above energy analysis in a one-to-one fashion and similarly lead to stability statements on the semidiscrete equations.

The proposed algorithm is constructed from differentiation matrices that live in computational space and for this purpose, Eq. (1) is transformed using the curvilinear coordinate transformation $x_m = x_m\left(\xi_1, \xi_2, \xi_3\right)$. Thus, after expanding the derivatives as

$$\frac{\partial}{\partial x_m} = \sum_{l=1}^{3} \frac{\partial \xi_l}{\partial x_m}\frac{\partial}{\partial \xi_l},$$

and multiplying by the metric Jacobian $(\mathcal{J}_\kappa)$, (1) becomes

$$\mathcal{J}_\kappa \frac{\partial \mathcal{U}}{\partial t} + \sum_{l,m=1}^{3} \mathcal{J}_\kappa \frac{\partial \xi_l}{\partial x_m}\frac{\partial \left(a_m \mathcal{U}\right)}{\partial \xi_l} = 0. \tag{4}$$

Herein, we refer to Eq. (4) as the chain rule form of Eq. (1) . Bringing the metric terms, $\mathcal{J}_\kappa \frac{\partial \xi_l}{\partial x_m}$, inside the derivative and using the product rule gives

$$\mathcal{J}_\kappa \frac{\partial \mathcal{U}}{\partial t} + \sum_{l,m=1}^{3} \frac{\partial}{\partial \xi_l}\left(\mathcal{J}_\kappa \frac{\partial \xi_l}{\partial x_m} a_m \mathcal{U}\right) - \sum_{l,m=1}^{3} a_m \mathcal{U} \frac{\partial}{\partial \xi_l}\left(\mathcal{J}_\kappa \frac{\partial \xi_l}{\partial x_m}\right) = 0. \tag{5}$$

The last term on the left-hand side of (5) is zero via the GCL relations

$$\sum_{l=1}^{3} \frac{\partial}{\partial \xi_l}\left(\mathcal{J}_\kappa \frac{\partial \xi_l}{\partial x_m}\right) = 0, \quad m = 1, 2, 3, \tag{6}$$

leading to the strong conservation form of the convection equation in curvilinear coordinates:

$$\mathcal{J}_\kappa \frac{\partial \mathcal{U}}{\partial t} + \sum_{l,m=1}^{3} \frac{\partial}{\partial \xi_l}\left(\mathcal{J}_\kappa \frac{\partial \xi_l}{\partial x_m} a_m \mathcal{U}\right) = 0. \tag{7}$$

Now, consider discretizing (7) by using the following differentiation matrices:

$$\mathsf{D}_{\xi_1} \equiv \mathsf{D}^{(1D)} \otimes \mathsf{I}_N \otimes \mathsf{I}_N, \quad \mathsf{D}_{\xi_2} \equiv \mathsf{I}_N \otimes \mathsf{D}^{(1D)} \otimes \mathsf{I}_N, \quad \mathsf{D}_{\xi_3} \equiv \mathsf{I}_N \otimes \mathsf{I}_N \otimes \mathsf{D}^{(1D)},$$

where I_N is an $N \times N$ identity matrix. The diagonal matrices containing the metric Jacobian and metric terms along their diagonals, respectively, are defined as follows:

$$\begin{aligned} \mathsf{J}_\kappa &\equiv \operatorname{diag}\left(\mathcal{J}_\kappa(\boldsymbol{\xi}^{(1)}), \ldots, \mathcal{J}_\kappa(\boldsymbol{\xi}^{(N_\kappa)})\right), \\ \left[\mathcal{J}\frac{\partial \xi_l}{\partial x_m}\right]_\kappa &\equiv \operatorname{diag}\left(\mathcal{J}_\kappa \frac{\partial \xi_l}{\partial x_m}(\boldsymbol{\xi}^{(1)}), \ldots, \mathcal{J}_\kappa \frac{\partial \xi_l}{\partial x_m}(\boldsymbol{\xi}^{(N_\kappa)})\right). \end{aligned}$$

where $N_\kappa \equiv N^3$ is the total number of nodes in element κ. With this nomenclature, the discretization of (7) on the κ^{th} element reads

$$\mathsf{J}_\kappa \frac{\mathrm{d}\boldsymbol{u}_\kappa}{\mathrm{d}t} + \sum_{l,m=1}^{3} \mathsf{D}_{\xi_l}\left[\mathcal{J}\frac{\partial \xi_l}{\partial x_m}\right]_\kappa a_m \boldsymbol{u}_\kappa = \boldsymbol{SAT}, \tag{8}$$

where $\boldsymbol{SAT}$ is the vector of the SATs used to impose both boundary conditions and or interelement connectivity. Unfortunately, the scheme (8) is not guaranteed to be stable. However, a well-known remedy is to consider a canonical splitting that is arrived at by summing one half of (4) and one half of (5), giving

$$\begin{aligned} &\mathcal{J}_\kappa \frac{\partial \mathcal{U}}{\partial t} + \frac{1}{2}\sum_{l,m=1}^{3}\left\{\frac{\partial}{\partial \xi_l}\left(\mathcal{J}_\kappa \frac{\partial \xi_l}{\partial x_m} a_m \mathcal{U}\right) + \mathcal{J}_\kappa \frac{\partial \xi_l}{\partial x_m}\frac{\partial}{\partial \xi_l}\left(a_m \mathcal{U}\right)\right\} \\ &- \frac{1}{2}\sum_{l,m=1}^{3}\left\{a_m \mathcal{U}\frac{\partial}{\partial \xi_l}\left(\mathcal{J}_\kappa \frac{\partial \xi_l}{\partial x_m}\right)\right\} = 0, \end{aligned} \tag{9}$$

where the last set of terms are zero by the GCL conditions (6). Then, a stable semidiscrete form is constructed in the same manner as the split form (9) by discretizing (4) and (5) using D_{ξ_l}, J_κ, and $\left[\mathcal{J}\frac{\partial \xi_l}{\partial x_m}\right]_\kappa$, and averaging the results. This procedure yields

$$\begin{aligned}\mathsf{J}_\kappa \frac{\mathrm{d}\boldsymbol{u}_\kappa}{\mathrm{d}t} + \frac{1}{2}\sum_{l,m=1}^{3} a_m \left\{ \mathsf{D}_{\xi_l}\left[\mathcal{J}\frac{\partial \xi_l}{\partial x_m}\right]_\kappa + \left[\mathcal{J}\frac{\partial \xi_l}{\partial x_m}\right]_\kappa \mathsf{D}_{\xi_l} \right\} \boldsymbol{u}_\kappa \\ - \frac{1}{2}\sum_{l,m=1}^{3} \left\{ a_m \,\mathrm{diag}\left(\boldsymbol{u}_\kappa\right) \mathsf{D}_{\xi_l}\left[\mathcal{J}\frac{\partial \xi_l}{\partial x_m}\right]_\kappa \mathbf{1}_\kappa \right\} = \boldsymbol{SAT},\end{aligned} \tag{10}$$

where $\mathbf{1}_\kappa$ is a vector of ones of the size of the number of nodes on the κ^{th} element. As in the continuous case, the semidiscrete form has a set of discrete GCL conditions

$$\sum_{l=1}^{3} \mathsf{D}_{\xi_l}\left[\mathcal{J}\frac{\partial \xi_l}{\partial x_m}\right]_\kappa \mathbf{1}_\kappa = \mathbf{0}, \quad m = 1,2,3, \tag{11}$$

that if satisfied, lead to the following telescoping (provably stable) semidiscrete form

$$\mathsf{J}_\kappa \frac{\mathrm{d}\boldsymbol{u}_\kappa}{\mathrm{d}t} + \frac{1}{2}\sum_{l,m=1}^{3} a_m \left\{ \mathsf{D}_{\xi_l}\left[\mathcal{J}\frac{\partial \xi_l}{\partial x_m}\right]_\kappa + \left[\mathcal{J}\frac{\partial \xi_l}{\partial x_m}\right]_\kappa \mathsf{D}_{\xi_l} \right\} \boldsymbol{u}_\kappa = \boldsymbol{SAT}. \tag{12}$$

Remark 1. *The linear stability of semidiscrete operators for constant coefficient hyperbolic systems, is not preserved by arbitrary design order approximations to the metric terms. Only approximations to the metric terms that satisfy discrete GCL* (11) *conditions lead to stable semidiscrete forms.*

Remark 2. *The satisfaction of the discrete GCL conditions* (11) *for tensor-product conforming discretizations has well-known solutions (Vinokur and Yee [59] or Thomas and Lombard [58]) which require that the differentiation matrices commute, i.e.* $\mathsf{D}_{\xi_1}\mathsf{D}_{\xi_2} = \mathsf{D}_{\xi_2}\mathsf{D}_{\xi_1}$*, etc..*

Remark 3. *The discrete GCL conditions can alternatively be derived by inputting a constant solution into* (10)*.*

3.2 Scalar convection and the nonconforming interface

The analysis and presentation of nonconforming semidiscrete algorithms is simplified by considering a single interface between two adjoining elements as shown in Figure 1. The elements have aligned computational coordinates and the shared interface is vertical. The nonconformity is assumed to arise from local approximations with differing polynomial degrees. Specifically, the left element has polynomial degree p_{L} (low: subscript/superscript L) and the right element has polynomial degree p_{H} (high: subscript/superscript H) where $p_{\mathrm{H}} > p_{\mathrm{L}}$ (see Figure 1). The first task is to construct SBP operators that span both elements: i.e., macroelement operators composed of elements L and H. A naive construction would be the following operators in the three coordinate directions:

$$\widetilde{\mathsf{D}}_{\xi_1} \equiv \begin{bmatrix} \mathsf{D}^{\mathrm{L}}_{\xi_1} & \\ & \mathsf{D}^{\mathrm{H}}_{\xi_1} \end{bmatrix} \quad ; \quad \widetilde{\mathsf{D}}_{\xi_2} \equiv \begin{bmatrix} \mathsf{D}^{\mathrm{L}}_{\xi_2} & \\ & \mathsf{D}^{\mathrm{H}}_{\xi_2} \end{bmatrix} \quad ; \quad \widetilde{\mathsf{D}}_{\xi_3} \equiv \begin{bmatrix} \mathsf{D}^{\mathrm{L}}_{\xi_3} & \\ & \mathsf{D}^{\mathrm{H}}_{\xi_3} \end{bmatrix}. \tag{13}$$

The $\widetilde{\mathsf{D}}_{\xi_2}$ and $\widetilde{\mathsf{D}}_{\xi_3}$ macroelement operators are by construction SBP operators; the action of their differentiation is parallel to the interface, and they telescope out to the boundaries. The $\widetilde{\mathsf{D}}_{\xi_1}$ is not by construction an SBP operator, despite the individual matrices composing $\widetilde{\mathsf{D}}_{\xi_1}$ being SBP operators. In addition, and more critically, there is no coupling between the two elements. Thus, interface coupling must be introduced between the two elements that render the operators on the macroelement as SBP operators. For this purpose, interpolation operators are needed that interpolate information from element H to element L and vice versa. For simplicity, the interpolation operators use only tensor product surface information from the adjoining interface surface.

With this background, general matrix difference operators between the two elements are constructed as

$$\widetilde{\mathsf{D}}_{\xi_l} = \widetilde{\mathsf{P}}^{-1}\widetilde{\mathsf{Q}}_{\xi_l} = \widetilde{\mathsf{P}}^{-1}\left(\widetilde{\mathsf{S}}_{\xi_l} + \frac{1}{2}\widetilde{\mathsf{E}}_{\xi_l}\right). \tag{14}$$

Focusing on the direction orthogonal to the interface (ξ_1) the relevant matrices are given by

$$\begin{aligned}
&\widetilde{\mathsf{P}} \equiv \mathrm{diag}\begin{bmatrix} \mathsf{P}^{\mathrm{L}} & \\ & \mathsf{P}^{\mathrm{H}} \end{bmatrix}, \\
&\widetilde{\mathsf{S}}_{\xi_1} \equiv \\
&\begin{bmatrix} \mathsf{S}^{\mathrm{L}}_{\xi_1} & \frac{1}{2}\left(\boldsymbol{e}_{N_{\mathrm{L}}}\boldsymbol{e}_{1_{\mathrm{H}}}^{\mathrm{T}} \otimes \mathsf{P}_{\mathrm{L}}^{(1D)}\mathsf{I}_{\mathrm{HtoL}}^{(1D)} \otimes \mathsf{P}_{\mathrm{L}}^{(1D)}\mathsf{I}_{\mathrm{HtoL}}^{(1D)}\right) \\ -\frac{1}{2}\left(\boldsymbol{e}_{1_{\mathrm{H}}}\boldsymbol{e}_{N_{\mathrm{L}}}^{\mathrm{T}} \otimes \mathsf{P}_{\mathrm{H}}^{(1D)}\mathsf{I}_{\mathrm{LtoH}}^{(1D)} \otimes \mathsf{P}_{\mathrm{H}}^{(1D)}\mathsf{I}_{\mathrm{LtoH}}^{(1D)}\right) & \mathsf{S}^{\mathrm{H}}_{\xi_1} \end{bmatrix}, \\
&\widetilde{\mathsf{E}}_{\xi_1} \equiv \\
&\begin{bmatrix} -\boldsymbol{e}_{1_{\mathrm{L}}}\boldsymbol{e}_{1_{\mathrm{L}}}^{\mathrm{T}} \otimes \mathsf{P}_{\mathrm{L}}^{(1D)} \otimes \mathsf{P}_{\mathrm{L}}^{(1D)} & \\ & \boldsymbol{e}_{N_{\mathrm{H}}}\boldsymbol{e}_{N_{\mathrm{H}}}^{\mathrm{T}} \otimes \mathsf{P}_{\mathrm{H}}^{(1D)} \otimes \mathsf{P}_{\mathrm{H}}^{(1D)} \end{bmatrix},
\end{aligned} \tag{15}$$

and $\mathsf{I}_{\mathrm{HtoL}}^{(1D)}$ and $\mathsf{I}_{\mathrm{LtoH}}^{(1D)}$ are one-dimensional interpolation operators from the H element to the L element and vice versa.

A necessary constraint the SBP formalism places on $\widetilde{\mathsf{D}}_{\xi_1}$, is skew-symmetry of the $\widetilde{\mathsf{S}}_{\xi_1}$ matrices. The block-diagonal matrices in $\widetilde{\mathsf{S}}_{\xi_1}$ are already skew-symmetric but the of diagonal blocks are not. Thus, it is necessary to satisfy the following condition:

$$\left(\boldsymbol{e}_{N_{\mathrm{L}}}\boldsymbol{e}_{1_{\mathrm{H}}}^{\mathrm{T}} \otimes \mathsf{P}_{\mathrm{L}}^{(1D)}\mathsf{I}_{\mathrm{HtoL}}^{(1D)} \otimes \mathsf{P}_{\mathrm{L}}^{(1D)}\mathsf{I}_{\mathrm{HtoL}}^{(1D)}\right) = \left\{\left(\boldsymbol{e}_{1_{\mathrm{H}}}\boldsymbol{e}_{N_{\mathrm{L}}}^{\mathrm{T}} \otimes \mathsf{P}_{\mathrm{H}}^{(1D)}\mathsf{I}_{\mathrm{LtoH}}^{(1D)} \otimes \mathsf{P}_{\mathrm{H}}^{(1D)}\mathsf{I}_{\mathrm{LtoH}}^{(1D)}\right)\right\}^{\mathrm{T}}.$$

This implies that the interpolation operators are related to each other as follows:

$$\mathsf{I}_{\mathrm{HtoL}}^{(1D)} = \left(\mathsf{P}_{\mathrm{L}}^{(1D)}\right)^{-1}\left(\mathsf{I}_{\mathrm{LtoH}}^{(1D)}\right)^{\mathrm{T}}\mathsf{P}_{\mathrm{H}}^{(1D)}.$$

This property is denoted as the SBP preserving property because it leads to a macroelement differentiation matrix that is an SBP operator. The optimal interpolation operator, $\mathsf{I}_{\mathrm{LtoH}}^{(1D)}$, is constructed to exactly interpolate polynomial of degree p_{L} and can be easily constructed as follows:

$$\mathsf{I}_{\mathrm{LtoH}}^{(1D)} = \left[\boldsymbol{\xi}_{\mathrm{H}}^{0}, \ldots, \boldsymbol{\xi}_{\mathrm{H}}^{p_{\mathrm{L}}}\right]\left[\boldsymbol{\xi}_{\mathrm{L}}^{0}, \ldots, \boldsymbol{\xi}_{\mathrm{L}}^{p_{\mathrm{L}}}\right]^{-1},$$

where $\boldsymbol{\xi}_{\mathrm{L}}$ and $\boldsymbol{\xi}_{\mathrm{H}}$ are the one-dimensional nodal distributions in computational space of the two elements. The companion interpolation operator $\mathsf{I}_{\mathrm{HtoL}}^{(1D)}$ is suboptimal by one degree $(p_{\mathrm{L}} - 1)$, a

consequence of satisfying the necessary SBP-preserving property (see Friedrich *et al.* [25] for a complete discussion).

The semidiscrete skew-symmetric split operator given in Eq. (10), discretized using the macroelement operators $\widetilde{\mathsf{D}}_{\xi_l}$, and metric information J, $\left[\mathcal{J}\frac{\partial \xi_l}{\partial x_m}\right]$, leads to the following:

$$\begin{aligned}\mathsf{J}\frac{\mathrm{d}\widetilde{\boldsymbol{u}}}{\mathrm{d}t} + \frac{1}{2}\sum_{l,m=1}^{3} a_m \left(\widetilde{\mathsf{D}}_{\xi_l}\left[\mathcal{J}\frac{\partial \xi_l}{\partial x_m}\right] + \left[\mathcal{J}\frac{\partial \xi_l}{\partial x_m}\right]\widetilde{\mathsf{D}}_{\xi_l}\right)\widetilde{\boldsymbol{u}} \\ - \frac{1}{2}\sum_{l,m=1}^{3} a_m \,\mathrm{diag}\left(\widetilde{\boldsymbol{u}}\right)\widetilde{\mathsf{D}}_{\xi_l}\left[\mathcal{J}\frac{\partial \xi_l}{\partial x_m}\right]\tilde{\mathbf{1}} = \mathbf{0},\end{aligned} \tag{16}$$

where

$$\widetilde{\boldsymbol{u}} \equiv \left[\boldsymbol{u}_{\mathrm{L}}^{\mathrm{T}}, \boldsymbol{u}_{\mathrm{H}}^{\mathrm{T}}\right]^{\mathrm{T}}, \mathsf{J} \equiv \mathrm{diag}\begin{bmatrix} \mathsf{J}_{\mathrm{L}} & \\ & \mathsf{J}_{\mathrm{H}} \end{bmatrix}, \left[\mathcal{J}\frac{\partial \xi_l}{\partial x_m}\right] \equiv \begin{bmatrix} \left[\mathcal{J}\frac{\partial \xi_l}{\partial x_m}\right]_{\mathrm{L}} & \\ & \left[\mathcal{J}\frac{\partial \xi_l}{\partial x_m}\right]_{\mathrm{H}} \end{bmatrix}. \tag{17}$$

As was the case in Eq. (10), a necessary condition for stability is that the metric terms satisfy the following discrete GCL conditions:

$$\sum_{l=1}^{3} \widetilde{\mathsf{D}}_{\xi_l}\left[\mathcal{J}\frac{\partial \xi_l}{\partial x_m}\right]\tilde{\mathbf{1}} = \mathbf{0}. \tag{18}$$

Recognizing that $\widetilde{\mathsf{D}}_{\xi_1}$ is not a tensor product operator, discrete metrics constructed using the analytic formalism of Vinokur and Yee [59] or Thomas and Lombard [58] will not in general satisfy the discrete GCL condition required in Eq. (18). The only viable alternative is to solve for discrete metrics that directly satisfy the GCL constraints.

Remark 4. *Note that metric terms are assigned colors; e.g., the time-term Jacobian:* J *or the volume metric terms:* $\left[\mathcal{J}\frac{\partial \xi_l}{\partial x_m}\right]$. *Metric terms with common colors form a clique and must be formed consistently. For example, the time-term Jacobian and the volume metric Jacobian need not be equivalent. Another important clique: the surface metrics, will be introduced in the next subsection.*

3.3 Isolating the metrics

The system (18) is a highly underdetermined system that couples the approximation of the metrics in both elements. Worse still, whole clouds of nonconforming elements would in general need to be solved simultaneously, making the approach undesirable and even impracticable! A close

examination of the volume terms provides insight on how to overcome this issue:

$$\widetilde{\mathsf{P}}\left(\widetilde{\mathsf{D}}_{\xi_1}\left[\mathcal{J}\frac{\partial \xi_1}{\partial x_m}\right]+\left[\mathcal{J}\frac{\partial \xi_1}{\partial x_m}\right]\widetilde{\mathsf{D}}_{\xi_1}\right)=$$
$$\begin{bmatrix}\mathsf{A}_{11} & \mathsf{A}_{12}\\ -\mathsf{A}_{12}^{\mathrm{T}} & \mathsf{A}_{22}\end{bmatrix}+\left(\widetilde{\mathsf{E}}_{\xi_1}\left[\mathcal{J}\frac{\partial \xi_1}{\partial x_m}\right]+\left[\mathcal{J}\frac{\partial \xi_1}{\partial x_m}\right]\widetilde{\mathsf{E}}_{\xi_1}\right),$$

$$\begin{aligned}
\mathsf{A}_{11} &\equiv \left\{\mathsf{S}^{\mathrm{L}}_{\xi_1}\left[\mathcal{J}\frac{\partial \xi_1}{\partial x_m}\right]_{\mathrm{L}}+\left[\mathcal{J}\frac{\partial \xi_1}{\partial x_m}\right]_{\mathrm{L}}\mathsf{S}^{\mathrm{L}}_{\xi_1}\right\},\\
\mathsf{A}_{12} &= \frac{1}{2}\left\{\begin{array}{l}\left[\mathcal{J}\frac{\partial \xi_1}{\partial x_m}\right]_{\mathrm{L}}\left(\boldsymbol{e}_{N_{\mathrm{L}}}\boldsymbol{e}_{1_{\mathrm{H}}}^{\mathrm{T}}\otimes \mathsf{P}_{\mathrm{L}}^{(1D)}\mathsf{I}_{\mathrm{HtoL}}^{(1D)}\otimes \mathsf{P}_{\mathrm{L}}^{(1D)}\mathsf{I}_{\mathrm{HtoL}}^{(1D)}\right)\\ +\left(\boldsymbol{e}_{N_{\mathrm{L}}}\boldsymbol{e}_{1_{\mathrm{H}}}^{\mathrm{T}}\otimes \mathsf{P}_{\mathrm{L}}^{(1D)}\mathsf{I}_{\mathrm{HtoL}}^{(1D)}\otimes \mathsf{P}_{\mathrm{L}}^{(1D)}\mathsf{I}_{\mathrm{HtoL}}^{(1D)}\right)\left[\mathcal{J}\frac{\partial \xi_1}{\partial x_m}\right]_{\mathrm{H}}\end{array}\right\},\\
\mathsf{A}_{22} &\equiv \left\{\mathsf{S}^{\mathrm{H}}_{\xi_1}\left[\mathcal{J}\frac{\partial \xi_1}{\partial x_m}\right]_{\mathrm{H}}+\left[\mathcal{J}\frac{\partial \xi_1}{\partial x_m}\right]_{\mathrm{H}}\mathsf{S}^{\mathrm{H}}_{\xi_1}\right\}.
\end{aligned} \tag{19}$$

Replacing the highlighted off-diagonal metric terms in (19) with known metrics data, by construction preserves the skew-symmetry of the operator $\widetilde{\mathsf{S}}_{\xi_l}$, but decouples the discrete GCL conditions (18). The highlighted off-diagonal surface metric terms: L and H become forcing data for the GCL condition. Note that L and H need not be equivalent, provided they are design order close.

Remark 5. *More generally,* A_{12} *can be composed of any terms that are design order interpolations from one element to the other and these can be constructed in a very general way, for example, one might consider first interpolating data to an intermediate set of Gauss nodes on which the metric terms are specified. The theoretical results in this paper apply to any such approach that is design order, satisfied the structural requirements presented above, and that uses specified metric information in the coupling terms.*

With this approach, the discrete GCL conditions become (where contributions from the boundary SATs have been ignored)

$$\begin{aligned}
&2\mathsf{P}^{\mathrm{L}}\sum_{l=1}^{3}\mathsf{D}^{\mathrm{L}}_{\xi_l}\left[\mathcal{J}\frac{\partial \xi_l}{\partial x_m}\right]_{\mathrm{L}}\mathbf{1}_{\mathrm{L}}=\\
&\left\{\left(\boldsymbol{e}_{N_{\mathrm{L}}}\boldsymbol{e}_{N_{\mathrm{L}}}^{\mathrm{T}}\otimes \mathsf{P}_{\mathrm{L}}^{(1D)}\otimes \mathsf{P}_{\mathrm{L}}^{(1D)}\right)\left[\mathcal{J}\frac{\partial \xi_1}{\partial x_m}\right]_{\mathrm{L}}+\left[\mathcal{J}\frac{\partial \xi_1}{\partial x_m}\right]_{\mathrm{L}}\left(\boldsymbol{e}_{N_{\mathrm{L}}}\boldsymbol{e}_{N_{\mathrm{L}}}^{\mathrm{T}}\otimes \mathsf{P}_{\mathrm{L}}^{(1D)}\otimes \mathsf{P}_{\mathrm{L}}^{(1D)}\right)\right\}\mathbf{1}_{\mathrm{L}}\\
&-\left\{\left(\boldsymbol{e}_{N_{\mathrm{L}}}\otimes \mathsf{I}_{N_{\mathrm{L}}}\otimes \mathsf{I}_{N_{\mathrm{L}}}\right)\left[\mathcal{J}\frac{\partial \xi_1}{\partial x_m}\right]_{\mathrm{L}}^{\hat{\Gamma}}\left(\mathsf{P}_{\mathrm{L}}^{(1D)}\mathsf{I}_{\mathrm{HtoL}}^{(1D)}\otimes \mathsf{P}_{\mathrm{L}}^{(1D)}\mathsf{I}_{\mathrm{HtoL}}^{(1D)}\right)\left(\boldsymbol{e}_{1_{\mathrm{H}}}^{\mathrm{T}}\otimes \mathsf{I}_{N_{\mathrm{H}}}\otimes \mathsf{I}_{N_{\mathrm{H}}}\right)\right\}\mathbf{1}_{\mathrm{H}}\\
&-\left\{\left(\boldsymbol{e}_{N_{\mathrm{L}}}\otimes \mathsf{I}_{N_{\mathrm{L}}}\otimes \mathsf{I}_{N_{\mathrm{L}}}\right)\left(\mathsf{P}_{\mathrm{L}}^{(1D)}\mathsf{I}_{\mathrm{HtoL}}^{(1D)}\otimes \mathsf{P}_{\mathrm{L}}^{(1D)}\mathsf{I}_{\mathrm{HtoL}}^{(1D)}\right)\left[\mathcal{J}\frac{\partial \xi_1}{\partial x_m}\right]_{\mathrm{H}}^{\hat{\Gamma}}\left(\boldsymbol{e}_{1_{\mathrm{H}}}^{\mathrm{T}}\otimes \mathsf{I}_{N_{\mathrm{H}}}\otimes \mathsf{I}_{N_{\mathrm{H}}}\right)\right\}\mathbf{1}_{\mathrm{H}},
\end{aligned} \tag{20}$$

$$
\begin{aligned}
&2\mathsf{P}^{\mathrm{L}}\sum_{l=1}^{3}\mathsf{D}_{\xi_l}^{\mathrm{H}}\left[\mathcal{J}\frac{\partial\xi_l}{\partial x_m}\right]_{\mathrm{H}}\mathbf{1}_{\mathrm{H}} = \\
&-\left\{\left(\boldsymbol{e}_{1_{\mathrm{H}}}\boldsymbol{e}_{1_{\mathrm{H}}}^{\mathrm{T}}\otimes\mathsf{P}_{\mathrm{H}}^{(1D)}\otimes\mathsf{P}_{\mathrm{H}}^{(1D)}\right)\left[\mathcal{J}\frac{\partial\xi_1}{\partial x_m}\right]_{\mathrm{H}}+\left[\mathcal{J}\frac{\partial\xi_1}{\partial x_m}\right]_{\mathrm{H}}\left(\boldsymbol{e}_{1_{\mathrm{L}}}\boldsymbol{e}_{1_{\mathrm{H}}}^{\mathrm{T}}\otimes\mathsf{P}_{\mathrm{H}}^{(1D)}\otimes\mathsf{P}_{\mathrm{H}}^{(1D)}\right)\right\}\mathbf{1}_{\mathrm{H}} \\
&+\left\{(\boldsymbol{e}_{1_{\mathrm{H}}}\otimes\mathsf{I}_{N_{\mathrm{H}}}\otimes\mathsf{I}_{N_{\mathrm{L}}})\left[\mathcal{J}\frac{\partial\xi_1}{\partial x_m}\right]_{\mathrm{H}}^{\hat{\Gamma}}\left(\mathsf{P}_{\mathrm{H}}^{(1D)}\mathsf{I}_{\mathrm{LtoH}}^{(1D)}\otimes\mathsf{P}_{\mathrm{H}}^{(1D)}\mathsf{I}_{\mathrm{LtoH}}^{(1D)}\right)(\boldsymbol{e}_{N_{\mathrm{L}}}^{\mathrm{T}}\otimes\mathsf{I}_{N_{\mathrm{L}}}\otimes\mathsf{I}_{N_{\mathrm{L}}})\right\}\mathbf{1}_{\mathrm{L}} \\
&+\left\{(\boldsymbol{e}_{1_{\mathrm{H}}}\otimes\mathsf{I}_{N_{\mathrm{H}}}\otimes\mathsf{I}_{N_{\mathrm{H}}})\left(\mathsf{P}_{\mathrm{H}}^{(1D)}\mathsf{I}_{\mathrm{LtoH}}^{(1D)}\otimes\mathsf{P}_{\mathrm{H}}^{(1D)}\mathsf{I}_{\mathrm{LtoH}}^{(1D)}\right)\left[\mathcal{J}\frac{\partial\xi_1}{\partial x_m}\right]_{\mathrm{L}}^{\hat{\Gamma}}(\boldsymbol{e}_{N_{\mathrm{L}}}^{\mathrm{T}}\otimes\mathsf{I}_{N_{\mathrm{L}}}\otimes\mathsf{I}_{N_{\mathrm{L}}})\right\}\mathbf{1}_{\mathrm{L}}.
\end{aligned}
\tag{21}
$$

The matrix $\left[\mathcal{J}\frac{\partial\xi_1}{\partial x_m}\right]_{\mathrm{L}}^{\hat{\Gamma}}$ is of size $N_{\mathrm{L}}^2\times N_{\mathrm{L}}^2$ (N_{L} is the number of nodes in each computational direction on element L) and its diagonal elements are approximations to the metrics on the surface nodes of element L at the shared interface. An analogous definition holds for $\left[\mathcal{J}\frac{\partial\xi_1}{\partial x_m}\right]_{\mathrm{H}}^{\hat{\Gamma}}$. In order to decouple the two systems of equations in (20) and (21) the terms in $\left[\mathcal{J}\frac{\partial\xi_1}{\partial x_m}\right]_{\mathrm{L}}^{\hat{\Gamma}}$ and $\left[\mathcal{J}\frac{\partial\xi_1}{\partial x_m}\right]_{\mathrm{H}}^{\hat{\Gamma}}$ need to be specified, for example, using the analytic metrics, which is the approach used in this paper. For later use, we introduce notation for the macroelement $\widetilde{\mathsf{D}}_{l,m}$ that is the macroelement operator constructed as descried above for the metric terms $\mathcal{J}_\kappa\frac{\partial\xi_l}{\partial x_m}$.

The next section details how to construct the metrics so that the remaining discrete GCL conditions are satisfied.

3.4 Metric solution mechanics

In this section, to demonstrate the proposed approach for approximating the metric terms, the discrete GCL conditions associated with the element L (20) are used.

Note that for an arbitrary interior element, the discrete GCL system that needs to be solved includes the coupling terms on all six faces, while for the simplified problem considered above only the (nonconforming) coupling on the vertical interface appears.

Eq. (20) can be algebraically manipulated into a form that is more convenient for constructing a solution procedure for the metric terms. This form is derived by multiplying Eq. (20) by -1, using the SBP property $\mathsf{Q}_{\mathrm{L}}^{(1D)} = -\left(\mathsf{Q}_{\mathrm{L}}^{(1D)}\right)^{\mathrm{T}}+\mathsf{E}_{\mathrm{L}}^{(1D)}$, and canceling common terms. Doing so results in

$$
\begin{aligned}
&2\sum_{l=1}^{3}\left(\mathsf{Q}_{\xi_l}^{\mathrm{L}}\right)^{\mathrm{T}}\left[\mathcal{J}\frac{\partial\xi_l}{\partial x_m}\right]_{\mathrm{L}}\mathbf{1}_{\mathrm{L}} = \\
&-\left\{(\boldsymbol{e}_{N_{\mathrm{L}}}\otimes\mathsf{I}_{N_{\mathrm{L}}}\otimes\mathsf{I}_{N_{\mathrm{L}}})\left[\mathcal{J}\frac{\partial\xi_1}{\partial x_m}\right]_{\mathrm{L}}^{\hat{\Gamma}}\left(\mathsf{P}_{\mathrm{L}}^{(1D)}\mathsf{I}_{\mathrm{HtoL}}^{(1D)}\otimes\mathsf{P}_{\mathrm{L}}^{(1D)}\mathsf{I}_{\mathrm{HtoL}}^{(1D)}\right)(\boldsymbol{e}_{1_{\mathrm{H}}}^{\mathrm{T}}\otimes\mathsf{I}_{N_{\mathrm{H}}}\otimes\mathsf{I}_{N_{\mathrm{H}}})\right\}\mathbf{1}_{\mathrm{H}} \\
&-\left\{(\boldsymbol{e}_{N_{\mathrm{L}}}\otimes\mathsf{I}_{N_{\mathrm{L}}}\otimes\mathsf{I}_{N_{\mathrm{L}}})\left(\mathsf{P}_{\mathrm{L}}^{(1D)}\mathsf{I}_{\mathrm{HtoL}}^{(1D)}\otimes\mathsf{P}_{\mathrm{L}}^{(1D)}\mathsf{I}_{\mathrm{HtoL}}^{(1D)}\right)\left[\mathcal{J}\frac{\partial\xi_1}{\partial x_m}\right]_{\mathrm{H}}^{\hat{\Gamma}}(\boldsymbol{e}_{1_{\mathrm{H}}}^{\mathrm{T}}\otimes\mathsf{I}_{N_{\mathrm{H}}}\otimes\mathsf{I}_{N_{\mathrm{H}}})\right\}\mathbf{1}_{\mathrm{H}}, \\
&m=1,2,3,
\end{aligned}
\tag{22}
$$

where $\mathsf{Q}_{\xi_1}^{\mathrm{L}}\equiv\mathsf{Q}_{\mathrm{L}}^{(1D)}\otimes\mathsf{P}_{\mathrm{L}}^{(1D)}\otimes\mathsf{P}_{\mathrm{L}}^{(1D)}$, $\mathsf{Q}_{\xi_2}^{\mathrm{L}}\equiv\mathsf{P}_{\mathrm{L}}^{(1D)}\otimes\mathsf{Q}_{\mathrm{L}}^{(1D)}\otimes\mathsf{P}_{\mathrm{L}}^{(1D)}$, $\mathsf{Q}_{\xi_3}^{\mathrm{L}}\equiv\mathsf{P}_{\mathrm{L}}^{(1D)}\otimes\mathsf{P}_{\mathrm{L}}^{(1D)}\otimes\mathsf{Q}_{\mathrm{L}}^{(1D)}$. Note that the contributions from the E_{ξ_l} from the left-hand side (i.e., coming from the step $\mathsf{Q}=-\mathsf{Q}^{\mathrm{T}}+\mathsf{E}$)

related to the boundaries of the macroelement are ignored. This contributions interact with the boundary SATs in the same way as the interface does.

The metric terms in Eq. (22) are determined by solving a strictly convex quadratic optimization problem, following the algorithm given in Crean *et al.* [13]:

$$\begin{aligned} &\min_{\boldsymbol{a}_m} \frac{1}{2}\left(\boldsymbol{a}_m^{\mathrm{L}} - \boldsymbol{a}_{m,\mathrm{target}}^{\mathrm{L}}\right)^{\mathrm{T}}\left(\boldsymbol{a}_m^{\mathrm{L}} - \boldsymbol{a}_{m,\mathrm{target}}^{\mathrm{L}}\right), \quad \text{subject to} \quad \mathsf{M}^{\mathrm{L}}\boldsymbol{a}_m^{\mathrm{L}} = \boldsymbol{c}_m^{\mathrm{L}}, \\ &m = 1,2,3, \end{aligned} \tag{23}$$

where $\boldsymbol{a}_m^{\mathrm{L}}$ and $\boldsymbol{a}_{m,\mathrm{target}}^{\mathrm{L}}$ are the optimized and targeted metric terms, respectively, and

$$\left(\boldsymbol{a}_m^{\mathrm{L}}\right)^{\mathrm{T}} \equiv \mathbf{1}_{\mathrm{L}}^{\mathrm{T}}\left[\left[\mathcal{J}\frac{\partial\xi_1}{\partial x_m}\right]_{\mathrm{L}}, \left[\mathcal{J}\frac{\partial\xi_2}{\partial x_m}\right]_{\mathrm{L}}, \left[\mathcal{J}\frac{\partial\xi_3}{\partial x_m}\right]_{\mathrm{L}}\right], \; \mathsf{M}^{\mathrm{L}} \equiv \left[\left(\mathsf{Q}_{\xi_1}^{\mathrm{L}}\right)^{\mathrm{T}}, \left(\mathsf{Q}_{\xi_2}^{\mathrm{L}}\right)^{\mathrm{T}}, \left(\mathsf{Q}_{\xi_3}^{\mathrm{L}}\right)^{\mathrm{T}}\right],$$

$$\begin{aligned} 2\boldsymbol{c}_m^{\mathrm{L}} \equiv & \\ &- \left\{\left(\boldsymbol{e}_{N_{\mathrm{L}}} \otimes \mathsf{I}_{N_{\mathrm{L}}} \otimes \mathsf{I}_{N_{\mathrm{L}}}\right)\left[\mathcal{J}\frac{\partial\xi_1}{\partial x_m}\right]_{\mathrm{L}}^{\hat{\Gamma}}\left(\mathsf{P}_{\mathrm{L}}^{(1D)}\mathsf{I}_{\mathrm{HtoL}}^{(1D)} \otimes \mathsf{P}_{\mathrm{L}}^{(1D)}\mathsf{I}_{\mathrm{HtoL}}^{(1D)}\right)\left(\boldsymbol{e}_{1_{\mathrm{H}}}^{\mathrm{T}} \otimes \mathsf{I}_{N_{\mathrm{H}}} \otimes \mathsf{I}_{N_{\mathrm{H}}}\right)\right\}\mathbf{1}_{\mathrm{H}} \\ &- \left\{\left(\boldsymbol{e}_{N_{\mathrm{L}}} \otimes \mathsf{I}_{N_{\mathrm{L}}} \otimes \mathsf{I}_{N_{\mathrm{L}}}\right)\left(\mathsf{P}_{\mathrm{L}}^{(1D)}\mathsf{I}_{\mathrm{HtoL}}^{(1D)} \otimes \mathsf{P}_{\mathrm{L}}^{(1D)}\mathsf{I}_{\mathrm{HtoL}}^{(1D)}\right)\left[\mathcal{J}\frac{\partial\xi_1}{\partial x_m}\right]_{\mathrm{H}}^{\hat{\Gamma}}\left(\boldsymbol{e}_{1_{\mathrm{H}}}^{\mathrm{T}} \otimes \mathsf{I}_{N_{\mathrm{H}}} \otimes \mathsf{I}_{N_{\mathrm{H}}}\right)\right\}\mathbf{1}_{\mathrm{H}}, \end{aligned}$$

with $\boldsymbol{a}_m^{\mathrm{L}}$ of size $3(N_{\mathrm{L}})^3 \times 1$, M^{L} of size $(N_{\mathrm{L}})^3 \times 3(N_{\mathrm{L}})^3$ and $\boldsymbol{c}_m^{\mathrm{L}}$ of size $(N_{\mathrm{L}})^3 \times 1$. The optimal solution, in the Cartesian 2-norm, is given by (see Proposition 1 in Crean *et al.* [13])

$$\boldsymbol{a}_m^{\mathrm{L}} = \boldsymbol{a}_{m,\mathrm{target}}^{\mathrm{L}} - \left(\mathsf{M}^{\mathrm{L}}\right)^{\dagger}\left(\mathsf{M}^{\mathrm{L}}\boldsymbol{a}_{m,\mathrm{target}}^{\mathrm{L}} - \boldsymbol{c}_m^{\mathrm{L}}\right), \tag{24}$$

with $\left(\mathsf{M}^{\mathrm{L}}\right)^{\dagger}$ the Moore-Penrose pseudoinverse of M^{L}. The pseudoinverse is computed using a singular value decomposition (SVD) of M^{L}

$$\mathsf{M}^{\mathrm{L}} = \mathsf{U}^{\mathrm{L}}\Sigma^{\mathrm{L}}\left(\mathsf{V}^{\mathrm{L}}\right)^{\mathrm{T}}, \quad \left(\mathsf{M}^{\mathrm{L}}\right)^{\dagger} = \mathsf{V}^{\mathrm{L}}\left(\Sigma^{\mathrm{L}}\right)^{\dagger}\left(\mathsf{U}^{\mathrm{L}}\right)^{\mathrm{T}},$$

with U^{L} an $(N_{\mathrm{L}})^3 \times (N_{\mathrm{L}})^3$ unitary matrix, Σ^{L} an $(N_{\mathrm{L}})^3 \times (N_{\mathrm{L}})^3$ diagonal matrix containing the singular values of M^{L}, and $\left(\mathsf{V}^{\mathrm{L}}\right)^{\mathrm{T}}$ an $(N_{\mathrm{L}})^3 \times 3(N_{\mathrm{L}})^3$ matrix with orthonormal rows. Although the solution ($\boldsymbol{a}_m^{\mathrm{L}}$ given by Eq. (24)) is optimal, it is not guaranteed to **exactly** satisfy Eq. (23) (i.e., machine precision). The following theorem establishes an additional constrain on the surface metrics.

Theorem 1. *The surface metrics, $\boldsymbol{c}_m^{\mathrm{L}}$, must satisfy the additional constraint*

$$\mathbf{1}_{\mathrm{L}}^{\mathrm{T}}\boldsymbol{c}_m^{\mathrm{L}} = 0\,, \tag{25}$$

to guarantee an exact solution of the discrete GCL condition given in Eq. (23)*.*

Proof. The matrix M^{L} is constructed from the transposes of three derivative operators: $\left(\mathsf{D}_{\xi_l}^{\mathrm{L}}\right)^{\mathrm{T}}\mathsf{P}^{\mathrm{L}} = \left(\mathsf{Q}_{\xi_l}^{\mathrm{L}}\right)^{\mathrm{T}}$, with the constant vector $\mathbf{1}_{\mathrm{L}}$, in its null space, i.e., $\mathbf{1}_{\mathrm{L}}^{\mathrm{T}}\left(\mathsf{Q}_{\xi_l}^{\mathrm{L}}\right)^{\mathrm{T}} = \mathbf{0}^{\mathrm{T}}$. Thus, the matrix M^{L} has a row rank of $(N_{\mathrm{L}})^3 - 1$ and one zero singular value.

Assemble the singular values in the diagonal matrix $\left(\Sigma^{\mathrm{L}}\right)$ in descending order. This implies that i) the final singular value is zero, $\Sigma((N_{\mathrm{L}})^3,(N_{\mathrm{L}})^3)=0$, ii) the final orthonormal column vector in U^{L} is a constant multiple of the vector, $\mathbf{1}_{\mathrm{L}}$, and iii) the pseudoinverse is given by $\left(\Sigma^{\mathrm{L}}\right)^{\dagger}(i,i)=\frac{1}{\Sigma^{\mathrm{L}}(i,i)}$, $i=1,\ldots,(N_{\mathrm{L}})^3-1$.

The optimal solution given in Eq. (24) can thus be expressed as

$$\boldsymbol{a}_m^{\mathrm{L}}=\boldsymbol{a}_{m,\mathrm{target}}^{\mathrm{L}}-\mathsf{V}^{\mathrm{L}}\left(\Sigma^{\mathrm{L}}\right)^{\dagger}\left(\Sigma^{\mathrm{L}}\left(\mathsf{V}^{\mathrm{L}}\right)^{\mathrm{T}}\boldsymbol{a}_{m,\mathrm{target}}^{\mathrm{L}}-(\mathsf{U}^{\mathrm{L}})^{\mathrm{T}}\boldsymbol{c}_m^{\mathrm{L}}\right).$$

Since the diagonal matrices $\left(\Sigma^{\mathrm{L}}\right)^{\dagger}$ and Σ^{L} are rank deficient in their $((N_{\mathrm{L}})^3,(N_{\mathrm{L}})^3)$ positions, a zero solution exists only if the final constant vector, dotted with the metric data is zero, i.e., $(\mathsf{U}^{\mathrm{L}})^{\mathrm{T}}\boldsymbol{c}_m^{\mathrm{L}}=\mathbf{1}_{\mathrm{L}}^{\mathrm{T}}\boldsymbol{c}_m^{\mathrm{L}}=0$. The proof is established. □

Inspection of the definition for $\boldsymbol{c}_m^{\mathrm{L}}$ given in Eq. (25), reveals that the constraint $\mathbf{1}_{\mathrm{L}}^{\mathrm{T}}\boldsymbol{c}_m^{\mathrm{L}}=0$, may be interpreted as the discrete integral of surface metric data. This integral must be zero as is motivated by the following derivation.

Integrate the continuous GCL equations over the domain $\hat{\Omega}_{\mathrm{L}}$, and apply Gauss' divergence theorem to the integral. The resulting expressions are

$$\int_{\hat{\Omega}_{\mathrm{L}}}\sum_{l=1}^{3}\frac{\partial}{\partial\xi_l}\left(\mathcal{J}\frac{\partial\xi_l}{\partial x_m}\right)\mathrm{d}\hat{\Omega}_{\mathrm{L}}=\oint_{\hat{\Gamma}_{\mathrm{L}}}\sum_{l=1}^{3}\left(\mathcal{J}\frac{\partial\xi_l}{\partial x_m}\right)n_{\xi_l}\mathrm{d}\hat{\Gamma}_{\mathrm{L}}\approx\ \mathbf{1}_{\mathrm{L}}^{\mathrm{T}}\boldsymbol{c}_m^{\mathrm{L}}\ =\ 0.$$

Thus, the constraint $\mathbf{1}_{\mathrm{L}}^{\mathrm{T}}\boldsymbol{c}_m^{\mathrm{L}}\ =\ 0$ is the discrete surface metric equivalent of the analytic surface integral consistency constraint.

There are at least two convenient ways of enforcing this constraint: 1) polynomially exact (analytic) surface metrics or 2) metrics constructed using conventional FD approaches [58,59]. The adequacy of these approaches is demonstrated by a careful investigation of the surface metrics arising from tensor-product transformations.

Consider a degree p tensor-product curvilinear coordinate transformation. The surface metrics and the coupling terms constructed on the joint surface are of degree $2p-1$ in the surface orthogonal directions. Thus, a surface mass matrix with quadrature strength $2p-1$, (e.g., LGL) integrates the surface terms exactly and immediately satisfies the constraint: $\mathbf{1}_{\mathrm{L}}^{\mathrm{T}}\boldsymbol{c}_m^{\mathrm{L}}=0$. The following theorem establishes that the resulting coupling terms satisfy the required integral constraints.

Theorem 2. *The coupling terms constructed on a conforming face between a conforming element and an element that has at least one other face that is nonconforming satisfy the condition* (25) *if either 1) analytic or 2) standard FD approaches (e.g., Vinokur and Yee [59] or Thomas and Lombard), are used to seed the metric terms.*

Proof. This proof follows by inserting the approximation of the metric terms using 1) analytic, or 2) either Vinokur or Yee [59] or Thomas and Lombard [58], and the polynomial exactness of the differentiation matrices and the norm matrices, see Appendix F. □

Remark 6. *The 1) GCL optimized volume metrics on all faces of a nonconforming element, and the 2) surface metrics specified in the coupling matrices, are both surface normal approximations but in general differ by a design order term. They are weakly coupled through the GCL constraint given in equation* (22).

The following theorem summarizes the properties of the proposed coupling approach.

Theorem 3. *The proposed coupling procedure results in a scheme that has the following properties:*

- *The scheme is discretely entropy conservative (i.e., neutral discrete L^2 stability under the assumption of positive temperature and density)*
- *The scheme is discretely elementwise conservative and preserves freestream*
- *The scheme is of order $p_{\mathrm{L}} + d - 1$ where p_{L} is the lowest degree used (the $+d$ comes from the fact that the PDE and therefore the discretization have been multiplied by the metric Jacobian which scales as h^d)*

Proof. The proof of entropy conservation is given in Section (5.2) while appropriate interface dissipation leading to entropy stability is discussed in Section 6. Element-wise conservation is proven in Appendix E. The order of the scheme results from the fact that one of the interpolation operators is suboptimal ($p_{\mathrm{L}} - 1$). □

4 Nonlinearly stable schemes: Burgers' equation

The nonconforming interface coupling mechanics presented in the previous section will be generalized for the compressible Euler equations in Section 5. Proving stability of nonlinear conservation laws, in general requires elaborate techniques well beyond simply discretizing the derivatives of the fluxes directly with SBP operators. Next, the Hadamard derivative formalisem is introduced in the context of one-dimensional inviscid Burgers' equation, which has the desirable property of being amenable to either 1) a canonical derivative splitting, or 2) the Hadamard derivative approach. The equivalence between the two approaches for Burgers' equation, is established elsewhere [8, 22].

Inviscid Burgers' equation, and its well-known canonical splitting, are of the form

$$\frac{\partial \mathcal{U}}{\partial t} + \frac{\partial}{\partial x_1}\left(\frac{\mathcal{U}^2}{2}\right) = 0 \quad ; \quad \frac{\partial \mathcal{U}}{\partial t} + \frac{1}{3}\frac{\partial}{\partial x_1}\left(\mathcal{U}^2\right) + \frac{\mathcal{U}}{3}\frac{\partial \mathcal{U}}{\partial x_1} = 0. \tag{26}$$

Performing an energy analysis on the split form of (26) gives (see, for instance, Ref, [8] for details)

$$\frac{1}{2}\frac{\mathrm{d}\|\mathcal{U}\|^2}{\mathrm{d}t} + \oint_\Gamma \frac{\mathcal{U}^3}{3} n_{x_1} \mathrm{d}\Gamma = 0, \quad \|\mathcal{U}\|^2 \equiv \int_\Omega \mathcal{U}^2 \mathrm{d}\Omega. \tag{27}$$

In order to prove stability, the semidiscrete scheme needs to mimic (27) in the sense that when contracted with $\boldsymbol{u}^{\mathrm{T}}\mathsf{P}$ (the discrete analogue of multiplying by the solution and integrating in space) the result is given by the sum of spatial terms that telescope to the boundaries.

The discretization of (26) with SBP operators (ignoring the SATs) is given as

$$\frac{\mathrm{d}\boldsymbol{u}}{\mathrm{d}t} + \frac{1}{3}\mathsf{D}_{x_1}\,\mathrm{diag}\left(\boldsymbol{u}\right)\boldsymbol{u} + \frac{1}{3}\,\mathrm{diag}\left(\boldsymbol{u}\right)\mathsf{D}_{x_1}\boldsymbol{u} = 0. \tag{28}$$

Multiplying (28) by $\boldsymbol{u}^{\mathrm{T}}\mathsf{P}$ results in

$$\frac{1}{2}\frac{\mathrm{d}\boldsymbol{u}^{\mathrm{T}}\mathsf{P}\boldsymbol{u}}{\mathrm{d}t} + \frac{1}{3}\left(\boldsymbol{u}^3(N) - \boldsymbol{u}^3(1)\right) = 0, \tag{29}$$

for which each term mimics (27) and has the telescoping property, i.e., the remaining terms are at the boundaries.

Now the discretization (28) is recast using the Hadamard derivative formalism. The Hadamard derivative operator and the equivalent split form operators are given as follows

$$2\mathsf{D}_{x_1} \circ \mathsf{F}_{x_1}\left(\boldsymbol{u},\boldsymbol{u}\right)\mathbf{1}_1 \quad \leftrightarrow \quad \frac{1}{3}\mathsf{D}_{x_1}\,\mathrm{diag}\left(\boldsymbol{u}\right)\boldsymbol{u} + \frac{1}{3}\,\mathrm{diag}\left(\boldsymbol{u}\right)\mathsf{D}_{x_1}\boldsymbol{u}\,. \tag{30}$$

The Hadamard operator is capable of compactly representing various split forms, and more importantly, extends to nonlinear equations for which a canonical split form is inappropriate.

The Hadamard derivative operator is constructed from two components: 1) an SBP derivative operator, and 2) a two point flux function specific to the physics being modeled. Two point fluxes are constructed between the center point and all other points of dependency within the SBP stencil. The SBP telescoping property [22] that results from precise local cancellation of spatial terms, can then be extended directly to nonlinear operators. A simple example is now presented.

Consider the two point Burgers' flux function defined by [8, 57]

$$\boldsymbol{f}^{sc}_{x_m}\left(\boldsymbol{u}^{(i)},\boldsymbol{u}^{(j)}\right) \equiv \frac{\left\{\left(\boldsymbol{u}^{(i)}\right)^2 + \boldsymbol{u}^{(i)}\boldsymbol{u}^{(j)} + \left(\boldsymbol{u}^{(j)}\right)^2\right\}}{6},$$

where $\boldsymbol{u}^{(i)}$ and $\boldsymbol{u}^{(j)}$ are the i^{th} and j^{th} components of $\boldsymbol{u}$, and for the purpose of demonstration, a simple SBP operator constructed on the LGL nodes $(-1, 0, 1)$

$$\mathsf{D}_{x_1} = \begin{bmatrix} -\frac{3}{2} & 2 & -\frac{1}{2} \\ -\frac{1}{2} & 0 & \frac{1}{2} \\ \frac{1}{2} & -2 & \frac{3}{2} \end{bmatrix}.$$

The two argument Hadamard matrix flux, $\mathsf{F}_{x_m}\left(\boldsymbol{u},\boldsymbol{u}\right)$ is given as

$$\mathsf{F}_{x_m}\left(\boldsymbol{u},\boldsymbol{u}\right) = \begin{bmatrix} \frac{\left(\boldsymbol{u}^{(1)}\right)^2}{2} & \frac{\left(\boldsymbol{u}^{(1)}\right)^2+\boldsymbol{u}^{(1)}\boldsymbol{u}^{(2)}+\left(\boldsymbol{u}^{(2)}\right)^2}{6} & \frac{\left(\boldsymbol{u}^{(1)}\right)^2+\boldsymbol{u}^{(1)}\boldsymbol{u}^{(3)}+\left(\boldsymbol{u}^{(3)}\right)^2}{6} \\ \frac{\left(\boldsymbol{u}^{(2)}\right)^2+\boldsymbol{u}^{(2)}\boldsymbol{u}^{(1)}+\left(\boldsymbol{u}^{(1)}\right)^2}{6} & \frac{\left(\boldsymbol{u}^{(2)}\right)^2}{2} & \frac{\left(\boldsymbol{u}^{(2)}\right)^2+\boldsymbol{u}^{(2)}\boldsymbol{u}^{(3)}+\left(\boldsymbol{u}^{(3)}\right)^2}{6} \\ \frac{\left(\boldsymbol{u}^{(3)}\right)^2+\boldsymbol{u}^{(3)}\boldsymbol{u}^{(1)}+\left(\boldsymbol{u}^{(1)}\right)^2}{6} & \frac{\left(\boldsymbol{u}^{(3)}\right)^2+\boldsymbol{u}^{(3)}\boldsymbol{u}^{(2)}+\left(\boldsymbol{u}^{(2)}\right)^2}{6} & \frac{\left(\boldsymbol{u}^{(3)}\right)^2}{2} \end{bmatrix}.$$

Thus,

$$\mathsf{D}_{x_1} \circ \mathsf{F}_{x_m}\left(\boldsymbol{u},\boldsymbol{u}\right)\mathbf{1} = \begin{bmatrix} -\frac{3}{2}\frac{\left(\boldsymbol{u}^{(1)}\right)^2}{2} & 2\frac{\left(\boldsymbol{u}^{(1)}\right)^2+\boldsymbol{u}^{(1)}\boldsymbol{u}^{(2)}+\left(\boldsymbol{u}^{(2)}\right)^2}{6} & -\frac{1}{2}\frac{\left(\boldsymbol{u}^{(1)}\right)^2+\boldsymbol{u}^{(1)}\boldsymbol{u}^{(3)}+\left(\boldsymbol{u}^{(3)}\right)^2}{6} \\ -\frac{1}{2}\frac{\left(\boldsymbol{u}^{(2)}\right)^2+\boldsymbol{u}^{(2)}\boldsymbol{u}^{(1)}+\left(\boldsymbol{u}^{(1)}\right)^2}{6} & 0 & \frac{1}{2}\frac{\left(\boldsymbol{u}^{(2)}\right)^2+\boldsymbol{u}^{(2)}\boldsymbol{u}^{(3)}+\left(\boldsymbol{u}^{(3)}\right)^2}{6} \\ \frac{1}{2}\frac{\left(\boldsymbol{u}^{(3)}\right)^2+\boldsymbol{u}^{(3)}\boldsymbol{u}^{(1)}+\left(\boldsymbol{u}^{(1)}\right)^2}{6} & -2\frac{\left(\boldsymbol{u}^{(3)}\right)^2+\boldsymbol{u}^{(3)}\boldsymbol{u}^{(2)}+\left(\boldsymbol{u}^{(2)}\right)^2}{6} & \frac{3}{2}\frac{\left(\boldsymbol{u}^{(3)}\right)^2}{2} \end{bmatrix}\begin{bmatrix} 1 \\ 1 \\ 1 \end{bmatrix}.$$

The equivalence between the two approaches is evident by inspection.

Now the general notation applicable to the compressible Euler equations is described. Assume that what is required is the discretization of the derivative of a flux vector $\boldsymbol{\mathcal{F}}_{x_m}$ in the x_m Cartesian direction. The essential ingredients used above are an SBP matrix difference operator, D_{x_m}, and a two argument matrix flux function, $\mathsf{F}_{x_m}(\boldsymbol{u}_\kappa, \boldsymbol{u}_r)$, which is composed of diagonal matrices and is defined blockwise as

$$\left(\mathsf{F}_{x_m}(\boldsymbol{u}_\kappa, \boldsymbol{u}_r)\right)(e(i-1)+1:ei, e(j-1)+1:ej) \equiv \operatorname{diag}\left(\boldsymbol{f}^{sc}_{x_m}\left(\boldsymbol{u}^{(i)}_\kappa, \boldsymbol{u}^{(j)}_r\right)\right),$$

$$\boldsymbol{u}^{(i)}_\kappa \equiv \boldsymbol{u}_\kappa\left(e(i-1)+1:ei\right),\ \boldsymbol{u}^{(j)}_r \equiv \boldsymbol{u}_r\left(e(j-1)+1:ej\right),$$

$$i = 1\ldots, N^3_\kappa,\ j = 1, \ldots, N^3_r,$$

where e is the number of equations in the system of PDEs. For example, for the compressible Euler equations, $e = 5$ and the two argument matrix flux function is of size $\left(e\,N^3_\kappa\right) \times \left(e\,N^3_r\right)$, where eN^3_κ and eN^3_r are the total number of entries in the vectors $\boldsymbol{u}_\kappa$ and $\boldsymbol{u}_r$ corresponding the solution variables in elements κ and r, respectively. Thus, $\boldsymbol{u}^{(i)}_\kappa$ is the vector of the e solution variables evaluated at the i^{th} node. The vectors $\boldsymbol{f}^{sc}_{x_m}\left(\boldsymbol{u}^{(i)}_\kappa, \boldsymbol{u}^{(j)}_r\right)$ are constructed from two-point flux functions that are symmetric in their arguments, $\left(\boldsymbol{u}^{(i)}_\kappa, \boldsymbol{u}^{(j)}_r\right)$, and consistent. Thus,

$$\boldsymbol{f}^{sc}_{x_m}\left(\boldsymbol{u}^{(i)}_\kappa, \boldsymbol{u}^{(j)}_r\right) = \boldsymbol{f}^{sc}_{x_m}\left(\boldsymbol{u}^{(j)}_r, \boldsymbol{u}^{(i)}_\kappa\right), \quad \boldsymbol{f}^{sc}_{x_m}\left(\boldsymbol{u}^{(i)}_\kappa, \boldsymbol{u}^{(i)}_\kappa\right) = \boldsymbol{\mathcal{F}}_{x_m}\left(\boldsymbol{u}^{(i)}_\kappa\right),$$

where $\boldsymbol{\mathcal{F}}_{x_m}$ is the flux vector in the x^{th}_m Cartesian direction. Using these ingredients, an approximation to the derivative $\frac{\partial \boldsymbol{\mathcal{F}}_{x_m}}{\partial x_m}$ is constructed as

$$2\mathsf{D}_{x_m} \circ \mathsf{F}_{x_m}(\boldsymbol{q}_\kappa, \boldsymbol{q}_\kappa)\,\mathbf{1}_\kappa \approx \frac{\partial \boldsymbol{\mathcal{F}}_{x_m}}{\partial x_m}(\boldsymbol{\xi}^\kappa),$$

where $\boldsymbol{\xi}^\kappa$ is the vector of vectors containing the nodal locations. The resulting approximation has the same order properties as differentiating directly with the SBP operator D_{x_m} (see Theorem 1 in Crean *et al.* [13]).

5 Application to the compressible Euler equations

In this section, the nonconforming algorithm presented in Section 3 is combined with the mechanics presented in Section 4 to construct an entropy conservative discretization of the compressible Euler equations on p-nonconforming meshes. First, in Section 5.1 the continuous equations and the continuous entropy analysis are reviewed, then in Section 5.2 the semidiscrete algorithm for the Euler equations is presented and analyzed.

5.1 Review of the continuous entropy analysis

The strong form of the compressible Euler equations in Cartesian coordinates are given as

$$\begin{aligned} &\frac{\partial \boldsymbol{\mathcal{Q}}}{\partial t} + \sum_{m=1}^{3} \frac{\partial \boldsymbol{\mathcal{F}}_{x_m}}{\partial x_m} = 0, && \forall\,(x_1,x_2,x_3) \in \Omega, \quad t \geq 0, \\ &\boldsymbol{\mathcal{Q}}\,(x_1,x_2,x_3,t) = \boldsymbol{\mathcal{G}}^{(B)}\,(x_1,x_2,x_3,t)\,, && \forall\,(x_1,x_2,x_3) \in \Gamma, \quad t \geq 0, \\ &\boldsymbol{\mathcal{Q}}\,(x_1,x_2,x_3,0) = \boldsymbol{\mathcal{G}}^{(0)}\,(x_1,x_2,x_3,0)\,, && \forall\,(x_1,x_2,x_3) \in \Omega. \end{aligned} \tag{31}$$

The vectors $\boldsymbol{\mathcal{Q}}$ and $\boldsymbol{\mathcal{F}}_x$, respectively, denote the conserved variables and the inviscid fluxes. The boundary data, $\boldsymbol{\mathcal{G}}^{(B)}$, and the initial condition, $\boldsymbol{\mathcal{G}}^{(0)}$, are assumed to be in $L^2(\Omega)$, with the further assumption that $\boldsymbol{\mathcal{G}}^{(B)}$ will be set to coincide with linear well-posed boundary conditions and such that entropy conservation or stability is achieved.

It is well-known that the compressible Euler equations (31) possess a convex extension that, when integrated over the physical domain Ω, only depends on the boundary data on Γ. Such an extension yields the entropy function

$$\mathcal{S} = -\rho s, \tag{32}$$

where ρ and s are the density and the thermodynamic entropy, respectively. The entropy function, $\mathcal{S}$, is convex if the thermodynamic variables are positive and is a useful tool for proving stability in the L^2 norm [14]. Following the analysis described in [5, 9, 44], the system (31) is multiplied by the (local) entropy variables $\boldsymbol{\mathcal{W}}^{\mathrm{T}} = \partial\mathcal{S}/\partial\boldsymbol{\mathcal{Q}}$ and by using the fact that

$$\frac{\partial \mathcal{S}}{\partial \boldsymbol{\mathcal{Q}}}\frac{\partial \boldsymbol{\mathcal{F}}_{x_m}}{\partial x_m} = \frac{\partial \mathcal{S}}{\partial \boldsymbol{\mathcal{Q}}}\frac{\partial \boldsymbol{\mathcal{F}}_{x_m}}{\partial \boldsymbol{\mathcal{Q}}}\frac{\partial \boldsymbol{\mathcal{Q}}}{\partial x_m} = \frac{\partial \mathcal{F}_{x_m}}{\partial \boldsymbol{\mathcal{Q}}}\frac{\partial \boldsymbol{\mathcal{Q}}}{\partial x_m} = \frac{\partial \mathcal{F}_{x_m}}{\partial x_m}, \qquad m = 1,2,3, \tag{33}$$

gives that

$$\frac{\partial \mathcal{S}}{\partial t} + \sum_{m=1}^{3} \frac{\partial \mathcal{F}_{x_m}}{\partial x_m} = 0, \tag{34}$$

where the scalars $\mathcal{F}_{x_m}(\boldsymbol{\mathcal{Q}})$ are the entropy fluxes in the x_m-direction. Then, integrating over the domain, Ω, and using integration by parts yields

$$\int_{\Omega} \frac{\partial \mathcal{S}}{\partial t} \mathrm{d}\Omega \leq \oint_{\Gamma} \left(\sum_{m=1}^{3} \mathcal{F}_{x_m} n_{x_m} \right) \mathrm{d}\Gamma, \tag{35}$$

where n_{x_m} is the m^{th} component of the outward facing unit normal. Note that the equality in (35) holds for smooth flows; conversely, the inequality is valid for non smooth flow since the mathematical entropy decreases across shocks.

To obtain a bound on the solution, the inequality (35) is integrated in time and assuming boundary conditions and an initial condition that are nonlinearly well posed, and positivity of density and temperature, the result can be turned into a bound on the solution in terms of the data of the problem (see Refs. [14, 52]). Example of fully-discrete explicit entropy conservative/stable algorithms are presented, for instance, in Refs. [24, 45].

5.2 A p-nonconforming algorithm

As for the convection equation, a skew-symmetrically split form of the compressible Euler equations is used to construct an entropy conservative/stable algorithm:

$$\begin{aligned}&\mathcal{J}_\kappa \frac{\partial \boldsymbol{\mathcal{Q}}_{\boldsymbol{\kappa}}}{\partial t} + \sum_{l,m=1}^{3} \frac{1}{2}\left\{ \frac{\partial}{\partial \xi_l}\left(\mathcal{J}_\kappa \frac{\partial \xi_l}{\partial x_m} \boldsymbol{\mathcal{F}}_{x_m} \right) + \mathcal{J}_\kappa \frac{\partial \xi_l}{\partial x_m} \frac{\partial \boldsymbol{\mathcal{F}}_{x_m}}{\partial \xi_1} \right\} \\ &- \frac{1}{2} \sum_{l,m=1}^{3} \boldsymbol{\mathcal{F}}_{x_m} \frac{\partial}{\partial \xi_l}\left(\mathcal{J}_\kappa \frac{\partial \xi_l}{\partial x_m} \right) = 0,\end{aligned} \tag{36}$$

where the last term on the left-hand side is zero as a result of the GCL conditions (6).

The discretization is developed using the same macroelement SBP operator as in Section 3. Thus, the discretization of (36) over the macroelement is given as

$$\begin{aligned}&\mathsf{J}\frac{\mathrm{d}\widetilde{\boldsymbol{q}}}{\partial t} + \sum_{l,m=1}^{3} \widetilde{\mathsf{D}}_{l,m} \circ \mathsf{F}_{x_m}\left(\widetilde{\boldsymbol{q}}, \widetilde{\boldsymbol{q}}\right) \tilde{\mathbf{1}} - \frac{1}{2} \sum_{l,m=1}^{3} \operatorname{diag}\left(\boldsymbol{f}_{x_m}\right) \widetilde{\mathsf{D}}_{\xi_l}\left[\mathcal{J} \frac{\partial \xi_l}{\partial x_m} \right] \tilde{\mathbf{1}} = \mathbf{0}, \\ &\widetilde{\boldsymbol{q}} \equiv \left[\boldsymbol{q}_{\mathrm{L}}^{\mathrm{T}}, \boldsymbol{q}_{\mathrm{H}}^{\mathrm{T}}\right]^{\mathrm{T}},\end{aligned} \tag{37}$$

where $\boldsymbol{f}_{x_m}$ is a vector of vectors constructed by evaluating $\boldsymbol{\mathcal{F}}_{x_m}$ at the mesh nodes. That the factor of $\frac{1}{2}$ on the skew-symmetric volume terms disappears as a result of using the nonlinear operator, e.g., $2\mathsf{D}_{\xi_l} \circ \mathsf{F}_{x_m}\left(\boldsymbol{q}_\kappa, \boldsymbol{q}_\kappa\right) \mathbf{1}_\kappa \approx \frac{\partial \boldsymbol{\mathcal{F}}_{x_m}}{\partial \xi_l}(\boldsymbol{\xi}^\kappa)$. Moreover, the flux function matrix, $\mathsf{F}_{x_m}\left(\widetilde{\boldsymbol{q}}, \widetilde{\boldsymbol{q}}\right)$, is constructed using a two point flux function, $\boldsymbol{f}_{x_m}^{sc}\left(\tilde{\boldsymbol{q}}^{(i)}, \tilde{\boldsymbol{q}}^{(i)}\right)$, that satisfies the Tadmor shuffle condition [57]

$$\left(\tilde{\boldsymbol{w}}^{(i)} - \tilde{\boldsymbol{w}}^{(j)}\right)^{\mathrm{T}} \boldsymbol{f}_{x_m}^{sc}\left(\tilde{\boldsymbol{q}}^{(i)}, \tilde{\boldsymbol{q}}^{(i)}\right) = \tilde{\boldsymbol{\psi}}_{x_m}^{(i)} - \tilde{\boldsymbol{\psi}}_{x_m}^{(j)}. \tag{38}$$

The $\widetilde{\mathsf{D}}_{l,m}$ operators are constructed as in Section (3) by tensoring the contributing matrices with an identity matrix I_5 to accommodate the system of 5 equations. For example,

$$\mathsf{D}_{\xi_1}^{\mathrm{L}} \equiv \overline{\mathsf{D}}_{\xi_1} \otimes \mathsf{I}_5, \quad \overline{\mathsf{D}}_{\xi_1}^{\mathrm{L}} \equiv \mathsf{D}_{\mathrm{L}}^{(1D)} \otimes \mathsf{I}_{N_{\mathrm{L}}} \otimes \mathsf{I}_{N_{\mathrm{L}}}.$$

Nonlinear stability requires that the last set of terms on the left-hand side of (37) be zero. This requirement leads to discrete GCL conditions which are identical to those obtained for the convection equation (with D_{ξ_l} replaced with $\overline{\mathsf{D}}_{\xi_l}$), i.e., conditions (20) and (21).

The procedure to demonstrate that the proposed scheme is entropy conservative (i.e., it telescopes to the element boundaries) follows the continuous analysis in a one-to-one fashion (see Section 5.1). To simplify the derivation, the following matrices are introduced:

$$\hat{\mathsf{D}}_m \equiv \sum_{l=1}^{3} \widetilde{\mathsf{D}}_{l,m}, \quad \hat{\mathsf{Q}}_m \equiv \widetilde{\mathsf{P}}\hat{\mathsf{D}}_m, \quad \hat{\mathsf{E}}_m \equiv \hat{\mathsf{Q}}_m + \hat{\mathsf{Q}}_m^{\mathrm{T}}.$$

Thus, assuming that the discrete GCL conditions are satisfied, (37) becomes

$$\mathsf{J}\frac{\mathrm{d}\widetilde{\boldsymbol{q}}}{\partial t} + \sum_{m=1}^{3} \hat{\mathsf{D}}_m \circ \mathsf{F}_{x_m}\left(\widetilde{\boldsymbol{q}}, \widetilde{\boldsymbol{q}}\right) \tilde{\mathbf{1}} = \mathbf{0}. \tag{39}$$

The first step is to contract (39), pointwise, with the entropy variables (at the continuous level this was the step $\mathcal{W}\frac{\partial \boldsymbol{\mathcal{F}}_{x_m}}{\partial x_m} = \frac{\partial \mathcal{F}_{x_m}}{\partial x_m}$). This is accomplished by multiplying (39) by $\mathsf{I}_{\tilde{N}} \otimes \mathbf{1}_5^{\mathrm{T}} \operatorname{diag}(\boldsymbol{w}_\kappa)$, which results in

$$\mathsf{J}\,\mathsf{I}_{\tilde{N}} \otimes \mathbf{1}_5^{\mathrm{T}} \operatorname{diag}(\boldsymbol{w}_\kappa) \frac{\mathrm{d}\widetilde{\boldsymbol{q}}}{\partial t} + \mathsf{I}_{\tilde{N}} \otimes \mathbf{1}_5^{\mathrm{T}} \operatorname{diag}(\boldsymbol{w}_\kappa) \sum_{m=1}^{3} \hat{\mathsf{D}}_m \circ \mathsf{F}_{x_m}(\widetilde{\boldsymbol{q}}, \widetilde{\boldsymbol{q}})\, \tilde{\mathbf{1}} = \mathbf{0}, \tag{40}$$

where $\tilde{N}$ is the total number of nodes in the macroelement. Adding and subtracting terms to (40) gives

$$\begin{aligned}\mathsf{J}\frac{\mathrm{d}\widetilde{\boldsymbol{s}}}{\partial t} + \mathsf{I}_{\tilde{N}} \otimes \mathbf{1}_5^{\mathrm{T}} \sum_{m=1}^{3} \Bigg\{ &\frac{1}{2} \operatorname{diag}(\boldsymbol{w}_\kappa) \hat{\mathsf{D}}_m \circ \mathsf{F}_{x_m}(\widetilde{\boldsymbol{q}}, \widetilde{\boldsymbol{q}})\, \tilde{\mathbf{1}} + \frac{1}{2} \hat{\mathsf{D}}_m \operatorname{diag}(\boldsymbol{w}_\kappa) \circ \mathsf{F}_{x_m}(\widetilde{\boldsymbol{q}}, \widetilde{\boldsymbol{q}})\, \tilde{\mathbf{1}} \\ &+ \frac{1}{2} \operatorname{diag}(\boldsymbol{w}_\kappa) \hat{\mathsf{D}}_m \circ \mathsf{F}_{x_m}(\widetilde{\boldsymbol{q}}, \widetilde{\boldsymbol{q}})\, \tilde{\mathbf{1}} - \frac{1}{2} \hat{\mathsf{D}}_m \operatorname{diag}(\boldsymbol{w}_\kappa) \circ \mathsf{F}_{x_m}(\widetilde{\boldsymbol{q}}, \widetilde{\boldsymbol{q}})\, \tilde{\mathbf{1}} \Bigg\} = \mathbf{0}.\end{aligned} \tag{41}$$

Consider the i^{th} term of the spatial terms of (41) (denoted Vol(i) where $i = 1, \ldots, \tilde{N}$),

$$\mathrm{Vol(i)} \equiv \sum_{\mathrm{j}=1}^{\tilde{\mathrm{N}}} \overline{\hat{\mathsf{D}}}_{\mathrm{m}}(\mathrm{i},\mathrm{j}) \left\{ \frac{\left(\widetilde{\mathrm{w}}^{(\mathrm{i})} + \widetilde{\mathrm{w}}^{(\mathrm{j})}\right)}{2} \mathrm{f}^{\mathrm{sc}}_{\mathrm{x_m}}\left(\widetilde{\mathrm{q}}^{(\mathrm{i})}, \widetilde{\mathrm{q}}^{(\mathrm{j})}\right) + \frac{\left(\widetilde{\mathrm{w}}^{(\mathrm{i})} - \widetilde{\mathrm{w}}^{(\mathrm{j})}\right)}{2} \mathrm{f}^{\mathrm{sc}}_{\mathrm{x_m}}\left(\widetilde{\mathrm{q}}^{(\mathrm{i})}, \widetilde{\mathrm{q}}^{(\mathrm{j})}\right) \right\}, \tag{42}$$

where $\hat{\mathsf{D}}_m = \overline{\hat{\mathsf{D}}}_m \otimes \mathsf{I}_5$. Using the Tadmor shuffle condition (38) on the second set of terms results in

$$\mathrm{Vol(i)} = \sum_{\mathrm{j}=1}^{\tilde{\mathrm{N}}} \overline{\hat{\mathsf{D}}}_{\mathrm{m}}(\mathrm{i},\mathrm{j}) \left\{ \frac{\left(\widetilde{\mathrm{w}}^{(\mathrm{i})} + \widetilde{\mathrm{w}}^{(\mathrm{j})}\right)}{2} \mathrm{f}^{\mathrm{sc}}_{\mathrm{x_m}}\left(\widetilde{\mathrm{q}}^{(\mathrm{i})}, \widetilde{\mathrm{q}}^{(\mathrm{j})}\right) + \frac{\left(\tilde{\boldsymbol{\psi}}^{(\mathrm{i})}_{\mathrm{x_m}} - \tilde{\boldsymbol{\psi}}^{(\mathrm{j})}_{\mathrm{x_m}}\right)}{2} \right\}. \tag{43}$$

Adding and subtracting terms to (43) gives

$$\begin{aligned}\mathrm{Vol(i)} = &\sum_{j=1}^{\tilde{N}} \overline{\hat{\mathsf{D}}}_m(i,j) \left\{ \frac{\left(\widetilde{\boldsymbol{w}}^{(i)} + \widetilde{\boldsymbol{w}}^{(j)}\right)}{2} \boldsymbol{f}^{sc}_{x_m}\left(\widetilde{\boldsymbol{q}}^{(i)}, \widetilde{\boldsymbol{q}}^{(j)}\right) - \frac{\left(\tilde{\boldsymbol{\psi}}^{(i)}_{x_m} + \tilde{\boldsymbol{\psi}}^{(j)}_{x_m}\right)}{2} \right\} \\ &+ \sum_{j=1}^{\tilde{N}} \overline{\hat{\mathsf{D}}}_m(i,j) \tilde{\boldsymbol{\psi}}^{(i)}_{x_m}\end{aligned} \tag{44}$$

The last set of terms can be expanded into matrix form as (i.e., the vector constructed from Vol(i) for $i = 1, .., \tilde{N}$)

$$\left(\tilde{\boldsymbol{\psi}}_{x_m}\right)^{\mathrm{T}} \sum_{l=1}^{3} \left\{ \overline{\mathsf{D}}_{\xi_l} \overline{\left[\mathcal{J} \frac{\partial \xi_l}{\partial x_m}\right]} + \overline{\left[\mathcal{J} \frac{\partial \xi_l}{\partial x_m}\right]} \overline{\mathsf{D}}_{\xi_l} \right\} \overline{\mathbf{1}} = \mathbf{0}, \tag{45}$$

where the equality follows from the assumption that the discrete GCL conditions and consistency of the first derivative operator, i.e., $\overline{\mathsf{D}}_{\xi_l} \overline{\mathbf{1}} = \mathbf{0}$. Eq. (44) can now be recast in terms of a new flux function matrix, $\tilde{\mathsf{F}}_{x_m}(\widetilde{\boldsymbol{q}}, \widetilde{\boldsymbol{q}})$ constructed from the two-point flux function

$$\tilde{\boldsymbol{f}}^{sc}_{x_m}\left(\widetilde{\boldsymbol{q}}^{(i)}, \widetilde{\boldsymbol{q}}^{(i)}\right) \equiv \frac{\left(\widetilde{\boldsymbol{w}}^{(i)} + \widetilde{\boldsymbol{w}}^{(j)}\right)}{2} \boldsymbol{f}^{sc}_{x_m}\left(\widetilde{\boldsymbol{q}}^{(i)}, \widetilde{\boldsymbol{q}}^{(j)}\right) - \frac{\left(\tilde{\boldsymbol{\psi}}^{(i)}_{x_m} + \tilde{\boldsymbol{\psi}}^{(j)}_{x_m}\right)}{2}.$$

Note that $\tilde{\boldsymbol{f}}^{sc}_{x_n}$ is symmetric and consistent with $\mathcal{F}_{x_m}$; thus, (40) reduces to

$$\mathsf{J}\frac{\mathrm{d}\widetilde{\boldsymbol{s}}}{\partial t} + \sum_{m=1}^{3} \overline{\hat{\mathsf{D}}}_m \circ \tilde{\mathsf{F}}_{x_m}\left(\widetilde{\boldsymbol{q}}, \widetilde{\boldsymbol{q}}\right) \overline{\mathbf{1}} = \mathbf{0}, \tag{46}$$

where (see Appendix A for details on the approximation properties of the nonlinear operators)

$$\overline{\hat{\mathsf{D}}}_m \circ \tilde{\mathsf{F}}_{x_m}\left(\widetilde{\boldsymbol{q}}, \widetilde{\boldsymbol{q}}\right) \overline{\mathbf{1}} \approx \frac{1}{2}\sum_{l=1}^{3}\left\{\frac{\partial}{\partial \xi_l}\left(\mathcal{J}_\kappa \frac{\partial \xi_l}{\partial x_m}\mathcal{F}_{x_m}\right) + \mathcal{J}_\kappa \frac{\partial \xi_l}{\partial x_m}\frac{\partial \mathcal{F}_{x_m}}{\partial \xi_l}\right\}\left(\tilde{\boldsymbol{\xi}}\right).$$

Next, (46) is discretely integrated over the domain by left multiplying by $\overline{\mathbf{1}}^{\mathrm{T}}\overline{\mathsf{P}}$ and rearranging, results in

$$\begin{aligned}
\overline{\mathbf{1}}^{\mathrm{T}}\overline{\mathsf{P}}\mathsf{J}\frac{\mathrm{d}\widetilde{\boldsymbol{s}}}{\partial t} &= -\sum_{m=1}^{3} \overline{\mathbf{1}}^{\mathrm{T}}\overline{\hat{\mathsf{Q}}}_m \circ \tilde{\mathsf{F}}_{x_m}\left(\widetilde{\boldsymbol{q}}, \widetilde{\boldsymbol{q}}\right) \overline{\mathbf{1}}, \\
&= -\frac{1}{2}\sum_{m=1}^{3}\left\{\overline{\mathbf{1}}^{\mathrm{T}}\overline{\hat{\mathsf{Q}}}_m \circ \tilde{\mathsf{F}}_{x_m}\left(\widetilde{\boldsymbol{q}}, \widetilde{\boldsymbol{q}}\right) \overline{\mathbf{1}} + \overline{\mathbf{1}}^{\mathrm{T}}\overline{\hat{\mathsf{Q}}}_m^{\mathrm{T}} \circ \tilde{\mathsf{F}}_{x_m}\left(\widetilde{\boldsymbol{q}}, \widetilde{\boldsymbol{q}}\right) \overline{\mathbf{1}}\right\} \\
&= -\frac{1}{2}\sum_{m=1}^{3}\left\{\overline{\mathbf{1}}^{\mathrm{T}}\overline{\hat{\mathsf{Q}}}_m \circ \tilde{\mathsf{F}}_{x_m}\left(\widetilde{\boldsymbol{q}}, \widetilde{\boldsymbol{q}}\right) \overline{\mathbf{1}} - \overline{\mathbf{1}}^{\mathrm{T}}\overline{\hat{\mathsf{Q}}}_m \circ \tilde{\mathsf{F}}_{x_m}\left(\widetilde{\boldsymbol{q}}, \widetilde{\boldsymbol{q}}\right) \overline{\mathbf{1}} + \overline{\mathbf{1}}^{\mathrm{T}}\overline{\hat{\mathsf{E}}}_m \circ \tilde{\mathsf{F}}_{x_m}\left(\widetilde{\boldsymbol{q}}, \widetilde{\boldsymbol{q}}\right) \overline{\mathbf{1}}\right\} \\
&= -\frac{1}{2}\sum_{m=1}^{3} \overline{\mathbf{1}}^{\mathrm{T}}\overline{\hat{\mathsf{E}}}_m \circ \tilde{\mathsf{F}}_{x_m}\left(\widetilde{\boldsymbol{q}}, \widetilde{\boldsymbol{q}}\right) \overline{\mathbf{1}} \\
&= -\frac{1}{2}\sum_{m=1}^{3}\sum_{i,j=1}^{N} \overline{\hat{\mathsf{E}}}_m(i,j)\left\{\frac{\left(\widetilde{\boldsymbol{w}}^{(i)} + \widetilde{\boldsymbol{w}}^{(j)}\right)}{2}\boldsymbol{f}^{sc}_{x_m}\left(\widetilde{\boldsymbol{q}}^{(i)}, \widetilde{\boldsymbol{q}}^{(j)}\right) - \frac{\left(\tilde{\boldsymbol{\psi}}^{(i)}_{x_m} + \tilde{\boldsymbol{\psi}}^{(j)}_{x_m}\right)}{2}\right\} \\
&= -\frac{1}{2}\sum_{m=1}^{3} \widetilde{\boldsymbol{w}}^{\mathrm{T}}\hat{\mathsf{E}}_m \circ \mathsf{F}_{x_m}\left(\widetilde{\boldsymbol{q}}, \widetilde{\boldsymbol{q}}\right) \tilde{\mathbf{1}} + \frac{1}{2}\overline{\mathbf{1}}^{\mathrm{T}}\overline{\hat{\mathsf{E}}}_m\widetilde{\boldsymbol{\psi}_m}.
\end{aligned} \tag{47}$$

Thus,

$$\overline{\mathbf{1}}^{\mathrm{T}}\overline{\mathsf{P}}\mathsf{J}\frac{\mathrm{d}\widetilde{\boldsymbol{s}}}{\partial t} = -\frac{1}{2}\sum_{m=1}^{3} \widetilde{\boldsymbol{w}}^{\mathrm{T}}\hat{\mathsf{E}}_m \circ \mathsf{F}_{x_m}\left(\widetilde{\boldsymbol{q}}, \widetilde{\boldsymbol{q}}\right) \tilde{\mathbf{1}} + \frac{1}{2}\overline{\mathbf{1}}^{\mathrm{T}}\overline{\hat{\mathsf{E}}}_m\widetilde{\boldsymbol{\psi}_m}. \tag{48}$$

The right-hand side of (48) contains terms constructed from the E matrices. As a result, these terms can be decomposed into the contributions of the separate surfaces of the element (nodewise). For periodic problems, these terms would cancel out with the contributions from face SATs coupling terms leading to entropy conservation. For nonperiodic problems appropriate SATs need to be constructed so that an entropy inequality or equality is attained (this is an active area of research; see, for example, Refs. [15, 44, 53]). It is important to highlight that when nonlinear systems of PDEs are considered, it is not possible to attain the telescoping property (41) by simply using SBP operators to discretely differentiate fluxes.

This section is finished by presenting the discretization for each element separately. Therefore, for the element L the semidiscrete form reads

$$
\begin{aligned}
&\mathsf{J}_{\mathrm{L}}\frac{\mathrm{d}\boldsymbol{q}_{\mathrm{L}}}{\mathrm{d}t}+\sum_{l,m=1}^{3}\left(\mathsf{D}_{\xi_l}^{\mathrm{L}}\left[\mathcal{J}\frac{\partial\xi_l}{\partial x_m}\right]_{\mathrm{L}}+\left[\mathcal{J}\frac{\partial\xi_m}{\partial x_l}\right]_{\mathrm{L}}\mathsf{D}_{\xi_l}^{\mathrm{L}}\right)\circ\mathsf{F}_{x_m}\left(\boldsymbol{q}_{\mathrm{L}},\boldsymbol{q}_{\mathrm{L}}\right)\mathbf{1}_{\mathrm{L}}=\\
&\left(\mathsf{P}^{\mathrm{L}}\right)^{-1}\sum_{m=1}^{3}\left\{\left(\boldsymbol{e}_{N_{\mathrm{L}}}\boldsymbol{e}_{N_{\mathrm{L}}}^{\mathrm{T}}\mathsf{P}_{\mathrm{L}}^{(1D)}\otimes\mathsf{P}_{\mathrm{L}}^{(1D)}\otimes\mathsf{I}_5\right)\left[\mathcal{J}\frac{\partial\xi_1}{\partial x_m}\right]_{\mathrm{L}}\right\}\circ\mathsf{F}_{x_m}\left(\boldsymbol{q}_{\mathrm{L}},\boldsymbol{q}_{\mathrm{L}}\right)\mathbf{1}_{\mathrm{L}}\\
&\left(\mathsf{P}^{\mathrm{L}}\right)^{-1}\sum_{m=1}^{3}\left\{\left[\mathcal{J}\frac{\partial\xi_1}{\partial x_m}\right]_{\mathrm{L}}\left(\boldsymbol{e}_{N_{\mathrm{L}}}\boldsymbol{e}_{N_{\mathrm{L}}}^{\mathrm{T}}\mathsf{P}_{\mathrm{L}}^{(1D)}\otimes\mathsf{P}_{\mathrm{L}}^{(1D)}\otimes\mathsf{I}_5\right)\right\}\circ\mathsf{F}_{x_m}\left(\boldsymbol{q}_{\mathrm{L}},\boldsymbol{q}_{\mathrm{L}}\right)\mathbf{1}_{\mathrm{L}}\\
&-\left(\mathsf{P}^{\mathrm{L}}\right)^{-1}\sum_{m=1}^{3}\left\{\left(\boldsymbol{e}_{N_{\mathrm{L}}}\otimes\mathsf{I}_{N_{\mathrm{L}}}\otimes\mathsf{I}_{N_{\mathrm{L}}}\otimes\mathsf{I}_5\right)\left[\mathcal{J}\frac{\partial\xi_1}{\partial x_m}\right]_{\mathrm{L}}^{\hat{\Gamma}}\left(\mathsf{P}_{\mathrm{L}}^{(1D)}\mathsf{I}_{\mathrm{HtoL}}^{(1D)}\otimes\mathsf{P}_{\mathrm{L}}^{(1D)}\mathsf{I}_{\mathrm{HtoL}}^{(1D)}\otimes\mathsf{I}_5\right)\right.\\
&\left.\left(\boldsymbol{e}_{1_{\mathrm{H}}}^{\mathrm{T}}\otimes\mathsf{I}_{N_{\mathrm{H}}}\otimes\mathsf{I}_{N_{\mathrm{H}}}\otimes\mathsf{I}_5\right)\right\}\circ\mathsf{F}_{x_m}\left(\boldsymbol{q}_{\mathrm{L}},\boldsymbol{q}_{\mathrm{H}}\right)\mathbf{1}_{\mathrm{H}}\\
&-\left(\mathsf{P}^{\mathrm{L}}\right)^{-1}\sum_{m=1}^{3}\left\{\left(\boldsymbol{e}_{N_{\mathrm{L}}}\otimes\mathsf{I}_{N_{\mathrm{L}}}\otimes\mathsf{I}_{N_{\mathrm{L}}}\otimes\mathsf{I}_5\right)\left(\mathsf{P}_{\mathrm{L}}^{(1D)}\mathsf{I}_{\mathrm{HtoL}}^{(1D)}\otimes\mathsf{P}_{\mathrm{L}}^{(1D)}\mathsf{I}_{\mathrm{HtoL}}^{(1D)}\otimes\mathsf{I}_5\right)\left[\mathcal{J}\frac{\partial\xi_1}{\partial x_m}\right]_{\mathrm{H}}^{\hat{\Gamma}}\right.\\
&\left.\left(\boldsymbol{e}_{1_{\mathrm{H}}}^{\mathrm{T}}\otimes\mathsf{I}_{N_{\mathrm{H}}}\otimes\mathsf{I}_{N_{\mathrm{H}}}\otimes\mathsf{I}_5\right)\right\}\circ\mathsf{F}_{x_m}\left(\boldsymbol{q}_{\mathrm{L}},\boldsymbol{q}_{\mathrm{H}}\right)\mathbf{1}_{\mathrm{H}},
\end{aligned}
\tag{49}
$$

whereas for the element H the semidiscrete form reads

$$
\begin{aligned}
&\mathsf{J}_{\mathrm{H}}\frac{\mathrm{d}\boldsymbol{q}_{\mathrm{H}}}{\mathrm{d}t}+\sum_{l,m=1}^{3}\left(\mathsf{D}_{\xi_l}^{\mathrm{H}}\left[\mathcal{J}\frac{\partial\xi_l}{\partial x_m}\right]_{\mathrm{H}}+\left[\mathcal{J}\frac{\partial\xi_m}{\partial x_l}\right]_{\mathrm{H}}\mathsf{D}_{\xi_l}^{\mathrm{H}}\right)\circ\mathsf{F}_{x_m}\left(\boldsymbol{q}_{\mathrm{H}},\boldsymbol{q}_{\mathrm{H}}\right)\mathbf{1}_{\mathrm{L}}=\\
&-\left(\mathsf{P}^{\mathrm{H}}\right)^{-1}\sum_{m=1}^{3}\left\{\left(\boldsymbol{e}_{1_{\mathrm{H}}}\boldsymbol{e}_{1_{\mathrm{H}}}^{\mathrm{T}}\mathsf{P}_{\mathrm{H}}^{(1D)}\otimes\mathsf{P}_{\mathrm{H}}^{(1D)}\otimes\mathsf{I}_5\right)\left[\mathcal{J}\frac{\partial\xi_1}{\partial x_m}\right]_{\mathrm{H}}\right\}\circ\mathsf{F}_{x_m}\left(\boldsymbol{q}_{\mathrm{H}},\boldsymbol{q}_{\mathrm{H}}\right)\mathbf{1}_{\mathrm{H}}\\
&-\left(\mathsf{P}^{\mathrm{H}}\right)^{-1}\sum_{m=1}^{3}\left\{\left[\mathcal{J}\frac{\partial\xi_1}{\partial x_m}\right]_{\mathrm{H}}\left(\boldsymbol{e}_{1_{\mathrm{H}}}\boldsymbol{e}_{1_{\mathrm{H}}}^{\mathrm{T}}\mathsf{P}_{\mathrm{H}}^{(1D)}\otimes\mathsf{P}_{\mathrm{H}}^{(1D)}\otimes\mathsf{I}_5\right)\right\}\circ\mathsf{F}_{x_m}\left(\boldsymbol{q}_{\mathrm{H}},\boldsymbol{q}_{\mathrm{H}}\right)\mathbf{1}_{\mathrm{H}}\\
&+\left(\mathsf{P}^{\mathrm{H}}\right)^{-1}\sum_{m=1}^{3}\left\{\left(\boldsymbol{e}_{1_{\mathrm{H}}}\otimes\mathsf{I}_{N_{\mathrm{H}}}\otimes\mathsf{I}_{N_{\mathrm{H}}}\otimes\mathsf{I}_5\right)\left[\mathcal{J}\frac{\partial\xi_1}{\partial x_m}\right]_{\mathrm{H}}^{\hat{\Gamma}}\left(\mathsf{P}_{\mathrm{H}}^{(1D)}\mathsf{I}_{\mathrm{LtoH}}^{(1D)}\otimes\mathsf{P}_{\mathrm{H}}^{(1D)}\mathsf{I}_{\mathrm{LtoH}}^{(1D)}\otimes\mathsf{I}_5\right)\right.\\
&\left.\left(\boldsymbol{e}_{N_{\mathrm{L}}}^{\mathrm{T}}\otimes\mathsf{I}_{N_{\mathrm{L}}}\otimes\mathsf{I}_{N_{\mathrm{L}}}\otimes\mathsf{I}_5\right)\right\}\circ\mathsf{F}_{x_m}\left(\boldsymbol{q}_{\mathrm{H}},\boldsymbol{q}_{\mathrm{L}}\right)\mathbf{1}_{\mathrm{L}}\\
&+\left(\mathsf{P}^{\mathrm{H}}\right)^{-1}\sum_{m=1}^{3}\left\{\left(\boldsymbol{e}_{1_{\mathrm{H}}}\otimes\mathsf{I}_{N_{\mathrm{H}}}\otimes\mathsf{I}_{N_{\mathrm{H}}}\otimes\mathsf{I}_5\right)\left(\mathsf{P}_{\mathrm{H}}^{(1D)}\mathsf{I}_{\mathrm{LtoH}}^{(1D)}\otimes\mathsf{P}_{\mathrm{H}}^{(1D)}\mathsf{I}_{\mathrm{LtoH}}^{(1D)}\otimes\mathsf{I}_5\right)\left[\mathcal{J}\frac{\partial\xi_1}{\partial x_m}\right]_{\mathrm{L}}^{\hat{\Gamma}}\right.\\
&\left.\left(\boldsymbol{e}_{N_{\mathrm{L}}}^{\mathrm{T}}\otimes\mathsf{I}_{N_{\mathrm{L}}}\otimes\mathsf{I}_{N_{\mathrm{L}}}\otimes\mathsf{I}_5\right)\right\}\circ\mathsf{F}_{x_m}\left(\boldsymbol{q}_{\mathrm{H}},\boldsymbol{q}_{\mathrm{L}}\right)\mathbf{1}_{\mathrm{L}}.
\end{aligned}
\tag{50}
$$

The algorithm presented above leads to an entropy conservative discretization (modulo what boundary conditions are imposed). However, the main interest is in entropy stable algorithms and the approach used herein to achieve this is to augment the entropy conservative scheme with an appropriate interface dissipation. How this is accomplished is discussed in the next section.

6 Inviscid interface dissipation and boundary SATs

To make the inviscid entropy conservative scheme entropy stable, an interface dissipation needs to be added. Herein, as in the conforming algorithms [5, 9, 42, 44], the numerical dissipation is motivated by the upwinding used in a Roe approximate Riemann solver which has the form

$$\boldsymbol{\mathcal{F}}^* = \frac{\boldsymbol{\mathcal{F}}^+ + \boldsymbol{\mathcal{F}}^-}{2} - \frac{1}{2}\mathsf{Y}\,|\boldsymbol{\Lambda}|\,\mathsf{Y}^{-1}\left(\boldsymbol{\mathcal{Q}}^+ - \boldsymbol{\mathcal{Q}}^-\right), \tag{51}$$

where + and − refer to quantities evaluated on the side of the interface in the positive and negative face normal directions, respectively (see Figure 1).

The original Roe flux: $\boldsymbol{\mathcal{F}}^*$ is composed of an inviscid flux average: $(\boldsymbol{\mathcal{F}}^+ + \boldsymbol{\mathcal{F}}^-)/2$ and a dissipation term. The flux average term is not in general entropy conservative, and is replaced with an entropy conservative two-point flux, e.g., Chandrashekar [11] or Ismail and Roe [28]. The remaining dissipation term, is reformulated in quadratic form to facilitate an entropy stability proof. This step is accomplished by using the flux Jacobian with respect to the entropy variables, $\boldsymbol{\mathcal{W}}$, rather than the conservative variables, $\boldsymbol{\mathcal{Q}}$. A unique scaling of the eigenvectors of the conservative variable flux Jacobian facilitates the reformulation [37].

$$\frac{\partial \boldsymbol{\mathcal{Q}}}{\partial \boldsymbol{\mathcal{W}}} = \mathsf{Y}\mathsf{Y}^{\mathrm{T}} \quad ; \quad \frac{\partial \boldsymbol{\mathcal{F}}_{\xi_l}}{\partial \boldsymbol{\mathcal{W}}} = \frac{\partial \boldsymbol{\mathcal{F}}_{\xi_l}}{\partial \boldsymbol{\mathcal{Q}}}\frac{\partial \boldsymbol{\mathcal{Q}}}{\boldsymbol{\mathcal{W}}} = \mathsf{Y}\boldsymbol{\Lambda}_{\xi_l}\mathsf{Y}^{-1}\ \mathsf{Y}\mathsf{Y}^{\mathrm{T}} = \mathsf{Y}\boldsymbol{\Lambda}_{\xi_l}\mathsf{Y}^{\mathrm{T}}$$

A full description of the various required matrices appears in Fisher [20].

The interface dissipation term: $\mathsf{Y}|\boldsymbol{\Lambda}|\mathsf{Y}^{-1}\left(\boldsymbol{\mathcal{Q}}^+ - \boldsymbol{\mathcal{Q}}^-\right)$ is replaced with the equivalent quadratic dissipation term: $\mathsf{Y}|\boldsymbol{\Lambda}|\mathsf{Y}^{\mathrm{T}}\left(\boldsymbol{\mathcal{W}}^+ - \boldsymbol{\mathcal{W}}^-\right)$. The final form of the interface flux is

$$\boldsymbol{\mathcal{F}}^* = \boldsymbol{f}^{sc}_{x_m}\left(\boldsymbol{\mathcal{W}}^+, \boldsymbol{\mathcal{W}}^-\right) - \frac{1}{2}\mathsf{Y}\,|\boldsymbol{\Lambda}|\,\mathsf{Y}^{\mathrm{T}}\left(\boldsymbol{\mathcal{W}}^+ - \boldsymbol{\mathcal{W}}^-\right). \tag{52}$$

and leads to an entropy stable scheme. The extension to the curvilinear case follows immediately by constructing all three computational fluxes followed by the dot product with the outward facing normal.

Therefore, the dissipation on element L is given as

$$\begin{aligned}\boldsymbol{diss}_{\mathrm{L}} \equiv &-\frac{1}{2}\left(\mathsf{P}^{\mathrm{L}}\right)^{-1}\mathsf{R}_{\mathrm{L}}^{\mathrm{T}}\mathsf{P}^{\mathrm{L}}_{\perp\xi_1}\left|\frac{\partial \boldsymbol{\mathcal{F}}_{\xi_1}}{\partial \boldsymbol{\mathcal{W}}}\right|_{\mathrm{L}}\left(\mathsf{R}_{\mathrm{L}}\boldsymbol{w}_{\mathrm{L}} - \mathsf{I}_{\mathrm{HtoL}}\mathsf{R}_{\mathrm{H}}\boldsymbol{w}_{\mathrm{H}}\right)\\ &-\frac{1}{2}\left(\mathsf{P}^{\mathrm{L}}\right)^{-1}\mathsf{R}_{\mathrm{L}}^{\mathrm{T}}\mathsf{P}^{\mathrm{L}}_{\perp\xi_1}\mathsf{I}_{\mathrm{HtoL}}\left|\frac{\partial \boldsymbol{\mathcal{F}}_{\xi_1}}{\partial \boldsymbol{\mathcal{W}}}\right|_{\mathrm{H}}\left(\mathsf{I}_{\mathrm{LtoH}}\mathsf{R}_{\mathrm{L}}\boldsymbol{w}_{\mathrm{L}} - \mathsf{R}_{\mathrm{H}}\boldsymbol{w}_{\mathrm{H}}\right),\end{aligned} \tag{53}$$

and on element H takes the following form

$$\begin{aligned}\boldsymbol{diss}_{\mathrm{H}} \equiv &-\frac{1}{2}\left(\mathsf{P}^{\mathrm{H}}\right)^{-1}\mathsf{R}_{\mathrm{H}}^{\mathrm{T}}\mathsf{P}^{\mathrm{H}}_{\perp\xi_1}\left|\frac{\partial \boldsymbol{\mathcal{F}}_{\xi_1}}{\partial \boldsymbol{\mathcal{W}}}\right|_{\mathrm{H}}\left(\mathsf{R}_{\mathrm{H}}\boldsymbol{w}_{\mathrm{H}} - \mathsf{I}_{\mathrm{LtoH}}\mathsf{R}_{\mathrm{L}}\boldsymbol{w}_{\mathrm{L}}\right)\\ &-\frac{1}{2}\left(\mathsf{P}^{\mathrm{H}}\right)^{-1}\mathsf{R}_{\mathrm{H}}^{\mathrm{T}}\mathsf{P}^{\mathrm{H}}_{\perp\xi_1}\mathsf{I}_{\mathrm{LtoH}}\left|\frac{\partial \boldsymbol{\mathcal{F}}_{\xi_1}}{\partial \boldsymbol{\mathcal{W}}}\right|_{\mathrm{L}}\left(\mathsf{I}_{\mathrm{HtoL}}\mathsf{R}_{\mathrm{H}}\boldsymbol{w}_{\mathrm{H}} - \mathsf{R}_{\mathrm{L}}\boldsymbol{w}_{\mathrm{L}}\right),\end{aligned} \tag{54}$$

where $\left|\frac{\partial \boldsymbol{\mathcal{F}}_{\xi_1}}{\partial \boldsymbol{\mathcal{W}}}\right|_{\mathrm{L}}$ is constructed from the Roe average of the states $\boldsymbol{w}_{\mathrm{L}}$ and $\mathsf{I}_{\mathrm{HtoL}}\boldsymbol{w}_{\mathrm{H}}$, and $\left|\frac{\partial \boldsymbol{\mathcal{F}}_{\xi_1}}{\partial \boldsymbol{\mathcal{W}}}\right|_{\mathrm{H}}$ is constructed from the Roe average of the states $\boldsymbol{w}_{\mathrm{H}}$ and $\mathsf{I}_{\mathrm{LtoH}}\boldsymbol{w}_{\mathrm{L}}$. Furthermore, the various operators

which appear in (53) and (54) are defined as follows:

$$\begin{aligned}
&\mathsf{R}_{\mathrm{L}} \equiv \boldsymbol{e}_{N_{\mathrm{L}}}^{\mathrm{T}} \otimes \mathsf{I}_{N_{\mathrm{L}}} \otimes \mathsf{I}_{N_{\mathrm{L}}} \otimes \mathsf{I}_5, \quad \mathsf{R}_{\mathrm{H}} \equiv \boldsymbol{e}_{1_{\mathrm{H}}}^{\mathrm{T}} \otimes \mathsf{I}_{N_{\mathrm{H}}} \otimes \mathsf{I}_{N_{\mathrm{H}}} \otimes \mathsf{I}_5, \\
&\mathsf{P}_{\perp\xi_l}^{\mathrm{L}} \equiv \mathsf{P}_{\mathrm{L}}^{(1D)} \otimes \mathsf{P}_{\mathrm{L}}^{(1D)} \otimes \mathsf{I}_5, \quad \mathsf{P}_{\perp\xi_l}^{\mathrm{H}} \equiv \mathsf{P}_{\mathrm{H}}^{(1D)} \otimes \mathsf{P}_{\mathrm{H}}^{(1D)} \otimes \mathsf{I}_5, \\
&\mathsf{I}_{\mathrm{HtoL}} \equiv \mathsf{I}_{\mathrm{HtoL}}^{(1D)} \otimes \mathsf{I}_{\mathrm{HtoL}}^{(1D)} \otimes \mathsf{I}_5, \quad \mathsf{I}_{\mathrm{LtoH}} \equiv \mathsf{I}_{\mathrm{LtoH}}^{(1D)} \otimes \mathsf{I}_{\mathrm{LtoH}}^{(1D)} \otimes \mathsf{I}_5.
\end{aligned}$$

All the theorems regarding the accuracy and the entropy stability are presented (elementwise conservation is discussed in Appendix E while it is straightforward to see that free-stream preservation is attained if the discrete GCL are satisfied).

Theorem 4. *The dissipation term* $\boldsymbol{diss}_{\mathrm{L}}$ *is a term of order* $p_{\mathrm{L}} + d - 1$ *and the dissipation term* $\boldsymbol{diss}_{\mathrm{H}}$ *is a term of order* $p_{\mathrm{L}} + d - 1$.

Proof. This follows from the accuracy of the interpolation operators. □

Theorem 5. *The dissipation terms* (53) *and* (54) *lead to an entropy stable scheme.*

Proof. Contracting the global dissipation operator with the entropy variables results in contractions of the interface dissipation terms $\boldsymbol{diss}_{\mathrm{L}}$ and $\boldsymbol{diss}_{\mathrm{H}}$ by $\boldsymbol{w}_{\mathrm{L}}^{\mathrm{T}}\mathsf{P}^{\mathrm{L}}$ and $\boldsymbol{w}_{\mathrm{H}}^{\mathrm{T}}\mathsf{P}^{\mathrm{H}}$, respectively. Summing the interface contributions $\boldsymbol{w}_{\mathrm{L}}^{\mathrm{T}}\mathsf{P}^{\mathrm{L}}\boldsymbol{diss}_{\mathrm{L}}$ and $\boldsymbol{w}_{\mathrm{H}}^{\mathrm{T}}\mathsf{P}^{\mathrm{H}}\boldsymbol{diss}_{\mathrm{H}}$, using the property $\mathsf{I}_{\mathrm{HtoL}} = \left(\mathsf{P}^{\mathrm{L}}\right)^{-1}\mathsf{I}_{\mathrm{LtoH}}^{\mathrm{T}}\mathsf{P}^{\mathrm{H}}$ and rearranging terms, results in

$$\begin{aligned}
&\boldsymbol{w}_{\mathrm{L}}^{\mathrm{T}}\mathsf{P}^{\mathrm{L}}\boldsymbol{diss}_{\mathrm{L}} + \boldsymbol{w}_{\mathrm{H}}^{\mathrm{T}}\mathsf{P}^{\mathrm{H}}\boldsymbol{diss}_{\mathrm{H}} = \\
&-\frac{1}{2}\left(\mathsf{R}_{\mathrm{L}}\boldsymbol{w}_{\mathrm{L}} - \mathsf{I}_{\mathrm{HtoL}}\mathsf{R}_{\mathrm{H}}\boldsymbol{w}_{\mathrm{H}}\right)^{\mathrm{T}}\mathsf{P}_{\perp\xi_1}^{\mathrm{L}}\left|\frac{\partial\boldsymbol{\mathcal{F}}_{\xi_1}}{\partial\boldsymbol{\mathcal{W}}}\right|_{\mathrm{L}}\left(\mathsf{R}_{\mathrm{L}}\boldsymbol{w}_{rmL} - \mathsf{I}_{\mathrm{HtoL}}\mathsf{R}_{\mathrm{H}}\boldsymbol{w}_{rmH}\right) \\
&-\frac{1}{2}\left(\mathsf{R}_{\mathrm{H}}\boldsymbol{w}_{rmH} - \mathsf{I}_{\mathrm{LtoH}}\mathsf{R}_{\mathrm{L}}\boldsymbol{w}_{\mathrm{L}}\right)^{\mathrm{T}}\mathsf{P}_{\perp\xi_1}^{\mathrm{H}}\left|\frac{\partial\boldsymbol{\mathcal{F}}_{\xi_1}}{\partial\boldsymbol{\mathcal{W}}}\right|_{\mathrm{H}}\left(\mathsf{R}_{\mathrm{H}}\boldsymbol{w}_{\mathrm{H}} - \mathsf{I}_{\mathrm{LtoH}}\mathsf{R}_{\mathrm{H}}\boldsymbol{w}_{\mathrm{L}}\right),
\end{aligned}$$

which is a negative semidefinite term. Therefore, the added interface terms are entropy dissipative. □

In Section 7, two problems are used to characterize the nonconforming algorithms: 1) the propagation of an isentropic vortex and 2) the inviscid Taylor-Green vortex problem. For all of them, the boundary conditions are weakly imposed by reusing the interface SAT mechanics (see, for instance, Refs. [15, 44]).

7 Numerical experiments

This section presents numerical evidence that demonstrates that the proposed p-nonconforming algorithm retains the accuracy and robustness of the spatial conforming discretization reported in [5, 9, 42, 44].

Herein, the conforming [5, 9, 42, 44] and p-adaptive solver for unstructured grids developed at the Extreme Computing Research Center (ECRC) at KAUST is used to perform numerical experiments. This parallel solver is built on top of the Portable and Extensible Toolkit for Scientific computing (PETSc) [4], its mesh topology abstraction (DMPLEX) [30] and scalable ordinary differential equation (ODE)/differential algebraic equations (DAE) solver library [1]. The systems of ordinary differential equations arising from the spatial discretizations are integrated using the

fourth-order accurate Dormand–Prince method [19] endowed with an adaptive time stepping technique based on digital signal processing [50,51]. To make the temporal error negligible, a tolerance of 10^{-8} is always used for the time-step adaptivity. The two-point entropy consistent flux of Chandrashekar [11] is used for all the test cases.

The errors are computed using volume scaled (for the L^1 and L^2 norms) discrete norms as follows:

$$\|\boldsymbol{u}\|_{L^1} = \Omega_c^{-1} \sum_{\kappa=1}^{K} \mathbf{1}_\kappa^{\mathrm{T}} \mathsf{P}^\kappa \mathsf{J}_\kappa \mathrm{abs}\left(\boldsymbol{u}_\kappa\right), \; \|\boldsymbol{u}\|_{L^2}^2 = \Omega_c^{-1} \sum_{\kappa=1}^{K} \boldsymbol{u}_\kappa \mathsf{P}^\kappa \mathsf{J}_\kappa \boldsymbol{u}_\kappa,$$
$$\|\boldsymbol{u}\|_{L^\infty} = \max_{\kappa=1\ldots K} \mathrm{abs}\left(\boldsymbol{u}_\kappa\right),$$

where Ω_c indicates the volume of Ω computed as $\Omega_c \equiv \sum_{\kappa=1}^{K} \mathbf{1}_\kappa^{\mathrm{T}} \mathsf{P}^\kappa \mathsf{J}_\kappa \mathbf{1}_\kappa$.

7.1 Isentropic Euler vortex propagation

For verification and characterization of the inviscid components of the algorithm, the propagation of an isentropic vortex is used. This benchmark problem has an analytical solution, which is given by

$$\mathcal{G}\left(x_1, x_2, x_3, t\right) = 1 - \left\{\left[\left(x_1 - x_{1,0}\right) - U_\infty \cos\left(\alpha\right) t\right]^2 + \left[\left(x_2 - x_{2,0}\right) - U_\infty \sin\left(\alpha\right) t\right]^2\right\},$$
$$\rho = T^{\frac{1}{\gamma-1}},$$
$$\mathcal{U}_1 = U_\infty \cos(\alpha) - \epsilon_\nu \frac{\left(x_2 - x_{2,0}\right) - U_\infty \sin\left(\alpha\right) t}{2\pi} \exp\left(\frac{\mathcal{G}}{2}\right),$$
$$\mathcal{U}_2 = U_\infty \sin(\alpha) - \epsilon_\nu \frac{\left(x_1 - x_{1,0}\right) - U_\infty \cos\left(\alpha\right) t}{2\pi} \exp\left(\frac{\mathcal{G}}{2}\right),$$
$$\mathcal{U}_3 = 0,$$
$$T = \left[1 - \epsilon_\nu^2 M_\infty^2 \frac{\gamma - 1}{8\pi^2} \exp\left(\mathcal{G}\right)\right],$$

where U_∞, M_∞, and $(x_{1,0}, x_{2,0}, x_{3,0})$ are the modulus of the freestream velocity, the freestream Mach number, and the vortex center, respectively. In this paper, the following values are used: $U_\infty = M_\infty c_\infty$, $\epsilon_\nu = 5$, $M_\infty = 0.5$, $\gamma = 1.4$, $\alpha = 45^\circ$, and $(x_{1,0}, x_{2,0}, x_{3,0}) = (0, 0, 0)$. The computational domain is $x_1 \in [-5, 5]$, $x_2 \in [-5, 5]$, $x_3 \in [-5, 5]$, and $t \in [0, 2]$. The analytical solution is used to furnish data for the initial condition.

First, results aimed at validating the entropy conservation properties of the interior domain SBP-SAT algorithm are reported. Thus, periodic boundary conditions are used on all six faces of the computational domain. Furthermore, all the dissipation terms used for the interface coupling are turned off. The discrete integral over the computational domain of the time rate of change of the entropy function, $\int_\Omega \frac{\partial \mathcal{S}}{\partial t} \mathrm{d}\Omega$ in Eq. (35), is monitored at every time step.

The computational domain is subdivided using ten hexahedrons in each coordinate direction and the solution polynomial degree in each element is assigned a random integer chosen uniformly from the set $p_s = \{2, 3, 4, 5\}$ (i.e., each member in the set has an equal probability of being chosen). To test the conservation of entropy and therefore the freestream condition when curved element

interfaces are used, the LGL collocation point coordinates at element interfaces are constructed[1] as follows:

- Construct a mesh by describing the element interfaces with a second-order polynomial representation. Note that many mesh generators use a uniform distribution of points (or nodes) to construct such a geometrical representation.

- Perturb the nodes that are used to define the second-order polynomial approximation of the element interfaces as follows:

$$x_1 = x_{1,*} + \frac{1}{15} L_1 \cos(a) \cos(3b) \sin(4c), \; x_2 = x_{2,*} + \frac{1}{15} L_2 \sin(4a) \cos(b) \cos(3c),$$
$$x_3 = x_{3,*} + \frac{1}{15} L_3 \cos(3a) \sin(4b) \cos(c),$$

  where

$$a = \frac{\pi}{L_1} \left(x_{1,*} - \frac{x_{1,H} + x_{1,L}}{2} \right), b = \frac{\pi}{L_2} \left(x_{2,*} - \frac{x_{2,H} + x_{2,L}}{2} \right),$$
$$c = \frac{\pi}{L_3} \left(x_{3,*} - \frac{x_{3,H} + x_{3,L}}{2} \right).$$

  The lengths L_1, L_2 and L_3 are the dimensions of the computational domain in the three coordinate directions and the sub-script $*$ indicates the unperturbed coordinates of the nodes. This step yields a "perturbed" second-order interface polynomial representation.

- Compute the coordinate of the LGL points at the element interface by evaluating the "perturbed" second-order polynomial at the tensor-product LGL points used to define the cell solution polynomial of order p_s.

Figure 2 shows a cut of the mesh and the polynomial order distribution used for this first test case. The propagation of the vortex is simulated for two time units. Figure 3 plots the integral of the time derivative of the entropy function. It is seen that the global variation of the time rate of the of $\mathcal{S}$ is practically zero. This implies that the spatially nonconforming algorithm is entropy conservative.

Second, a grid convergence study is performed to investigate the order of convergence of the nonconforming algorithm. The base grid (i.e., the coarsest grid) is constructed as follows:

- Divide the computational domain with four hexahedral elements in each coordinate direction.

- Assign the solution polynomial degree in each element to a random integer chosen uniformly from the set $\{p_s, p_s + 1\}$.

- Approximate with a p_sth-order accurate polynomial the element interfaces.

- Construct the perturbed elements and their corresponding LGL points as described previously.

From the base grid, which is similar to the one depicted in Figure 2, a sequence of nested grids is then generated to perform the convergence study. The results are reported in Tables 7.1 through 6 for the error on the density. The number listed in the first column denoted by"Grid" indicates the number of hexahedrons in each coordinate direction.

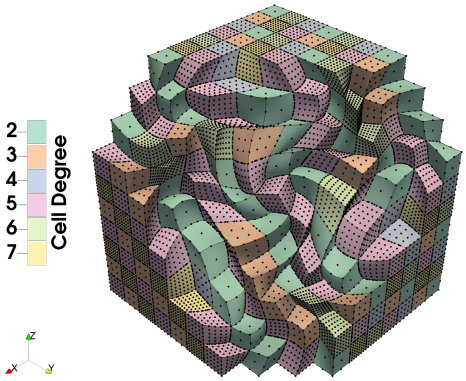

Figure 2. Isentropic vortex: mesh cut and polynomial order distribution.

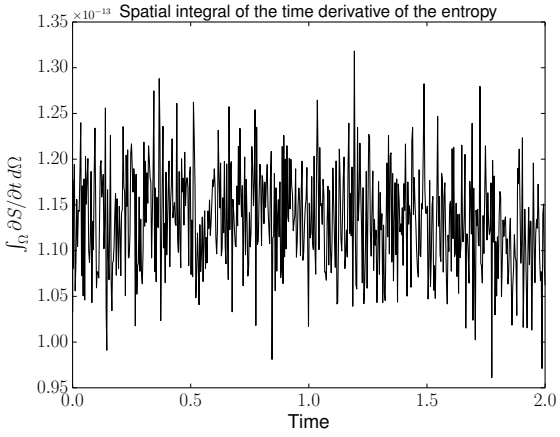

Figure 3. Isentropic vortex: time rate of change of the entropy function.

Table 1: Convergence study of the isentropic vortex propagation: $p = 1$ with $p = 2$; density error.

	Conforming, $p = 1$						Nonconforming, $p = 1$ and $p = 2$					
Grid	L^1	Rate	L^2	Rate	L^∞	Rate	L^1	Rate	L^2	Rate	L^∞	Rate
4	2.74E-02	-	1.32E-03	-	1.55E-01	-	1.87E-02	-	9.48E-04	-	1.20E-01	-
8	1.14E-02	-1.26	6.61E-04	-1.00	1.12E-01	-0.47	1.02E-02	-0.87	5.87E-04	-0.69	1.23E-01	+0.04
16	5.13E-03	-1.16	3.31E-04	-1.00	7.29E-02	-0.62	4.55E-03	-1.17	2.99E-04	-0.97	7.06E-02	-0.80
32	1.70E-03	-1.59	1.15E-04	-1.52	3.01E-02	-1.28	1.52E-03	-1.58	1.07E-04	-1.49	3.97E-02	-0.83
64	4.76E-04	-1.84	3.24E-05	-1.83	8.53E-03	-1.82	4.36E-04	-1.81	3.15E-05	-1.76	2.15E-02	-0.88
128	1.23E-04	-1.96	8.33E-06	-1.96	2.13E-03	-2.00	1.14E-04	-1.93	8.72E-06	-1.85	1.05E-02	-1.03
256	3.08E-05	-1.99	2.09E-06	-1.99	5.24E-04	-2.02	2.91E-05	-1.98	2.46E-06	-1.83	5.10E-03	-1.05
512	7.68E-06	-2.00	5.23E-07	-2.00	1.30E-04	-2.01	7.23E-06	-2.01	6.17E-07	-2.00	2.26E-03	-1.17

Table 2: Convergence study of the isentropic vortex propagation: $p = 2$ with $p = 3$; density error.

	Conforming, $p = 2$						Nonconforming, $p = 2$ and $p = 3$					
Grid	L^1	Rate	L^2	Rate	L^∞	Rate	L^1	Rate	L^2	Rate	L^∞	Rate
4	9.75E-03	-	5.32E-04	-	1.24E-01	-	8.57E-03	-	5.05E-04	-	1.21E-01	-
8	3.18E-03	-1.61	2.09E-04	-1.35	6.97E-02	-0.83	2.70E-03	-1.67	1.84E-04	-1.46	8.55E-02	-0.50
16	5.18E-04	-2.62	3.88E-05	-2.43	2.51E-02	-1.47	4.25E-04	-2.67	3.58E-05	-2.36	3.23E-02	-1.40
32	6.38E-05	-3.02	5.50E-06	-2.82	7.23E-03	-1.79	4.99E-05	-3.09	5.14E-06	-2.80	7.20E-03	-2.17
64	7.61E-06	-3.07	7.23E-07	-2.93	1.21E-03	-2.58	5.78E-06	-3.11	7.05E-07	-2.87	1.42E-03	-2.35
128	9.48E-07	-3.00	9.95E-08	-2.86	2.75E-04	-2.14	7.14E-07	-3.02	1.06E-07	-2.74	3.52E-04	-2.01
256	1.23E-07	-2.94	1.43E-08	-2.83	3.41E-05	-3.01	9.46E-08	-2.92	1.52E-08	-2.80	9.16E-05	-1.94

Table 3: Convergence study of the isentropic vortex propagation: $p = 3$ with $p = 4$; density error.

	Conforming, $p = 3$						Nonconforming, $p = 3$ and $p = 4$					
Grid	L^1	Rate	L^2	Rate	L^∞	Rate	L^1	Rate	L^2	Rate	L^∞	Rate
4	5.22E-03	-	3.38E-04	-	9.16E-02	-	4.58E-03	-	3.07E-04	-	8.90E-02	-
8	6.84E-04	-2.93	5.30E-05	-2.67	4.71E-02	-0.96	5.81E-04	-2.98	4.94E-05	-2.63	5.26E-02	-0.76
16	5.50E-05	-3.64	4.54E-06	-3.55	6.61E-03	-2.83	4.51E-05	-3.69	4.15E-06	-3.58	5.04E-03	-3.38
32	3.48E-06	-3.98	3.33E-07	-3.77	5.47E-04	-3.59	2.88E-06	-3.97	3.06E-07	-3.76	4.98E-04	-3.34
64	2.10E-07	-4.05	2.45E-08	-3.76	4.93E-05	-3.47	1.78E-07	-4.01	2.34E-08	-3.71	5.42E-05	-3.20
128	1.39E-08	-3.92	1.87E-09	-3.71	6.32E-06	-2.96	1.24E-08	-3.85	1.90E-09	-3.63	7.96E-06	-2.77

Table 4: Convergence study of the isentropic vortex propagation: $p = 4$ with $p = 5$; density error.

	Conforming, $p = 4$						Nonconforming, $p = 4$ and $p = 5$					
Grid	L^1	Rate	L^2	Rate	L^∞	Rate	L^1	Rate	L^2	Rate	L^∞	Rate
4	2.34E-03	-	1.56E-04	-	9.92E-02	-	2.10E-03	-	1.48E-04	-	9.28E-02	-
8	1.70E-04	-3.78	1.43E-05	-3.45	2.32E-02	-2.09	1.48E-04	-3.82	1.37E-05	-3.43	2.30E-02	-2.01
16	6.07E-06	-4.81	6.41E-07	-4.48	1.27E-03	-4.19	5.17E-06	-4.85	6.00E-07	-4.51	1.26E-03	-4.19
32	1.99E-07	-4.93	2.25E-08	-4.83	5.13E-05	-4.64	1.64E-07	-4.98	2.07E-08	-4.86	5.50E-05	-4.52
64	7.11E-09	-4.81	8.60E-10	-4.71	3.01E-06	-4.09	6.36E-09	-4.69	7.95E-10	-4.70	2.99E-06	-4.20

Table 5: Convergence study of the isentropic vortex propagation: $p = 5$ with $p = 6$; density error.

	Conforming, $p = 5$						Nonconforming, $p = 5$ and $p = 6$					
Grid	L^1	Rate	L^2	Rate	L^∞	Rate	L^1	Rate	L^2	Rate	L^∞	Rate
4	1.01E-03	-	6.88E-05	-	4.53E-02	-	9.14E-04	-	6.63E-05	-	4.45E-02	-
8	3.81E-05	-4.73	3.80E-06	-4.18	6.37E-03	-2.83	3.26E-05	-4.81	3.61E-06	-4.20	6.44E-03	-2.79
16	7.23E-07	-5.72	7.95E-08	-5.58	2.23E-04	-4.84	5.93E-07	-5.78	7.30E-08	-5.63	1.63E-04	-5.30
32	1.24E-08	-5.87	1.59E-09	-5.65	4.99E-06	-5.48	1.05E-08	-5.82	1.46E-09	-5.65	4.99E-06	-5.03

Table 6: Convergence study of the isentropic vortex propagation: $p = 6$ with $p = 7$; density error.

	Conforming, $p = 6$						Nonconforming, $p = 6$ and $p = 7$					
Grid	L^1	Rate	L^2	Rate	L^∞	Rate	L^1	Rate	L^2	Rate	L^∞	Rate
4	4.28E-04	-	3.14E-05	-	2.17E-02	-	3.84E-04	-	3.03E-05	-	2.35E-02	-
8	8.58E-06	-5.64	9.16E-07	-5.10	1.57E-03	-3.78	7.27E-06	-5.72	8.72E-07	-5.12	1.58E-03	-3.89
16	7.97E-08	-6.75	1.02E-08	-6.49	2.20E-05	-6.16	6.58E-08	-6.79	9.41E-09	-6.53	2.37E-05	-6.06
32	5.95E-10	-7.07	8.17E-11	-6.96	2.55E-07	-6.43	6.05E-10	-6.76	7.71E-11	-6.93	3.55E-07	-6.06

For all the degrees tested (i.e., $p = 1$ to $p = 7$), the order of convergence of the conforming algorithm is very close to that of the nonconforming. However, note that in the L^1 and L^2 norms the nonconforming algorithm is more accurate than the conforming one. In the discrete L^∞ norm, the nonconforming scheme is sometimes slightly worse than the conforming scheme; this results from the interpolation matrices being suboptimal at nonconforming interfaces.

7.2 Inviscid Taylor–Green vortex propagation

The purpose of this section is to numerically demonstrate the robustness of the nonconforming entropy stable algorithm. To do so, the inviscid Taylor–Green vortex problem is solved using a coarse grid with four elements in each coordinate direction.

The test case is solved on a periodic cube $[-\pi L \leq x, y, z \leq \pi L]$, where the initial condition is given by the initial condition used for the simulation of the standard (viscous) Taylor–Green problem:

$$\mathcal{U}_1 = \mathcal{V}_0 \sin\left(\frac{x_1}{L}\right) \cos\left(\frac{x_2}{L}\right) \cos\left(\frac{x_3}{L}\right), \mathcal{U}_2 = -\mathcal{V}_0 \cos\left(\frac{x_1}{L}\right) \sin\left(\frac{x_2}{L}\right) \cos\left(\frac{x_3}{L}\right),$$
$$\mathcal{U}_3 = 0, \mathcal{P} = \mathcal{P}_0 + \frac{\rho_0 \mathcal{V}_0^2}{16} \left[\cos\left(\frac{2x_1}{L} + \cos\left(\frac{2x_2}{L}\right)\right)\right] \left[\cos\left(\frac{2x_3}{L} + 2\right)\right].$$

The flow is initialized using $\mathcal{P}/\rho = \mathcal{P}_0/\rho_0 = R\mathcal{T}_0$, and $\mathcal{P}_0 = 1$, $\mathcal{T}_0 = 1$, $L = 1$, and $\mathcal{V}_0 = 1$. In order to obtain results that are reasonably close to those found for the incompressible equations, a Mach number of $M = 0.05$ is used.

The problem is simulated for twenty time units using an unstructured grid constructed as follows:

- Divide the computational domain with four hexahedral elements in each coordinate direction.
- Assign the solution polynomial degree in each element to a random integer chosen uniformly from a set $\{p_{min}, p_{max}\}$.
- Approximate the element interfaces with a p_{min}th accurate polynomial.
- Construct the perturbed elements and their corresponding LGL points as described in Section 7.1.

Figure 4 shows the time rate of change of the kinetic energy, dke/dt, for the nonconforming algorithm using a random distribution of solution polynomial order between i) $p_{min} = 2$ and $p_{max} = 7$ and ii) $p_{min} = 2$ and $p_{max} = 10$. The main takeaway from the figure is that all simulations are stable. This is numerical evidence that the p-nonconforming scheme inherits the stability characteristics of the conforming and fully staggered algorithms [5, 6, 9, 42, 44].

8 Conclusions

In this paper, the entropy conservative $p-$refinement/coarsening nonconforming algorithm of Friedrich *et al.* [25] is extended to curvilinear coordinates applicable to the compressible Euler equations. The coupling between nonconforming interfaces is achieved using SBP preserving interpolation operators and prescribed metric terms. To maintain entropy conservation/stability,

[1] In a general setting, element interfaces can also be boundary element interfaces.

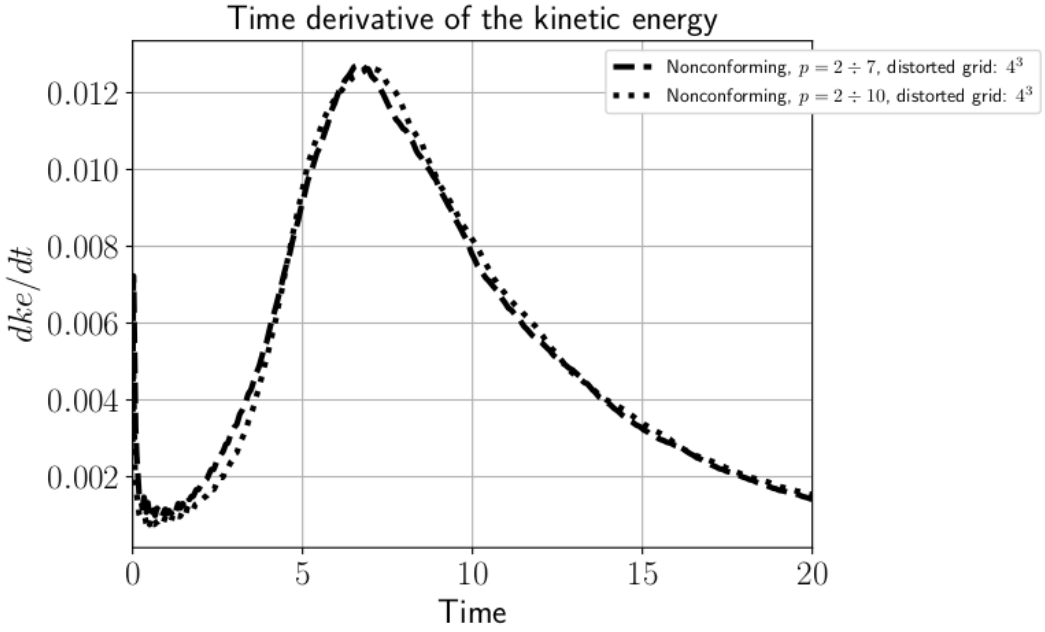

Figure 4. Evolution of the time derivative of the kinetic energy for the inviscid Taylor–Green vortex at $M = 0.05$.

elementwise conservation, and the order of the parent element, the procedure of Crean *et al.* [13] is used to approximate grid metrics. Finally, the accuracy and stability characteristics of the resulting numerical schemes are shown to be comparable to those of the original conforming scheme [5, 44], in the context of two canonical tests.

References

1. S. Abhyankar, J. Brown, E. M. Constantinescu, D. Ghosh, B. F. Smith, and H. Zhang, *PETSc/TS: A modern scalable ODE/DAE solver library*, arXiv preprint arXiv:1806.01437, (2018).

2. M. Almquist, S. Wang, and J. Werpers, *Order-preserving interpolation for summation-by-parts operators at nonconforming grid interfaces*, SIAM Journal on Scientific Computing, 41 (2019), p. A1201A1227.

3. O. Ålund and J. Nordström, *Encapsulated high order difference operators on curvilinear non-conforming grids*, Journal of Computational Physics, 385 (2019), pp. 209–224.

4. S. Balay, S. Abhyankar, M. F. Adams, J. Brown, P. Brune, K. Buschelman, L. Dalcin, A. Dener, V. Eijkhout, W. D. Gropp, D. Karpeyev, D. Kaushik, M. G. Knepley, D. A. May, L. C. McInnes, R. T. Mills, T. Munson, K. Rupp, P. Sanan, B. F. Smith, S. Zampini, H. Zhang, and H. Zhang, *PETSc users manual*, Tech. Report ANL-95/11 - Revision 3.11, Argonne National Laboratory, 2019.

5. M. H. Carpenter, T. C. Fisher, E. J. Nielsen, and S. H. Frankel, *Entropy stable spectral collocation schemes for the Navier–Stokes equations: discontinuous interfaces*, SIAM Journal on Scientific Computing, 36 (2014), pp. B835–B867.

6. M. H. Carpenter, T. C. Fisher, E. J. Nielsen, M. Parsani, M. Svärd, and N. Yamaleev, *Entropy stable summation-by-parts formulations for computational fluid dynamics*, Handbook of Numerical Analysis, (2016), pp. 495–524.

7. M. H. Carpenter, D. Gottlieb, and S. Abarbanel, *Time-stable boundary conditions for finite-difference schemes solving hyperbolic systems: Methodology and application to high-order compact schemes*, Journal of Computational Physics, 111 (1994), pp. 220–236.

8. M. H. Carpenter, M. Parsani, T. C. Fisher, and E. J. Nielsen, *Entropy stable staggered grid spectral collocation for the Burgers' and compressible Navier–Stokes equations*, NASA TM-2015-218990, (2015).

9. M. H. Carpenter, M. Parsani, T. C. Fisher, and E. J. Nielsen, *Towards and entropy stable spectral element framework for computational fluid dynamics*, in 54th AIAA Aerospace Sciences Meeting, AIAA 2016-1058, American Institute of Aeronautics and Astronautics (AIAA), 2016.

10. J. Chan, *On discretely entropy conservative and entropy stable discontinuous Galerkin methods*, Journal of Computational Physics, 362 (2018), pp. 346 – 374.

11. P. Chandrashekar, *Kinetic energy preserving and entropy stable finite volume schemes for compressible Euler and Navier–Stokes equations*, Communications in Computational Physics, 14 (2013), pp. 1252–1286.

12. T. Chen and C.-W. Shu, *Entropy stable high order discontinuous Galerkin methods with suitable quadrature rules for hyperbolic conservation laws*, Journal of Computational Physics, 345 (2017), pp. 427 – 461.

13. J. Crean, J. E. Hicken, D. C. Del Rey Fernández, D. W. Zingg, and M. H. Carpenter, *Entropy-stable summation-by-parts discretization of the Euler equations on general curved elements*, Journal of Computational Physics, 356 (2018), pp. 410 –438.

14. C. M. Dafermos, *Hyperbolic conservation laws in continuum physics*, Springer-Verlag, Berlin, 2010.

15. L. Dalcin, D. Rojas, S. Zampini, D. C. Del Rey Fernández, M. H. Carpenter, and M. Parsani, *Conservative and entropy stable solid wall boundary conditions for the compressible Navier–Stokes equations: Adiabatic wall and heat entropy transfer*, Journal of Computational Physics, 397 (2019).

16. D. C. Del Rey Fernández, P. D. Boom, and D. W. Zingg, *A generalized framework for nodal first derivative summation-by-parts operators*, Journal of Computational Physics, 266 (2014), pp. 214–239.

17. D. C. Del Rey Fernández, J. Crean, M. H. Carpenter, and J. E. Hicken, *Staggered entropy-stable summation-by-parts discretization of the Euler equations on general curved elements*, Journal of Computational Physics, 392 (2019), pp. 161–186.

18. D. C. Del Rey Fernández, J. E. Hicken, and D. W. Zingg, *Review of summation-by-parts operators with simultaneous approximation terms for the numerical solution of partial differential equations*, Computers & Fluids, 95 (2014), pp. 171–196.

19. J. R. Dormand and P. J. Prince, *A family of embedded Runge–Kutta formulae*, Journal of Computational and Applied Mathematics, 6 (1980), pp. 19 – 26.

20. T. C. Fisher, *High-order L^2 stable multi-domain finite difference method for compressible flows*, PhD thesis, Purdue University, August 2012.

21. T. C. Fisher and M. H. Carpenter, *High-order entropy stable finite difference schemes for nonlinear conservation laws: Finite domains*, Journal of Computational Physics, 252 (2013), pp. 518–557.

22. T. C. Fisher, M. H. Carpenter, J. Nordström, and N. K. Yamaleev, *Discretely conservative finite-difference formulations for nonlinear conservation laws in split form: Theory and boundary conditions*, Journal of Computational Physics, 234 (2013), pp. 353–375.

23. U. S. Fjordholm, S. Mishra, and E. Tadmor, *Arbitrarily high-order accurate entropy stable essentially nonoscillatory schemes for systems of conservation laws*, Communications in Computational Physics, 50 (2012), pp. 554–573.

24. L. Friedrich, G. Shnücke, A. R. Winters, D. C. Del Rey Fernández, G. J. Gassner, and M. H. Carpenter, *Entropy stable space-time discontinuous Galerkin schemes with summation-by-parts property for hyperbolic conservation laws*, Journal of Scientific Computing, 80 (2019), pp. 175–222.

25. L. Friedrich, A. R. Winters, D. C. Del Rey Fernández, G. J. Gassner, M. Parsani, and M. H. Carpenter, *An entropy stable h/p non-conforming discontinuous Galerkin method with the summation-by-parts property*, Journal of Scientific Computing, (2018), pp. 1–37.

26. M. Gerritsen and P. Olsson, *Designing an efficient solution strategy for fluid flows 1. A stable high order finite difference scheme and sharp shock resolution for the Euler equations*, Journal of Computational Physics, 129 (1996), pp. 245–262.

27. T. J. R. Hughes, L. P. Franca, and M. Mallet, *A new finite element formulation for computational fluid dynamics, I: symmetric forms of the compressible Navier–Stokes equations and the second law of thermodynamics*, Computer Methods in Applied Mechanics and Engineering, 54 (1986), pp. 223 – 234.

28. F. Ismail and P. L. Roe, *Affordable, entropy-consistent Euler flux functions II: entropy production at shocks*, Journal of Computational Physics, 228 (2009), pp. 5410–5436.

29. W. P. Johnsor, *The curious history of Fáa du Bruno's formula*, The American Mathematical Monthly, 109 (2002), pp. 217–234.

30. M. G. Knepley and D. A. Karpeev, *Mesh algorithms for PDE with Sieve I: Mesh distribution*, Scientific Programming, 17 (2009), pp. 215–230.

31. J. E. Kozdon and L. C. Wilcox, *Stable coupling of nonconforming, high-order finite difference methods*, SIAM Journal on Scientific Computing, 38 (2016), p. A923A952.

32. H.-O. Kreiss and J. Oliger, *Comparison of accurate methods for the integration of hyperbolic equations*, Tellus, 24 (1972), pp. 199–215.

33. P. Lax, *Hyperbolic Systems of Conservation Laws and the Mathematical Theory of Shock Waves*, Society for Industrial and Applied Mathematics, 1973.

34. P. D. Lax and B. Wendroff, *Systems of conservation laws*, Communications on pure and applied mathematics, 13 (1960), pp. 217–237.

35. R. J. LeVeque, *Numerical Methods for Conservation Laws*, Lectures in Mathematics ETH Zürich, Birkhäuser, 1992.

36. K. Mattsson and M. H. Carpenter, *Stable and accurate interpolation operators for high-order multiblock finite difference methods*, SIAM Journal on Scientific Computing, 32 (2010), pp. 2298–2320.

37. M. L. Merriam, *An entropy-based approach to nonlinear stability*, NASA TM-101086, (1989).

38. A. Nissen, K. Kormann, M. Grandin, and K. Virta, *Stable difference methods for block-oriented adaptive grids*, Journal of Scientific Computing, 65 (2015), pp. 486–511.

39. A. Nissen, G. Kreiss, and M. Gerritsen, *Stability at nonconforming grid interfaces for a high order discretization of the schrödinger equation*, Journal of Scientific Computing, 53 (2012), pp. 528–551.

40. J. Nordström and M. H. Carpenter, *Boundary and interface conditions for high-order finite-difference methods applied to the Euler and Navier–Stokes equations*, Journal of Computational Physics, 148 (1999), pp. 621–645.

41. P. Olsson and J. Oliger, *Energy and maximum norm estimates for nonlinear conservation laws*, Tech. Report 94–01, The Research Institute of Advanced Computer Science, 1994.

42. M. Parsani, M. H. Carpenter, T. C. Fisher, and E. J. Nielsen, *Entropy stable staggered grid discontinuous spectral collocation methods of any order for the compressible Navier–Stokes equations*, SIAM Journal on Scientific Computing, 38 (2016), pp. A3129–A3162.

43. M. Parsani, M. H. Carpenter, and E. J. Nielsen, *Entropy stable discontinuous interfaces coupling for the three-dimensional compressible Navier–Stokes equations*, Journal of Computational Physics, 290 (2015), pp. 132–138.

44. M. Parsani, M. H. Carpenter, and E. J. Nielsen, *Entropy stable wall boundary conditions for the three-dimensional compressible Navier–Stokes equations*, Journal of Computational Physics, 292 (2015), pp. 88–113.

45. H. Ranocha, M. Sayyari, L. Dalcin, M. Parsani, and D. I. Ketcheson, *Relaxation Runge–Kutta methods: Fully-discrete explicit entropy-stable schemes for the Euler and Navier–Stokes equations*, (2019). Submitted to SIAM Journal on Scientific Computing.

46. D. Ray, P. Chandrashekar, U. S. Fjordhom, and S. Mishra, *Entropy stable scheme on two-dimensional unstructured grids for Euler equations*, Communications in Computational Physics, 19 (2016), pp. 1111–1140.

47. N. D. Sandham, Q. Li, and H. C. Yee, *Entropy splitting for high-order numerical simulation of compressible turbulence*, Journal of Computational Physics, 178 (2002), pp. 307–322.

48. C. Shi and C.-W. Shu, *On local conservation of numerical methods for conservation laws*, Computers & Fluids, 169 (2018), pp. 3–9.

49. B. Sjögren and H. C. Yee, *High order entropy conservative central schemes for wide ranges of compressible gas dynamics and MHD flows*, Journal of Computational Physics, 364 (2018), pp. 153–185.

50. G. Söderlind, *Digital filters in adaptive time-stepping*, ACM Transactions on Mathematical Software, 29 (2003), pp. 1–26.

51. G. Söderlind and L. Wang, *Adaptive time-stepping and computational stability*, Journal of Computational and Applied Mathematics, 185 (2006), pp. 225–243.

52. M. Svärd, *Weak solutions and convergent numerical schemes of modified compressible Navier–Stokes equations*, Journal of Computational Physics, 288 (2015), pp. 19–51.

53. M. Svärd, M. H. Carpenter, and M. Parsani, *Entropy stability and the no-slip wall boundary condition*, SIAM Journal on Numerical Analysis, 56 (2018), pp. 256–273.

54. M. Svärd and J. Nordström, *Review of summation-by-parts schemes for initial-boundary-value-problems*, Journal of Computational Physics, 268 (2014), pp. 17–38.

55. B. Swartz and B. Wendroff, *The relative efficiency of finite difference and finite element methods. I: Hyperbolic problems and splines*, SIAM Journal on Numerical Analysis, 11 (1974), pp. 979–993.

56. E. Tadmor, *The numerical viscosity of entropy stable schemes for systems of conservation laws I*, Mathematics of Computation, 49 (1987), pp. 91–103.

57. E. Tadmor, *Entropy stability theory for difference approximations of nonlinear conservation laws and related time-dependent problems*, Acta Numerica, 12 (2003), pp. 451–512.

58. D. Thomas and C. K. Lombard, *Geometric conservation law and its application to flow computations on moving grids*, AIAA Journal, 17 (1979), pp. 1030–1037.

59. M. Vinokur and H. C. Yee, *Extension of efficient low dissipation high order schemes for 3-d curvilinear moving grids*, in Frontiers of Computational Fluid Dynamics, D. A. Caughey and M. Hafez, eds., World Scientific Publishing Company, 2002, pp. 129–164.

60. S. Wang, *An improved high order finite difference method for non-conforming grid interfaces for the wave equation*, Journal of Scientific Computing, 77 (2018), pp. 775–792.

61. S. Wang, K. Virta, and G. Kreiss, *High order finite difference methods for the wave equation with non-conforming grid interfaces*, Journal of Scientific Computing, 68 (2016), pp. 1002–1028.

62. A. R. Winters, D. Derigs, G. J. Gassner, and S. Walch, *Uniquely defined entropy stable matrix dissipation operator for high Mach number ideal MHD and compressible Euler simulations*, Journal of Computational Physics, 332 (2017), pp. 274–289.

63. A. R. Winters and G. J.Gassner, *A comparison of two entropy stable discontinuous Galerkin spectral element approximations to the shallow water equations with non-constant topography*, Journal of Computational Physics, 301 (2015), pp. 357–376.

64. N. K. Yamaleev and M. H. Carpenter, *A family of fourth-order entropy stable non-oscillatory spectral collocation schemes for the 1-d Navier-Stokes equations*, Journal of Computational Physics, 331 (2017), pp. 90–107.

65. H. C. Yee, M. Vinokur, and M. J. Djomehri, *Entropy splitting and numerical dissipation*, Journal of Computational Physics, 162 (2000), pp. 33–81.

Appendix A

Generalized notation and nonlinear analysis

The various proofs presented in these appendices are greatly simplified (and also generalized) by using notation appropriate for multidimensional SBP operators. In this section, the notation that will be used in the appendices is presented and linked to the tensor-product notation used in the paper. Furthermore, the nonlinear approximation used to construct entropy conservative discretizations will be analyzed in detail.

A.1 Generalized notation

The derivative operators that are used are constructed using tensor-products. For a system of e PDEs they read

$$\begin{aligned}
\mathsf{D}_{\xi_1} &\equiv \overline{\mathsf{D}}_{\xi_1} \otimes \mathsf{I}_e, \quad \overline{\mathsf{D}}_{\xi_1} \equiv \mathsf{D}_{\xi_1}^{(1D)} \otimes \mathsf{I}_{N_2} \otimes \mathsf{I}_{N_3}, \\
\mathsf{D}_{\xi_2} &\equiv \overline{\mathsf{D}}_{\xi_2} \otimes \mathsf{I}_e, \quad \overline{\mathsf{D}}_{\xi_2} \equiv \mathsf{I}_{N_1} \otimes \mathsf{D}_{\xi_2}^{(1D)} \otimes \mathsf{I}_{N_3}, \\
\mathsf{D}_{\xi_3} &\equiv \overline{\mathsf{D}}_{\xi_3} \otimes \mathsf{I}_e, \quad \overline{\mathsf{D}}_{\xi_3} \equiv \mathsf{I}_{N_1} \otimes \mathsf{I}_{N_2} \otimes \mathsf{D}_{\xi_3}^{(1D)}.
\end{aligned}$$

The above tensor-product SBP operators can be recast as multidimensional SBP operators as follows:

$$\begin{aligned}
\mathsf{D}_{\xi_1} &= \mathsf{P}^{-1}\mathsf{Q}_{\xi_1}, \quad \mathsf{Q}_{\xi_1} \equiv \overline{\mathsf{Q}}_{\xi_1} \otimes \mathsf{I}_e, \quad \overline{\mathsf{Q}}_{\xi_1} \equiv \mathsf{Q}_{\xi_1}^{(1D)} \otimes \mathsf{P}_{\xi_2}^{(1D)} \otimes \mathsf{P}_{\xi_3}^{(1D)}, \\
\mathsf{D}_{\xi_2} &= \mathsf{P}^{-1}\mathsf{Q}_{\xi_2}, \quad \mathsf{Q}_{\xi_2} \equiv \overline{\mathsf{Q}}_{\xi_2} \otimes \mathsf{I}_e, \quad \overline{\mathsf{Q}}_{\xi_2} \equiv \mathsf{P}_{\xi_1}^{(1D)} \otimes \mathsf{Q}_{\xi_2}^{(1D)} \otimes \mathsf{P}_{\xi_3}^{(1D)}, \\
\mathsf{D}_{\xi_3} &= \mathsf{P}^{-1}\mathsf{Q}_{\xi_3}, \quad \mathsf{Q}_{\xi_3} \equiv \overline{\mathsf{Q}}_{\xi_3} \otimes \mathsf{I}_e, \quad \overline{\mathsf{Q}}_{\xi_3} \equiv \mathsf{P}_{\xi_1}^{(1D)} \otimes \mathsf{P}_{\xi_2}^{(1D)} \otimes \mathsf{Q}_{\xi_3}^{(1D)}, \\
\mathsf{P} &\equiv \overline{\mathsf{P}} \otimes \mathsf{I}_e, \quad \overline{\mathsf{P}} \equiv \mathsf{P}_{\xi_1}^{(1D)} \otimes \mathsf{P}_{\xi_2}^{(1D)} \otimes \mathsf{P}_{\xi_3}^{(1D)}.
\end{aligned}$$

The resulting recast of the tensor-product SBP operators as multidimensional SBP operators respects the SBP property, i.e., $\mathsf{Q}_{\xi_l} + \mathsf{Q}_{\xi_l}^{\mathrm{T}} = \mathsf{E}_{\xi_l}$, where the surface matrices E_{ξ_l} are given as

$$\begin{aligned}
\mathsf{E}_{\xi_1} &= \overline{\mathsf{E}}_{\xi_1} \otimes \mathsf{I}_e, \quad \overline{\mathsf{E}}_{\xi_1} \equiv \left(\boldsymbol{e}_{N_1}\boldsymbol{e}_{N_1}^{\mathrm{T}} - \boldsymbol{e}_{1_1}\boldsymbol{e}_{1_1}^{\mathrm{T}}\right) \otimes \mathsf{P}_{\xi_2}^{(1D)} \otimes \mathsf{P}_{\xi_3}^{(1D)}, \\
\mathsf{E}_{\xi_2} &= \overline{\mathsf{E}}_{\xi_2} \otimes \mathsf{I}_e, \quad \overline{\mathsf{E}}_{\xi_2} \equiv \mathsf{P}_{\xi_1}^{(1D)} \otimes \left(\boldsymbol{e}_{N_2}\boldsymbol{e}_{N_2}^{\mathrm{T}} - \boldsymbol{e}_{1_2}\boldsymbol{e}_{1_2}^{\mathrm{T}}\right) \otimes \mathsf{P}_{\xi_3}^{(1D)}, \\
\mathsf{E}_{\xi_3} &= \overline{\mathsf{E}}_{\xi_3} \otimes \mathsf{I}_e, \quad \overline{\mathsf{E}}_{\xi_3} \equiv \mathsf{P}_{\xi_1}^{(1D)} \otimes \mathsf{P}_{\xi_2}^{(1D)} \otimes \left(\boldsymbol{e}_{N_3}\boldsymbol{e}_{N_3}^{\mathrm{T}} - \boldsymbol{e}_{1_3}\boldsymbol{e}_{1_3}^{\mathrm{T}}\right).
\end{aligned}$$

In precisely the same way that the one-dimensional E can be decomposed into separate surface contributions, i.e., $\mathsf{E} = \boldsymbol{e}_N\boldsymbol{e}_N^{\mathrm{T}} - \boldsymbol{e}_1\boldsymbol{e}_1^{\mathrm{T}}$, the multidimensional E given above can be decomposed into contributions to the faces of the hexahedral element. Thus, E_{ξ_1} is decomposed as

$$\begin{aligned}
&\mathsf{E}_{\xi_1} = \mathsf{E}_{\beta_1} - \mathsf{E}_{\alpha_1}, \quad \mathsf{E}_{\beta_1} \equiv \mathsf{R}_{\beta_1}^{\mathrm{T}}\mathsf{P}_{\perp\xi_1}\mathsf{R}_{\beta_1}, \qquad \mathsf{E}_{\alpha_1} \equiv \mathsf{R}_{\alpha_1}^{\mathrm{T}}\mathsf{P}_{\perp\xi_1}\mathsf{R}_{\alpha_1}, \\
&\mathsf{R}_{\beta_1} \equiv \overline{\mathsf{R}}_{\beta_1} \otimes \mathsf{I}_e, \quad \overline{\mathsf{R}}_{\beta_1} \equiv \boldsymbol{e}_{1_{N_1}}^{\mathrm{T}} \otimes \mathsf{I}_{N_2} \otimes \mathsf{I}_{N_3}, \\
&\mathsf{R}_{\alpha_1} \equiv \overline{\mathsf{R}}_{\alpha_1} \otimes \mathsf{I}_e, \quad \overline{\mathsf{R}}_{\alpha_1} \equiv \boldsymbol{e}_{1_1}^{\mathrm{T}} \otimes \mathsf{I}_{N_2} \otimes \mathsf{I}_{N_3}, \\
&\mathsf{P}_{\perp\xi_1} \equiv \overline{\mathsf{P}}_{\perp\xi_1} \otimes \mathsf{I}_e, \quad \overline{\mathsf{P}}_{\perp\xi_1} \equiv \mathsf{P}_{\xi_2}^{(1D)} \otimes \mathsf{P}_{\xi_3}^{(1D)},
\end{aligned}$$

E_{ξ_2} is decomposed as

$$\begin{aligned}
&\mathsf{E}_{\xi_2} = \mathsf{E}_{\beta_2} - \mathsf{E}_{\alpha_2}, \quad \mathsf{E}_{\beta_2} \equiv \mathsf{R}_{\beta_2}^{\mathrm{T}} \mathsf{P}_{\perp\xi_2} \mathsf{R}_{\beta_2}, \quad \mathsf{E}_{\alpha_2} \equiv \mathsf{R}_{\alpha_2}^{\mathrm{T}} \mathsf{P}_{\perp\xi_2} \mathsf{R}_{\alpha_2},\\
&\mathsf{R}_{\beta_2} \equiv \overline{\mathsf{R}}_{\beta_2} \otimes \mathsf{I}_e, \quad \overline{\mathsf{R}}_{\beta_2} \equiv \mathsf{I}_{N_1} \otimes \boldsymbol{e}_{1_{N_2}}^{\mathrm{T}} \otimes \mathsf{I}_{N_3},\\
&\mathsf{R}_{\alpha_2} \equiv \overline{\mathsf{R}}_{\alpha_2} \otimes \mathsf{I}_e, \quad \overline{\mathsf{R}}_{\alpha_2} \equiv \mathsf{I}_{N_1} \otimes \boldsymbol{e}_{1_1}^{\mathrm{T}} \otimes \mathsf{I}_{N_3},\\
&\mathsf{P}_{\perp\xi_2} \equiv \overline{\mathsf{P}}_{\perp\xi_2} \otimes \mathsf{I}_e, \quad \overline{\mathsf{P}}_{\perp\xi_2} \equiv \mathsf{P}_{\xi_1}^{(1D)} \otimes \mathsf{P}_{\xi_3}^{(1D)},
\end{aligned}$$

and E_{ξ_3} is decomposed as

$$\begin{aligned}
&\mathsf{E}_{\xi_3} = \mathsf{E}_{\beta_3} - \mathsf{E}_{\alpha_3}, \quad \mathsf{E}_{\beta_2} \equiv \mathsf{R}_{\beta_3}^{\mathrm{T}} \mathsf{P}_{\perp\xi_3} \mathsf{R}_{\beta_3}, \quad \mathsf{E}_{\alpha_3} \equiv \mathsf{R}_{\alpha_3}^{\mathrm{T}} \mathsf{P}_{\perp\xi_3} \mathsf{R}_{\alpha_3},\\
&\mathsf{R}_{\beta_3} \equiv \overline{\mathsf{R}}_{\beta_3} \otimes \mathsf{I}_e, \quad \overline{\mathsf{R}}_{\beta_3} \equiv \mathsf{I}_{N_1} \otimes \mathsf{I}_{N_2} \otimes \boldsymbol{e}_{1_{N_3}}^{\mathrm{T}},\\
&\mathsf{R}_{\alpha_3} \equiv \overline{\mathsf{R}}_{\alpha_3} \otimes \mathsf{I}_e, \quad \overline{\mathsf{R}}_{\alpha_3} \equiv \mathsf{I}_{N_1} \otimes \mathsf{I}_{N_2} \otimes \boldsymbol{e}_{1_3}^{\mathrm{T}},\\
&\mathsf{P}_{\perp\xi_3} \equiv \overline{\mathsf{P}}_{\perp\xi_3} \otimes \mathsf{I}_e, \quad \overline{\mathsf{P}}_{\perp\xi_3} \equiv \mathsf{P}_{\xi_1}^{(1D)} \otimes \mathsf{P}_{\xi_2}^{(1D)}.
\end{aligned}$$

To give further insight into the properties of the above operators, a connection to various bilinear forms is given:

$$\boldsymbol{v}^{\mathrm{T}} \overline{\mathsf{P}} \boldsymbol{u} \equiv \int_{\hat{\Omega}} \mathcal{V}\mathcal{U} \mathrm{d}\hat{\Omega}, \qquad \boldsymbol{v}^{\mathrm{T}} \overline{\mathsf{Q}}_{\xi_l} \boldsymbol{u} \equiv \int_{\hat{\Omega}} \mathcal{V} \frac{\partial \mathcal{U}}{\partial \xi_l} \mathrm{d}\hat{\Omega},$$

$$\boldsymbol{v}^{\mathrm{T}} \overline{\mathsf{E}}_{\xi_l} \boldsymbol{u} \approx \oint_{\hat{\Gamma}} \mathcal{V}\mathcal{U} n_{\xi_l} \mathrm{d}\hat{\Gamma},$$

$$\boldsymbol{v}^{\mathrm{T}} \bar{\mathsf{E}}_{\beta_l} \boldsymbol{u} \approx \oint_{\hat{\Gamma}_{\beta_l}} \mathcal{V}\mathcal{U} n_{\xi_l} \mathrm{d}\hat{\Gamma}, \quad \boldsymbol{v}^{\mathrm{T}} \bar{\mathsf{E}}_{\alpha_l} \boldsymbol{u} \approx \oint_{\hat{\Gamma}_{\alpha_l}} \mathcal{V}\mathcal{U} n_{\xi_l} \mathrm{d}\hat{\Gamma},$$

where $\hat{\Gamma}_{\beta_l}$ is the surface of the hexahedral element where ξ_l is at a maximum and $\hat{\Gamma}_{\alpha_l}$ is the surface where ξ_l is at a minimum. Furthermore, the operators $\overline{\mathsf{R}}_{\beta_l}$ and $\overline{\mathsf{R}}_{\alpha_l}$ interpolate to the nodes of the $\hat{\Gamma}_{\beta_l}$ and $\hat{\Gamma}_{\alpha_l}$ surfaces, respectively.

A.2 Analysis of the nonlinear discretization

SBP operators are constructed so that the continuous stability proofs can be mimicked at the semidiscrete and fully-discrete levels. The critical property that is needed is that, like the continuous analysis, the spatial (and temporal in the fully discrete case) terms telescope to the boundaries. Then, if appropriate numerical boundary closures can be found, discrete stability statements can be constructed. Often times this is linked to the schemes mimicking integration by parts (this is what is used at the continuous level). However, any combination of differentiation matrix D and norm matrix P is mimetic of integration by parts. It is the fact that SBP operators result into (nodewise) separable approximations to surface integrals that allows stability estimates to be constructed.

The telescoping notion is best explained by carefully examining how SBP operators mimic integration by parts. In multiple dimensions, integration by parts on a hexahedral element is given as

$$\oint_{\hat{\Omega}} \left(\mathcal{V} \frac{\partial \mathcal{U}}{\partial \xi_l} + \mathcal{U} \frac{\partial \mathcal{V}}{\partial \xi_l} \right) \mathrm{d}\hat{\Omega} = \oint_{\hat{\Gamma}} \left(\mathcal{V}\mathcal{U} n_{\xi_l} \right) \mathrm{d}\hat{\Gamma} = \oint_{\hat{\Gamma}_{\beta l}} \left(\mathcal{V}\mathcal{U} n_{\xi_l} \right) \mathrm{d}\hat{\Gamma} + \oint_{\hat{\Gamma}_{\alpha l}} \left(\mathcal{V}\mathcal{U} n_{\xi_l} \right) \mathrm{d}\hat{\Gamma}. \tag{A1}$$

Discretizing the left-hand side of (A1) using SBP operators and their properties results in the following equality:

$$\boldsymbol{v}^{\mathrm{T}} \overline{\mathsf{PD}}_{\xi_l} \boldsymbol{u} + \boldsymbol{u} \overline{\mathsf{PD}}_{\xi_l} \boldsymbol{v} = \boldsymbol{v}^{\mathrm{T}} \overline{\mathsf{E}}_{\xi_l} \boldsymbol{u}. \tag{A2}$$

Each term in (A2) is a high-order approximation to the analogous term in integration by parts formula (A1). Notice, though, that this would also occur for a discretization of (A1) constructed for any combination of a high-order norm matrix, that approximates the inner product, and a high-order derivative operator.

However, the SBP operator has an E matrix that can be further decomposed into separate contributions from opposing surfaces (this property does not in general hold for arbitrary combinations of P and D), namely

$$\boldsymbol{v}^{\mathrm{T}}\overline{\mathsf{PD}}_{\xi_l}\boldsymbol{u} + \boldsymbol{u}\overline{\mathsf{PD}}_{\xi_l}\boldsymbol{v} = \boldsymbol{v}^{\mathrm{T}}\bar{\mathsf{E}}_{\beta_l}\boldsymbol{u} - \boldsymbol{v}^{\mathrm{T}}\bar{\mathsf{E}}_{\alpha_l}\boldsymbol{u}. \tag{A3}$$

Now the right-hand side of (A2) has been decomposed in terms of contributions to the $\hat{\Gamma}^{\beta_l}$ and $\hat{\Gamma}^{\alpha_l}$ surfaces; this is still insufficient unless one is happy with imposing the same boundary condition over the entire face. What is needed is the ability to impose boundary conditions pointwise. The next decomposition demonstrates that a pointwise interpretation of the telescoping property is possible:

$$\boldsymbol{v}^{\mathrm{T}}\overline{\mathsf{PD}}_{\xi_l}\boldsymbol{u} + \boldsymbol{u}\overline{\mathsf{PD}}_{\xi_l}\boldsymbol{v} = \left(\overline{\mathsf{R}}_{\beta_l}\boldsymbol{v}\right)^{\mathrm{T}}\overline{\mathsf{P}}_{\perp\xi_l}\overline{\mathsf{R}}_{\beta_l}\boldsymbol{u} - \left(\overline{\mathsf{R}}_{\alpha_l}\boldsymbol{v}\right)^{\mathrm{T}}\overline{\mathsf{P}}_{\perp\xi_l}\overline{\mathsf{R}}_{\alpha_l}\boldsymbol{u}. \tag{A4}$$

To see why the right-hand side is separable, pointwise, consider the term $\left(\overline{\mathsf{R}}_{\beta_l}\boldsymbol{v}\right)^{\mathrm{T}}\overline{\mathsf{P}}_{\perp\xi_l}\overline{\mathsf{R}}_{\beta_l}\boldsymbol{u}$. The action of R_{α_l} is to interpolate $\boldsymbol{v}$ or $\boldsymbol{u}$ to the $\hat{\Gamma}_{\beta_l}$ boundary. Defining the vectors $\boldsymbol{v}_{\hat{\Gamma}_{\beta_l}} \equiv \overline{\mathsf{R}}_{\beta_l}\boldsymbol{v}$ and $\boldsymbol{u}_{\hat{\Gamma}_{\beta_l}} \equiv \overline{\mathsf{R}}_{\beta_l}\boldsymbol{u}$ gives

$$\left(\overline{\mathsf{R}}_{\beta_l}\boldsymbol{v}\right)^{\mathrm{T}}\overline{\mathsf{P}}_{\perp\xi_l}\overline{\mathsf{R}}_{\beta_l}\boldsymbol{u} = \boldsymbol{v}_{\hat{\Gamma}_{\beta_l}}^{\mathrm{T}}\,\overline{\mathsf{P}}_{\perp\xi_l}\boldsymbol{u}_{\hat{\Gamma}_{\beta_l}}. \tag{A5}$$

Since $\overline{\mathsf{P}}_{\perp\xi_l}$ is diagonal, this means that the surface nodes can be traversed and at each node an appropriate boundary condition can be imposed.

The nonlinear approximations used in this paper, constructed from SBP operators and two-point flux function matrices, poses the same type of properties as the above SBP operators. Namely, the result has the telescoping property and is mimetic of the following (nonlinear) form of integration by parts

$$\frac{1}{2}\sum_{l,m=1}^{3}\int_{\hat{\Omega}}\mathcal{W}^{\mathrm{T}}\left\{\frac{\partial}{\partial\xi_l}\left(\mathcal{J}_\kappa\frac{\partial\xi_l}{\partial x_m}\boldsymbol{\mathcal{F}}_{x_m}\right) + \mathcal{J}_\kappa\frac{\partial\xi_l}{\partial x_m}\frac{\partial\boldsymbol{\mathcal{F}}_{x_m}}{\partial\xi_l}\right\}\mathrm{d}\hat{\Omega} = \sum_{l,m=1}^{3}\oint_{\hat{\Gamma}}\left(\mathcal{J}_\kappa\frac{\partial\xi_l}{\partial x_m}\mathcal{F}_{x_m}n_{\xi_l}\right)\mathrm{d}\hat{\Gamma}. \tag{A6}$$

The steps that will be taken to demonstrate that the nonlinear approximation has the telescoping property and is mimetic of (A6) are as follows:

1. Characterize the error properties of the nonlinear approximations to the derivatives, i.e., the terms $\left(2\mathsf{D}_{\xi_l}^{\kappa}\left[\mathcal{A}\right]_\kappa\right)\circ\mathsf{F}_{x_m}\left(\boldsymbol{q}_\kappa,\boldsymbol{q}_\kappa\right)\mathbf{1}_\kappa$ and $\left(2\left[\mathcal{A}\right]_\kappa\mathsf{D}_{\xi_l}^{\kappa}\right)\circ\mathsf{F}_{x_m}\left(\boldsymbol{q}_\kappa,\boldsymbol{q}_\kappa\right)\mathbf{1}_\kappa$.

2. Contract the spatial terms with the entropy variables and discretely integrate over an element/macroelement, discretely mimicking the same steps at the continuous level, and demonstrate that the result telescopes.

3. Characterize the error properties of the discrete bilinear forms induced by the on-volume contributions to the SATs, i.e., the terms

$$\boldsymbol{v}_\kappa^{\mathrm{T}}\left(\overline{\mathsf{E}}_{\xi_l}^{\kappa}\overline{\left[\mathcal{J}\frac{\partial\xi_l}{\partial x_m}\right]}_\kappa\right)\circ\mathsf{F}_{x_m}^{[i]}\left(\boldsymbol{q}_\kappa,\boldsymbol{q}_\kappa\right)\overline{\mathbf{1}}_\kappa \text{ and } \boldsymbol{v}_\kappa^{\mathrm{T}}\left(\overline{\left[\mathcal{J}\frac{\partial\xi_l}{\partial x_m}\right]}_\kappa\overline{\mathsf{E}}_{\xi_l}^{\kappa}\right)\circ\mathsf{F}_{x_m}^{[i]}\left(\boldsymbol{q}_\kappa,\boldsymbol{q}_\kappa\right)\overline{\mathbf{1}}_\kappa$$

and therefore demonstrate that the telescoping form is discretely mimetic of (A6).

The starting point is to demonstrate that the nonlinear approximation is both telescoping and mimetic of (A6) is to analyze the error properties of the nonlinear approximation. The following is a general result on the accuracy of the nonlinear approximations and is an extension of the proof give in Crean *et al.* [13].

Theorem 6. *Let $\mathsf{D}_{\xi_l}^{\kappa}$ be any degree p finite-difference approximation to the first derivative $\partial/\partial\xi_l$, on a set of nodes $\boldsymbol{\xi}$. Consider a PDE whose fluxes in the x_m, $m=1,2,3$, coordinate directions are continuously differentiable functions $\boldsymbol{\mathcal{F}}_{x_m}:\mathbb{R}^5\to\mathbb{R}^5$ and a variable coefficient $\mathcal{A}_\kappa$ that is sufficiently smooth. If $\boldsymbol{f}_{x_m}^{sc}\left(\boldsymbol{u},\boldsymbol{v}\right):\mathbb{R}^5\times\mathbb{R}^5\to\mathbb{R}^5$ are dyadic functions that are continuously differentiable, symmetric in their arguments, and satisfy $\boldsymbol{f}_{x_m}^{sc}\left(\boldsymbol{q}_\kappa^{(i)},\boldsymbol{q}_\kappa^{(i)}\right)=\boldsymbol{\mathcal{F}}_{x_m}\left(\boldsymbol{q}_\kappa^{(i)}\right)$, then for sufficiently smooth solutions $\boldsymbol{\mathcal{Q}}$*

$$\begin{aligned}
\left(2\mathsf{D}_{\xi_l}^{\kappa}\left[\mathcal{A}\right]_\kappa\right)\circ\mathsf{F}_{x_m}\left(\boldsymbol{q}_\kappa,\boldsymbol{q}_\kappa\right)\mathbf{1}_\kappa&=\left(\frac{\partial\left(\mathcal{A}\boldsymbol{\mathcal{F}}_{x_m}\right)}{\partial\xi_l}\right)\left(\boldsymbol{\xi}_\kappa\right)+\left(\boldsymbol{\mathcal{F}}_{x_m}\frac{\partial\mathcal{A}}{\partial\xi_l}\right)\left(\boldsymbol{\xi}_\kappa\right)+\mathcal{O}\left(h^{p+1}\right),\\
\left(2\left[\mathcal{A}\right]_\kappa\mathsf{D}_{\xi_l}^{\kappa}\right)\circ\mathsf{F}_{x_m}\left(\boldsymbol{q}_\kappa,\boldsymbol{q}_\kappa\right)\mathbf{1}_\kappa&=\left(\mathcal{A}\frac{\partial\boldsymbol{\mathcal{F}}_{x_m}}{\partial\xi_l}\right)\left(\boldsymbol{\xi}_\kappa\right)+\mathcal{O}\left(h^{p+1}\right),
\end{aligned}\tag{A7}$$

where $\left[\mathcal{A}\right]_\kappa$ is a diagonal matrix containing, along its diagonal, the evaluation of the variable coefficient at the mesh nodes $\boldsymbol{\xi}_\kappa$, and h is some appropriate measure of the mesh spacing within the element.

Proof. The proof is given in B □

Theorem 6 implies that

$$\begin{aligned}
\left(2\mathsf{D}_{\xi_l}^{\kappa}\left[\mathcal{J}\frac{\partial\xi_l}{\partial x_m}\right]_\kappa\right)\circ\mathsf{F}_{x_m}\left(\boldsymbol{q}_\kappa,\boldsymbol{q}_\kappa\right)\mathbf{1}_\kappa&=\left(\frac{\partial\left(\mathcal{J}_\kappa\frac{\partial\xi_l}{\partial x_m}\boldsymbol{\mathcal{F}}_{x_m}\right)}{\partial\xi_l}\right)\left(\boldsymbol{\xi}_\kappa\right)+\left(\boldsymbol{\mathcal{F}}_{x_m}\frac{\partial\mathcal{J}_\kappa\frac{\partial\xi_l}{\partial x_m}}{\partial\xi_l}\right)\left(\boldsymbol{\xi}_\kappa\right)+\mathcal{O}\left(h^{p+d}\right),\\
\left(2\left[\mathcal{J}\frac{\partial\xi_l}{\partial x_m}\right]_\kappa\mathsf{D}_{\xi_l}^{\kappa}\right)\circ\mathsf{F}_{x_m}\left(\boldsymbol{q}_\kappa,\boldsymbol{q}_\kappa\right)\mathbf{1}_\kappa&=\left(\mathcal{J}_\kappa\frac{\partial\xi_l}{\partial x_m}\frac{\partial\boldsymbol{\mathcal{F}}_{x_m}}{\partial\xi_l}\right)\left(\boldsymbol{\xi}_\kappa\right)+\mathcal{O}\left(h^{p+d}\right),
\end{aligned}\tag{A8}$$

where the change in the truncation terms comes from the fact that $\mathcal{J}_\kappa\frac{\partial\xi_l}{\partial x_m}\propto h^{d-1}$, i.e., the variable coefficient $\mathcal{A}$ in Theorem 6 is treated as a dimensionless quantity. Notice that summing the first equality in the three computational directions and using the continuous GCL gives that

$$\sum_{l=1}^{3}\left(2\mathsf{D}_{\xi_l}^{\kappa}\left[\mathcal{J}\frac{\partial\xi_l}{\partial x_m}\right]_\kappa\right)\circ\mathsf{F}_{x_m}\left(\boldsymbol{q}_\kappa,\boldsymbol{q}_\kappa\right)\mathbf{1}_\kappa=\sum_{l=1}^{3}\left(\frac{\partial\left(\mathcal{J}_\kappa\frac{\partial\xi_l}{\partial x_m}\boldsymbol{\mathcal{F}}_{x_m}\right)}{\partial\xi_l}\right)\left(\boldsymbol{\xi}_\kappa\right)+\mathcal{O}\left(h^{p+d}\right).\tag{A9}$$

In order to demonstrate the telescoping flux form, the following general result is necessary

Theorem 7. *Consider the matrix of* $\overline{\mathsf{A}}$ *of size* $N_\kappa \times N_r$ *with a tensor extension* $\mathsf{A} \equiv \overline{\mathsf{A}} \otimes \mathsf{I}_5$, *and a two argument matrix flux function* $\mathsf{F}_{x_m}(\boldsymbol{q}_\kappa, \boldsymbol{q}_r)$ *constructed from the two point flux function* $\boldsymbol{f}^{sc}_{x_m}\left(\boldsymbol{q}^{(i)}_\kappa, \boldsymbol{q}^{(j)}_r\right)$ *that satisfies the Tadmor shuffle condition*

$$\left(\boldsymbol{w}^{(i)}_\kappa - \boldsymbol{w}^{(j)}_r\right)^{\mathrm{T}} \boldsymbol{f}^{sc}_{x_m}\left(\boldsymbol{q}^{(i)}_\kappa, \boldsymbol{q}^{(j)}_r\right) = \left(\boldsymbol{\psi}^\kappa_{x_m}\right)^{(i)} - \left(\boldsymbol{\psi}^r_{x_m}\right)^{(j)}$$

and is symmetric, i.e., $\boldsymbol{f}^{sc}_{x_m}\left(\boldsymbol{q}^{(i)}_\kappa, \boldsymbol{q}^{(j)}_r\right) = \boldsymbol{f}^{sc}_{x_m}\left(\boldsymbol{q}^{(j)}_r, \boldsymbol{q}^{(i)}_\kappa\right)$, *then*

$$\boldsymbol{w}_{\mathrm{T}}(\mathsf{A}) \circ \mathsf{F}_{x_m}(\boldsymbol{q}_\kappa, \boldsymbol{q}_r)\,\mathbf{1}_r - \mathbf{1}^{\mathrm{T}}_\kappa \mathsf{A} \circ \mathsf{F}_{x_m}(\boldsymbol{q}_\kappa, \boldsymbol{q}_r)\,\boldsymbol{w}_r = \left(\boldsymbol{\psi}^\kappa_{x_m}\right)^{\mathrm{T}} \overline{\mathsf{A}}\overline{\mathbf{1}}_r - \overline{\mathbf{1}}^{\mathrm{T}}_\kappa \overline{\mathsf{A}} \boldsymbol{\psi}^r_{x_m}.$$

Proof.

$$\begin{aligned}
&\boldsymbol{w}_{\mathrm{T}}(\mathsf{A}) \circ \mathsf{F}_{x_m}(\boldsymbol{q}_\kappa, \boldsymbol{q}_r)\,\mathbf{1}_r - \mathbf{1}^{\mathrm{T}}_\kappa \mathsf{A} \circ \mathsf{F}_{x_m}(\boldsymbol{q}_\kappa, \boldsymbol{q}_r)\,\boldsymbol{w}_r = \\
&\sum_{i=1}^{N_\kappa}\sum_{j=1}^{N_r}\left\{\overline{\mathsf{A}}(i,j)\left(\boldsymbol{w}^{(i)}_\kappa\right)^{\mathrm{T}} \mathsf{F}_{x_m}\left(\boldsymbol{q}^{(i)}_\kappa, \boldsymbol{q}^{(i)}_r\right) - \overline{\mathsf{A}}(i,j)\left(\boldsymbol{w}^{(j)}_r\right)^{\mathrm{T}} \mathsf{F}_{x_m}\left(\boldsymbol{q}^{(i)}_\kappa, \boldsymbol{q}^{(i)}_r\right)\right\} = \\
&\sum_{i=1}^{N_\kappa}\sum_{j=1}^{N_r}\left\{\overline{\mathsf{A}}(i,j)\left(\boldsymbol{w}^{(i)}_\kappa - \boldsymbol{w}^{(j)}_r\right)^{\mathrm{T}} \mathsf{F}_{x_m}\left(\boldsymbol{q}^{(i)}_\kappa, \boldsymbol{q}^{(i)}_r\right)\right\} = \\
&\sum_{i=1}^{N_\kappa}\sum_{j=1}^{N_r}\left\{\overline{\mathsf{A}}(i,j)\left(\left(\boldsymbol{\psi}^\kappa_{x_m}\right)^{(i)} - \left(\boldsymbol{\psi}^r_{x_m}\right)^{(j)}\right)\right\} = \left(\boldsymbol{\psi}^\kappa_{x_m}\right)^{\mathrm{T}} \overline{\mathsf{A}}\overline{\mathbf{1}}_r - \overline{\mathbf{1}}^{\mathrm{T}}_\kappa \overline{\mathsf{A}} \boldsymbol{\psi}^r_{x_m}.
\end{aligned}$$

□

Now it is demonstrated, using (A8), (A9), and Theorem 7, that the nonlinear approximation results in a telescoping form. Discretizing the left-hand side of (A6) using the nonlinear operator gives

$$\boldsymbol{lhs} \equiv \sum_{l,m=1}^{3} \boldsymbol{w}^{\mathrm{T}}_\kappa \left(\mathsf{Q}_{\xi_l}\left[\mathcal{J}\frac{\partial \xi_l}{\partial x_m}\right]_\kappa + \left[\mathcal{J}\frac{\partial \xi_l}{\partial x_m}\right]_\kappa \mathsf{Q}_{\xi_l}\right) \circ \mathsf{F}_{x_m}(\boldsymbol{q}_\kappa, \boldsymbol{q}_\kappa)\,\mathbf{1}_k, \tag{A10}$$

where for a nonconforming element the macroelement is considered. Using (A8), (A9), then it can be shown that Eq. (A10) is an approximation of the left-hand side of (A6), i.e.,

$$\begin{aligned}
&\sum_{l,m=1}^{3} \boldsymbol{w}^{\mathrm{T}}_\kappa \left(\mathsf{Q}_{\xi_l}\left[\mathcal{J}\frac{\partial \xi_l}{\partial x_m}\right]_\kappa + \left[\mathcal{J}\frac{\partial \xi_l}{\partial x_m}\right]_\kappa \mathsf{Q}_{\xi_l}\right) \circ \mathsf{F}_{x_m}(\boldsymbol{q}_\kappa, \boldsymbol{q}_\kappa)\,\mathbf{1}_k \approx \\
&\frac{1}{2}\sum_{l,m=1}^{3} \int_{\hat{\Omega}} \mathcal{W}^{\mathrm{T}} \left\{\frac{\partial}{\partial \xi_l}\left(\mathcal{J}_\kappa \frac{\partial \xi_l}{\partial x_m}\boldsymbol{\mathcal{F}}_{x_m}\right) + \mathcal{J}_\kappa \frac{\partial \xi_l}{\partial x_m}\frac{\partial \boldsymbol{\mathcal{F}}_{x_m}}{\partial \xi_l}\right\} \mathrm{d}\hat{\Omega}.
\end{aligned} \tag{A11}$$

Next, we demonstrate that Eq. (A10) reduces to a telescoping form. Transposing the second term in (A10) and using the symmetry of $\mathsf{F}_{x_m}(\boldsymbol{q}_\kappa, \boldsymbol{q}_\kappa)$ gives

$$\boldsymbol{lhs} = \sum_{l,m=1}^{3} \left\{\boldsymbol{w}^{\mathrm{T}}_\kappa \left(\mathsf{Q}_{\xi_l}\left[\mathcal{J}\frac{\partial \xi_l}{\partial x_m}\right]_\kappa\right) \circ \mathsf{F}_{x_m}(\boldsymbol{q}_\kappa, \boldsymbol{q}_\kappa)\,\mathbf{1}_k + \mathbf{1}^{\mathrm{T}}_k \left(\mathsf{Q}^{\mathrm{T}}_{\xi_l}\left[\mathcal{J}\frac{\partial \xi_l}{\partial x_m}\right]_\kappa\right) \circ \mathsf{F}_{x_m}(\boldsymbol{q}_\kappa, \boldsymbol{q}_\kappa)\,\boldsymbol{w}_\kappa\right\}. \tag{A12}$$

Using the SBP property $\mathsf{Q}_{\xi_l}^{\mathrm{T}} = -\mathsf{Q}_{\xi_l} + \mathsf{E}_{\xi_l}$ yields

$$\begin{aligned}\boldsymbol{lhs} = &\left\{ \boldsymbol{w}_\kappa^{\mathrm{T}} \left(\mathsf{Q}_{\xi_l} \left[\mathcal{J} \frac{\partial \xi_l}{\partial x_m} \right]_\kappa \right) \circ \mathsf{F}_{x_m}\left(\boldsymbol{q}_\kappa, \boldsymbol{q}_\kappa\right) \mathbf{1}_k - \mathbf{1}_k^{\mathrm{T}} \left(\mathsf{Q}_{\xi_l} \left[\mathcal{J} \frac{\partial \xi_l}{\partial x_m} \right]_\kappa \right) \circ \mathsf{F}_{x_m}\left(\boldsymbol{q}_\kappa, \boldsymbol{q}_\kappa\right) \boldsymbol{w}_\kappa \right\} \\ &+ \sum_{l,m=1}^{3} \boldsymbol{w}_\kappa^{\mathrm{T}} \mathsf{E}_{\xi_l} \left[\mathcal{J} \frac{\partial \xi_l}{\partial x_m} \right]_\kappa \circ \mathsf{F}_{x_m}\left(\boldsymbol{q}_\kappa, \boldsymbol{q}_\kappa\right) \mathbf{1}_k\end{aligned} \tag{A13}$$

Applying Theorem 7 on the first set of terms results in

$$\begin{aligned}\boldsymbol{lhs} = &\sum_{l,m=1}^{3} \left\{ \left(\boldsymbol{\psi}_{x_m}^\kappa\right)^{\mathrm{T}} \overline{\mathsf{Q}}_{\xi_l} \overline{\left[\mathcal{J} \frac{\partial \xi_l}{\partial x_m} \right]}_\kappa \overline{\mathbf{1}}_\kappa - \overline{\mathbf{1}}_\kappa^{\mathrm{T}} \overline{\mathsf{Q}}_{\xi_l} \overline{\left[\mathcal{J} \frac{\partial \xi_l}{\partial x_m} \right]}_\kappa \boldsymbol{\psi}_{x_m}^\kappa \right\} \\ &+ \sum_{l,m=1}^{3} \boldsymbol{w}_\kappa^{\mathrm{T}} \mathsf{E}_{\xi_l} \left[\mathcal{J} \frac{\partial \xi_l}{\partial x_m} \right]_\kappa \circ \mathsf{F}_{x_m}\left(\boldsymbol{q}_\kappa, \boldsymbol{q}_\kappa\right) \mathbf{1}_k.\end{aligned} \tag{A14}$$

The first set of terms on the right-hand side are the discrete GCL conditions and are therefore zero. The second set of terms is reduced by using the SBP property $\overline{\mathsf{Q}}_{\xi_l} = -\overline{\mathsf{Q}}_{\xi_l}^{\mathrm{T}} + \overline{\mathsf{E}}_{\xi_l}$ and the consistency of the derivative operator which implies that $\overline{\mathsf{Q}}_{\xi_l} \overline{\mathbf{1}}_\kappa = 0$. Therefore, (A14) reduces to

$$\boldsymbol{lhs} = \sum_{l,m=1}^{3} \left\{ \boldsymbol{w}_\kappa^{\mathrm{T}} \mathsf{E}_{\xi_l} \left[\mathcal{J} \frac{\partial \xi_l}{\partial x_m} \right]_\kappa \circ \mathsf{F}_{x_m}\left(\boldsymbol{q}_\kappa, \boldsymbol{q}_\kappa\right) \mathbf{1}_k - \overline{\mathbf{1}}_\kappa^{\mathrm{T}} \overline{\mathsf{E}}_{\xi_l} \overline{\left[\mathcal{J} \frac{\partial \xi_l}{\partial x_m} \right]}_\kappa \boldsymbol{\psi}_{x_m}^\kappa \right\}. \tag{A15}$$

In order to demonstrate that (A15) is mimetic of A6, like in the analysis of integration by parts, the accuracy of the on element surface matrix terms such as ,$\mathsf{E}_{\xi_l} \left[\mathcal{J} \frac{\partial \xi_l}{\partial x_m} \right]_\kappa \circ \mathsf{F}_{x_m}\left(\boldsymbol{q}_\kappa, \boldsymbol{q}_\kappa\right) \mathbf{1}_\kappa$, need to be determined.

For generality and so that the results of this section can be utilized for the elementwise conservation analysis, the considered bilinear forms are products of continuous scalar functions, $\mathcal{V}$, against one of the components of the derivative of the flux vector $\boldsymbol{\mathcal{F}}_{x_m}$. For this purpose, the scalar version of the flux function matrix is introduced as follows:

$$\mathsf{F}_{x_m}^{[i]}\left(\boldsymbol{q}_\kappa, \boldsymbol{q}_r\right) \equiv \begin{bmatrix} \left(\boldsymbol{f}_{x_m}^{sc}\left(\boldsymbol{q}_\kappa^{(1)}, \boldsymbol{q}_r^{(1)}\right)\right)(i) & \dots & \left(\boldsymbol{f}_{x_m}^{sc}\left(\boldsymbol{q}_\kappa^{(1)}, \boldsymbol{q}_r^{(N_r)}\right)\right)(i) \\ \vdots & & \vdots \\ \left(\boldsymbol{f}_{x_m}^{sc}\left(\boldsymbol{q}_\kappa^{(N_\kappa)}, \boldsymbol{q}_r^{(1)}\right)\right)(i) & \dots & \left(\boldsymbol{f}_{x_m}^{sc}\left(\boldsymbol{q}_\kappa^{(N_\kappa)}, \boldsymbol{q}_r^{(N_r)}\right)\right)(i) \end{bmatrix}, \quad i = 1, \dots, 5. \tag{A16}$$

Theorem 8. *Under the same conditions as in Thrm. 6 and considering the constituent matrices of a degree p SBP operator, $\overline{\mathsf{D}}_{\xi_l}^\kappa$, with a norm matrix $\overline{\mathsf{P}}$ of degree p_{P} and R matrices of degree r, for all smooth functions $\mathcal{V}$*

$$\begin{aligned}&\boldsymbol{v}_\kappa^{\mathrm{T}} \left(\overline{\mathsf{E}}_{\xi_l}^\kappa \overline{[\mathcal{A}]}_\kappa \right) \circ \mathsf{F}_{x_m}^{[i]}\left(\boldsymbol{q}_\kappa, \boldsymbol{q}_\kappa\right) \overline{\mathbf{1}}_\kappa = \oint_{\hat{\Gamma}_\kappa} \mathcal{V} \mathcal{A} \boldsymbol{\mathcal{F}}_{x_m}(i) n_{\xi_l} \mathrm{d}\hat{\Gamma} + \max\left[\mathcal{O}\left(h^{p_{\mathsf{P}}+1}\right), \mathcal{O}\left(h^{r+1}\right) \right], \\ &\boldsymbol{v}_\kappa^{\mathrm{T}} \left(\overline{[\mathcal{A}]}_\kappa \overline{\mathsf{E}}_{\xi_l}^\kappa \right) \circ \mathsf{F}_{x_m}^{[i]}\left(\boldsymbol{q}_\kappa, \boldsymbol{q}_\kappa\right) \overline{\mathbf{1}}_\kappa = \oint_{\hat{\Gamma}_\kappa} \mathcal{V} \mathcal{A} \boldsymbol{\mathcal{F}}_{x_m}(i) n_{\xi_l} \mathrm{d}\hat{\Gamma} + \max\left[\mathcal{O}\left(h^{p_{\mathsf{P}}+1}\right), \mathcal{O}\left(h^{r+1}\right) \right], \\ &i = 1, \dots, 5.\end{aligned} \tag{A17}$$

Proof. The proof is given in Appendix D. □

Theorem 8 implies that

$$\begin{aligned}
&\boldsymbol{v}_\kappa^{\mathrm{T}}\left(\overline{\mathsf{E}}_{\xi_l}^{\kappa}\overline{\left[\mathcal{J}\frac{\partial\xi_l}{\partial x_m}\right]}_{\kappa}\right)\circ\mathsf{F}_{x_m}^{[i]}\left(\boldsymbol{q}_\kappa,\boldsymbol{q}_\kappa\right)\overline{\mathbf{1}}_\kappa=\oint_{\hat{\Gamma}_\kappa}\mathcal{V}\mathcal{J}_\kappa\frac{\partial\xi_l}{\partial x_m}\boldsymbol{\mathcal{F}}_{x_m}(i)n_{\xi_l}\mathrm{d}\hat{\Gamma}+\max\left[\mathcal{O}\left(h^{p_{\mathrm{P}}+d}\right),\mathcal{O}\left(h^{r+d}\right)\right],\\
&\boldsymbol{v}_\kappa^{\mathrm{T}}\left(\overline{\left[\mathcal{J}\frac{\partial\xi_l}{\partial x_m}\right]}_{\kappa}\overline{\mathsf{E}}_{\xi_l}^{\kappa}\right)\circ\mathsf{F}_{x_m}^{[i]}\left(\boldsymbol{q}_\kappa,\boldsymbol{q}_\kappa\right)\overline{\mathbf{1}}_\kappa=\oint_{\hat{\Gamma}_\kappa}\mathcal{V}\mathcal{J}_\kappa\frac{\partial\xi_l}{\partial x_m}\boldsymbol{\mathcal{F}}_{x_m}(i)n_{\xi_l}\mathrm{d}\hat{\Gamma}+\max\left[\mathcal{O}\left(h^{p_{\mathrm{P}}+d}\right),\mathcal{O}\left(h^{r+d}\right)\right],\\
&i=1,\ldots,5.
\end{aligned}\tag{A18}$$

By (A18) and the exactness properties of $\overline{\mathsf{E}}_{\xi_l}$, the right-hand side of (A10) is an approximation to the right-hand side of (A6), i.e.,

$$\begin{aligned}
\boldsymbol{lhs}=&\sum_{l,m=1}^{3}\left(\boldsymbol{w}_\kappa^{\mathrm{T}}\mathsf{E}_{\xi_l}\left[\mathcal{J}\frac{\partial\xi_l}{\partial x_m}\right]_\kappa\circ\mathsf{F}_{x_m}\left(\boldsymbol{q}_\kappa,\boldsymbol{q}_\kappa\right)\mathbf{1}_\kappa-\overline{\mathbf{1}}_\kappa^{\mathrm{T}}\overline{\mathsf{E}}_{\xi_l}\overline{\left[\mathcal{J}\frac{\partial\xi_l}{\partial x_m}\right]}_{\kappa}\boldsymbol{\psi}_{x_m}^{\kappa}\right)\approx\\
&\sum_{l,m=1}^{3}\oint_{\hat{\Gamma}}\left\{\left(\boldsymbol{\mathcal{W}}^{\mathrm{T}}\boldsymbol{\mathcal{F}}_{x_m}-\psi_{x_m}\right)\mathcal{J}_\kappa\frac{\partial\xi_l}{\partial x_m}n_{\xi_l}\right\}\mathrm{d}\hat{\Gamma}=\sum_{l,m=1}^{3}\oint_{\hat{\Gamma}}\left(\mathcal{J}_\kappa\frac{\partial\xi_l}{\partial x_m}\mathcal{F}_{x_m}n_{\xi_l}\right)\mathrm{d}\hat{\Gamma}.
\end{aligned}\tag{A19}$$

Finally, and of critical importance, the right-hand side of (A10) is in a telescopic form, which when combined with appropriate interface SATs, telescopes to the boundaries of the domain.

The accuracy of the coupling terms in the SATs is necessary to prove that the scheme is elementwise conservative and is given below.

Theorem 9. *The coupling matrices constructed using the mortar-element approach satisfy the following accuracy conditions:*

$$\begin{aligned}
&\boldsymbol{v}_\kappa^{\mathrm{T}}\overline{\mathsf{E}}^{\mathrm{HtoL}}\left(\left[\mathcal{J}\frac{\partial\xi_1}{\partial x_m}\right]\right)\circ\mathsf{F}_{x_m}^{[i]}\left(\boldsymbol{q}_{\mathrm{L}},\boldsymbol{q}_{\mathrm{H}}\right)\overline{\mathbf{1}}_{N_{\mathrm{H}}}=\oint_{\hat{\Gamma}^{\mathrm{L}}}\mathcal{V}\boldsymbol{\mathcal{F}}_{x_m}(i)\mathcal{J}_\kappa\frac{\partial\xi_1}{\partial x_m}n_{\xi_1}\mathrm{d}\hat{\Gamma}+\mathcal{O}\left(h^{p_{\mathrm{L}}+d}\right)\\
&\boldsymbol{v}_\kappa^{\mathrm{T}}\overline{\mathsf{E}}^{\mathrm{LtoH}}\left(\left[\mathcal{J}\frac{\partial\xi_1}{\partial x_m}\right]\right)\circ\mathsf{F}_{x_m}^{[i]}\left(\boldsymbol{q}_{\mathrm{L}},\boldsymbol{q}_{\mathrm{H}}\right)\overline{\mathbf{1}}_{\mathrm{L}}=\oint_{\hat{\Gamma}^{\mathrm{H}}}\mathcal{V}\boldsymbol{\mathcal{F}}_{x_m}(i)\mathcal{J}_\kappa\frac{\partial\xi_1}{\partial x_m}n_{\xi_1}\mathrm{d}\hat{\Gamma}+\mathcal{O}\left(h^{p_{\mathrm{L}}+d}\right),
\end{aligned}\tag{A20}$$

where in the current context

$$\begin{aligned}
\overline{\mathsf{E}}^{\mathrm{HtoL}}\left(\left[\mathcal{J}\frac{\partial\xi_1}{\partial x_m}\right]\right)&\equiv\frac{1}{2}\left\{\left(\overline{\mathsf{R}}_{\beta_1}^{\mathrm{L}}\right)^{\mathrm{T}}\overline{\left[\mathcal{J}\frac{\partial\xi_1}{\partial x_m}\right]}_{\mathrm{L}}^{\hat{\Gamma}^{\mathrm{L}}}\overline{\mathsf{P}}_{\perp\xi_1}^{\mathrm{L}}\mathsf{I}_{\mathrm{HtoL}}\mathsf{R}_{\alpha_1}^{\mathrm{H}}+\left(\overline{\mathsf{R}}_{\beta_1}^{\mathrm{L}}\right)^{\mathrm{T}}\overline{\mathsf{P}}_{\perp\xi_1}^{\mathrm{L}}\mathsf{I}_{\mathrm{HtoL}}\overline{\left[\mathcal{J}\frac{\partial\xi_1}{\partial x_m}\right]}_{\mathrm{H}}^{\hat{\Gamma}^{\mathrm{H}}}\mathsf{R}_{\alpha_1}^{\mathrm{H}}\right\}\\
\overline{\mathsf{E}}^{\mathrm{LtoH}}\left(\left[\mathcal{J}\frac{\partial\xi_1}{\partial x_m}\right]\right)&\equiv-\frac{1}{2}\left\{\left(\overline{\mathsf{R}}_{\alpha_1}^{\mathrm{H}}\right)^{\mathrm{T}}\overline{\left[\mathcal{J}\frac{\partial\xi_1}{\partial x_m}\right]}_{\mathrm{H}}^{\hat{\Gamma}^{\mathrm{H}}}\overline{\mathsf{P}}_{\perp\xi_1}^{\mathrm{H}}\mathsf{I}_{\mathrm{LtoH}}\mathsf{R}_{\beta_1}^{\mathrm{L}}+\left(\overline{\mathsf{R}}_{\beta_1}^{\mathrm{L}}\right)^{\mathrm{T}}\overline{\mathsf{P}}_{\perp\xi_1}^{\mathrm{H}}\mathsf{I}_{\mathrm{HtoL}}\overline{\left[\mathcal{J}\frac{\partial\xi_1}{\partial x_m}\right]}_{\mathrm{H}}^{\hat{\Gamma}^{\mathrm{H}}}\mathsf{R}_{\beta_1}^{\mathrm{L}}\right\}
\end{aligned}$$

Proof. The proof follows identically to that given in Thrm. 8. □

Appendix B

Proof of Theorem. 6

In this appendix, we prove that the nonlinear approximations have the following error properties:

$$\left(2\mathsf{D}^{\kappa}_{\xi_l}\left[\mathcal{A}\right]_{\kappa}\right)\circ\mathsf{F}_{x_m}\left(\boldsymbol{q}_{\kappa},\boldsymbol{q}_{\kappa}\right)\mathbf{1}_{\kappa}=\left(\frac{\partial\left(\mathcal{A}\boldsymbol{\mathcal{F}}_{x_m}\right)}{\partial\xi_l}\right)\left(\boldsymbol{\xi}_{\kappa}\right)+\left(\boldsymbol{\mathcal{F}}_{x_m}\frac{\partial\mathcal{A}}{\partial\xi_l}\right)\left(\boldsymbol{\xi}_{\kappa}\right)+\mathcal{O}\left(h^{p+1}\right),$$
$$\left(2\left[\mathcal{A}\right]_{\kappa}\mathsf{D}^{\kappa}_{\xi_l}\right)\circ\mathsf{F}_{x_m}\left(\boldsymbol{q}_{\kappa},\boldsymbol{q}_{\kappa}\right)\mathbf{1}_{\kappa}=\left(\mathcal{A}\frac{\partial\boldsymbol{\mathcal{F}}_{x_m}}{\partial\xi_l}\right)\left(\boldsymbol{\xi}_{\kappa}\right)+\mathcal{O}\left(h^{p+1}\right),$$

where we note that the variable coefficient $\mathcal{A}$ is taken as a dimensionless quantity.

The first error estimate is not intuitive and is the focus of this appendix, while the second error estimate follows directly from the error estimate of the nonlinear approximation $\mathsf{D}_{\xi_l}\circ\mathsf{F}_{x_m}\left(\boldsymbol{q}_{\kappa},\boldsymbol{q}_{\kappa}\right)\mathbf{1}_{\kappa}$, which has been derived by several authors (for example see Ref. [13] Theorem 1). The approach that is taken is to examine, pointwise, what the action of the derivative operator is. Then a careful examination of the derivative of the two-point flux function, taking advantage of its consistency and symmetry, reveals the final error estimate.

Note that the dyadic flux vector is a function of two vector valued arguments, which is represented in a generic fashion as $\boldsymbol{f}^{sc}_{x_m}\left(\boldsymbol{\mathcal{Q}}_{\mathrm{L}},\boldsymbol{\mathcal{Q}}_{\mathrm{R}}\right)$ (note that the Tadmor shuffle condition (38) is not required here). Starting with the first equality,

$$\begin{aligned}
&\left(\left(2\mathsf{D}^{\kappa}_{\xi_l}\left[\mathcal{A}\right]_{\kappa}\right)\circ\mathsf{F}_{x_m}\left(\boldsymbol{q}_{\kappa},\boldsymbol{q}_{\kappa}\right)\mathbf{1}_{\kappa}\right)(i)=\sum_{j=1}^{N_{\kappa}}2\mathsf{D}^{\kappa}_{\xi_l}(i,j)\mathcal{A}(j)\boldsymbol{f}^{sc}_{x_m}\left(\boldsymbol{q}^{(i)}_{\kappa},\boldsymbol{q}^{(j)}_{\kappa}\right)\\
&=2\left(\frac{\partial\left(\mathcal{A}\boldsymbol{f}^{sc}_{x_m}\left(\boldsymbol{\mathcal{Q}}_{\mathrm{L}},\boldsymbol{\mathcal{Q}}_{\mathrm{R}}\right)\right)}{\partial\xi_l}\right)\left(\boldsymbol{\mathcal{Q}}_{\mathrm{L}}=\boldsymbol{\mathcal{Q}}_{\mathrm{R}}=\boldsymbol{q}^{(i)}_{\kappa}\right)+\mathcal{O}\left(h^{p+1}\right)\\
&=2\left(\mathcal{A}\frac{\partial\boldsymbol{f}^{sc}_{x_m}\left(\boldsymbol{\mathcal{Q}}_{\mathrm{L}},\boldsymbol{\mathcal{Q}}_{\mathrm{R}}\right)}{\partial\xi_l}\right)\left(\boldsymbol{\mathcal{Q}}_{\mathrm{L}}=\boldsymbol{\mathcal{Q}}_{\mathrm{R}}=\boldsymbol{q}^{(i)}_{\kappa}\right)+2\left(\boldsymbol{f}^{sc}_{x_m}\left(\boldsymbol{\mathcal{Q}}_{\mathrm{L}},\boldsymbol{\mathcal{Q}}_{\mathrm{R}}\right)\frac{\partial\mathcal{A}}{\partial\xi_l}\right)\left(\boldsymbol{\mathcal{Q}}_{\mathrm{L}}=\boldsymbol{\mathcal{Q}}_{\mathrm{R}}=\boldsymbol{q}^{(i)}_{\kappa}\right)\\
&+\mathcal{O}\left(h^{p+1}\right)\\
&=2\left(\mathcal{A}\frac{\boldsymbol{f}^{sc}_{x_m}\left(\boldsymbol{\mathcal{Q}}_{\mathrm{L}},\boldsymbol{\mathcal{Q}}_{\mathrm{R}}\right)}{\partial\boldsymbol{\mathcal{Q}}_{\mathrm{R}}}\frac{\partial\boldsymbol{\mathcal{Q}}_{\mathrm{R}}}{\partial\xi_l}\right)\left(\boldsymbol{\mathcal{Q}}_{\mathrm{L}}=\boldsymbol{\mathcal{Q}}_{\mathrm{R}}=\boldsymbol{q}^{(i)}_{\kappa}\right)+2\left(\boldsymbol{\mathcal{F}}_{x_m}\frac{\partial\mathcal{A}}{\partial\xi_l}\right)\left(\boldsymbol{\mathcal{Q}}_{\mathrm{L}}=\boldsymbol{\mathcal{Q}}_{\mathrm{R}}=\boldsymbol{q}^{(i)}_{\kappa}\right)\\
&+\mathcal{O}\left(h^{p+1}\right)
\end{aligned}\tag{B1}$$

where the following are used: 1) $\mathsf{D}^{\kappa}_{\xi_l}$ is a degree p differentiation operator, and therefore, of order $p+1$ (note that this occurs because the derivative that is being approximated is in computational space, see Appendix C for a thorough discussion), and 2) $\boldsymbol{f}^{sc}_{x_m}\left(\boldsymbol{\mathcal{Q}},\boldsymbol{\mathcal{Q}}\right)=\boldsymbol{\mathcal{F}}_{x_m}$. Now,

$$\begin{aligned}
\frac{\partial\boldsymbol{\mathcal{F}}_{x_m}\left(\boldsymbol{\mathcal{Q}}\right)}{\partial\xi_l}=&\frac{\partial\boldsymbol{f}^{sc}_{x_m}\left(\boldsymbol{\mathcal{Q}},\boldsymbol{\mathcal{Q}}\right)}{\partial\xi_l}=\left(\frac{\partial\boldsymbol{f}^{sc}_{x_m}\left(\boldsymbol{\mathcal{Q}}_{\mathrm{L}},\boldsymbol{\mathcal{Q}}_{\mathrm{R}}\right)}{\partial\xi_l}\right)\left(\boldsymbol{\mathcal{Q}}_{\mathrm{L}}=\boldsymbol{\mathcal{Q}}_{\mathrm{R}}=\boldsymbol{\mathcal{Q}}\right)\\
&=\left(\frac{\partial\boldsymbol{f}^{sc}_{x_m}\left(\boldsymbol{\mathcal{Q}}_{\mathrm{L}},\boldsymbol{\mathcal{Q}}_{\mathrm{R}}\right)}{\partial\boldsymbol{\mathcal{Q}}_{\mathrm{L}}}\frac{\partial\boldsymbol{\mathcal{Q}}_{\mathrm{L}}}{\partial\xi_l}+\frac{\partial\boldsymbol{f}^{sc}_{x_m}\left(\boldsymbol{\mathcal{Q}}_{\mathrm{L}},\boldsymbol{\mathcal{Q}}_{\mathrm{R}}\right)}{\partial\boldsymbol{\mathcal{Q}}_{\mathrm{R}}}\frac{\partial\boldsymbol{\mathcal{Q}}_{\mathrm{R}}}{\partial\xi_l}\right)\left(\boldsymbol{\mathcal{Q}}_{\mathrm{L}}=\boldsymbol{\mathcal{Q}}_{\mathrm{R}}=\boldsymbol{\mathcal{Q}}\right).
\end{aligned}\tag{B2}$$

It is now shown that

$$\left(\frac{\partial \boldsymbol{f}^{sc}_{x_m}(\boldsymbol{\mathcal{Q}}_{\mathrm{L}},\boldsymbol{\mathcal{Q}}_{\mathrm{R}})}{\partial \boldsymbol{\mathcal{Q}}_{\mathrm{L}}}\right)(\boldsymbol{\mathcal{Q}}_{\mathrm{L}}=\boldsymbol{\mathcal{Q}}_{\mathrm{R}}=\boldsymbol{\mathcal{Q}}) = \left(\frac{\partial \boldsymbol{f}^{sc}_{x_m}(\boldsymbol{\mathcal{Q}}_{\mathrm{L}},\boldsymbol{\mathcal{Q}}_{\mathrm{R}})}{\partial \boldsymbol{\mathcal{Q}}_{\mathrm{R}}}\right)(\boldsymbol{\mathcal{Q}}_{\mathrm{L}}=\boldsymbol{\mathcal{Q}}_{\mathrm{R}}=\boldsymbol{\mathcal{Q}}).$$

For the term on the left of the equality,

$$\begin{aligned}\frac{\partial \boldsymbol{f}^{sc}_{x_m}(\boldsymbol{\mathcal{Q}}_{\mathrm{L}},\boldsymbol{\mathcal{Q}}_{\mathrm{R}})}{\partial \boldsymbol{\mathcal{Q}}_{\mathrm{L}}}(\boldsymbol{\mathcal{Q}}_{\mathrm{L}}=\boldsymbol{\mathcal{Q}}_{\mathrm{R}}=\boldsymbol{\mathcal{Q}}) &= \left(\lim_{\Delta\boldsymbol{\mathcal{Q}}\to\mathbf{0}}\frac{\boldsymbol{f}^{sc}_{x_m}(\boldsymbol{\mathcal{Q}}+\Delta\boldsymbol{\mathcal{Q}},\boldsymbol{\mathcal{Q}}_{\mathrm{R}})}{\Delta\boldsymbol{\mathcal{Q}}}\right)(\boldsymbol{\mathcal{Q}}_{\mathrm{L}}=\boldsymbol{\mathcal{Q}}_{\mathrm{R}}=\boldsymbol{\mathcal{Q}})\\ &= \lim_{\Delta\boldsymbol{\mathcal{Q}}\to\mathbf{0}}\frac{\boldsymbol{f}^{sc}_{x_m}(\boldsymbol{\mathcal{Q}}+\Delta\boldsymbol{\mathcal{Q}},\boldsymbol{\mathcal{Q}})}{\Delta\boldsymbol{\mathcal{Q}}}.\end{aligned}$$

For the term on the right of the equality,

$$\begin{aligned}\left(\frac{\partial \boldsymbol{f}^{sc}_{x_m}(\boldsymbol{\mathcal{Q}}_{\mathrm{L}},\boldsymbol{\mathcal{Q}}_{\mathrm{R}})}{\partial \boldsymbol{\mathcal{Q}}_{\mathrm{R}}}\right)(\boldsymbol{\mathcal{Q}}_{\mathrm{L}}=\boldsymbol{\mathcal{Q}}_{\mathrm{R}}=\boldsymbol{\mathcal{Q}}) &= \left(\lim_{\Delta\boldsymbol{\mathcal{Q}}\to\mathbf{0}}\frac{\boldsymbol{f}^{sc}_{x_m}(\boldsymbol{\mathcal{Q}}_{\mathrm{L}},\boldsymbol{\mathcal{Q}}_{\mathrm{R}}+\Delta\boldsymbol{\mathcal{Q}})}{\Delta\boldsymbol{\mathcal{Q}}}\right)(\boldsymbol{\mathcal{Q}}_{\mathrm{L}}=\boldsymbol{\mathcal{Q}}_{\mathrm{R}}=\boldsymbol{\mathcal{Q}})\\ &= \lim_{\Delta\boldsymbol{\mathcal{Q}}\to\mathbf{0}}\frac{\boldsymbol{f}^{sc}_{x_m}(\boldsymbol{\mathcal{Q}},\boldsymbol{\mathcal{Q}}+\Delta\boldsymbol{\mathcal{Q}})}{\Delta\boldsymbol{\mathcal{Q}}}\\ &= \lim_{\Delta\boldsymbol{\mathcal{Q}}\to\mathbf{0}}\frac{\boldsymbol{f}^{sc}_{x_m}(\boldsymbol{\mathcal{Q}}+\Delta\boldsymbol{\mathcal{Q}},\boldsymbol{\mathcal{Q}})}{\Delta\boldsymbol{\mathcal{Q}}},\end{aligned}$$

where the last equality results from the symmetry of $\boldsymbol{f}^{sc}_{x_m}$; thus, (B2) becomes

$$\begin{aligned}\frac{\partial \boldsymbol{\mathcal{F}}_{x_m}(\boldsymbol{\mathcal{Q}})}{\partial \xi_l} =& \frac{\partial \boldsymbol{f}^{sc}_{x_m}(\boldsymbol{\mathcal{Q}},\boldsymbol{\mathcal{Q}})}{\partial \xi_l} = \left(\frac{\partial \boldsymbol{f}^{sc}_{x_m}(\boldsymbol{\mathcal{Q}}_{\mathrm{L}},\boldsymbol{\mathcal{Q}}_{\mathrm{R}})}{\partial \xi_l}\right)(\boldsymbol{\mathcal{Q}}_{\mathrm{L}}=\boldsymbol{\mathcal{Q}}_{\mathrm{R}}=\boldsymbol{\mathcal{Q}})\\ =& 2\left(\frac{\partial \boldsymbol{f}^{sc}_{x_m}(\boldsymbol{\mathcal{Q}}_{\mathrm{L}},\boldsymbol{\mathcal{Q}}_{\mathrm{R}})}{\partial \boldsymbol{\mathcal{Q}}_{\mathrm{L}}}\frac{\partial \boldsymbol{\mathcal{Q}}_{\mathrm{L}}}{\partial \xi_l}\right)(\boldsymbol{\mathcal{Q}}_{\mathrm{L}}=\boldsymbol{\mathcal{Q}}_{\mathrm{R}}=\boldsymbol{\mathcal{Q}}) = 2\left(\frac{\partial \boldsymbol{f}^{sc}_{x_m}(\boldsymbol{\mathcal{Q}}_{\mathrm{L}},\boldsymbol{\mathcal{Q}}_{\mathrm{R}})}{\partial \boldsymbol{\mathcal{Q}}_{\mathrm{R}}}\frac{\partial \boldsymbol{\mathcal{Q}}_{\mathrm{R}}}{\partial \xi_l}\right)(\boldsymbol{\mathcal{Q}}_{\mathrm{L}}=\boldsymbol{\mathcal{Q}}_{\mathrm{R}}=\boldsymbol{\mathcal{Q}}).\end{aligned} \tag{B3}$$

Therefore, by (B3), (B1) reduces to

$$\begin{aligned}\left(2\mathsf{D}^{\kappa}_{\xi_l}[\mathcal{A}]_{\circ}\,\mathsf{F}_{x_m}(\boldsymbol{q}_\kappa,\boldsymbol{q}_\kappa)\,\mathbf{1}_\kappa\right)(i) &= \left(\mathcal{A}\frac{\partial \boldsymbol{\mathcal{F}}_{x_m}}{\partial \xi_l}\right)\left(\boldsymbol{\mathcal{Q}}=\boldsymbol{q}^{(i)}_\kappa\right)+\left(2\boldsymbol{\mathcal{F}}_{x_m}\frac{\partial \mathcal{A}}{\partial \xi_l}\right)\left(\boldsymbol{\mathcal{Q}}=\boldsymbol{q}^{(i)}_\kappa\right)+\mathcal{O}\left(h^{p+1}\right)\\ &= \left(\frac{\partial \mathcal{A}\boldsymbol{\mathcal{F}}_{x_m}}{\partial \xi_l}\right)\left(\boldsymbol{\mathcal{Q}}=\boldsymbol{q}^{(i)}_\kappa\right)+\left(\boldsymbol{\mathcal{F}}_{x_m}\frac{\partial \mathcal{A}}{\partial \xi_l}\right)\left(\boldsymbol{\mathcal{Q}}=\boldsymbol{q}^{(i)}_\kappa\right)+\mathcal{O}\left(h^{p+1}\right).\end{aligned} \tag{B4}$$

The second equality in (A7) follows in a similar manner.

Appendix C

On order of polynomial exactness

In this section, a careful analysis is undertaken of the relation between polynomial exactness and order. This analysis is necessary in order to explain error estimates on quantities such as the plain derivative in computational space, i.e., $\mathsf{D}_{\xi_l}\boldsymbol{f}$ versus error estimates on quantities involving metric terms, i.e., $\mathsf{D}_{\xi_l}\left[\mathcal{J}\frac{\partial \xi_l}{\partial x_m}\right]\boldsymbol{f}$. To do so, it is convenient to examine the accuracy of a degree p approximation of the ξ derivative in one dimension using a degree p one-dimensional SBP operator $\mathsf{D}_{\xi_1}^{(1D)}$ on the N nodes $\boldsymbol{\xi}_1$ generated by a linear transformation

$$x_1(\xi_1) = \frac{h}{2}\xi_1 + \frac{x_{\mathrm{R}} + x_{\mathrm{L}}}{2}, \tag{C1}$$

where $h \equiv x_{\mathrm{R}} - x_{\mathrm{L}}$ and $\xi_{11} \in [-1, 1]$. The approximation at the i^{th} node of the derivative of the function $\mathcal{F}$ is given by

$$\frac{\partial \mathcal{F}}{\partial \xi}\left(\boldsymbol{\xi}^{(i)}\right) \approx \left(\mathsf{D}_{\xi_1}^{(1D)}\boldsymbol{f}\right)(i) = \sum_{j=1}^{N} \mathsf{D}_{\xi_1}^{(1D)}(i,j)\boldsymbol{f}(j).$$

The error at the i^{th} node is found by taking the difference between the approximation and the exact derivative, giving

$$\mathbf{error}(\boldsymbol{\xi}^{(i)}) = \sum_{j=1}^{n} \mathsf{D}_{\xi_l}^{(1D)}(i,j)\boldsymbol{f}(j) - \frac{\partial \mathcal{F}}{\partial \xi_1}\left(\boldsymbol{\xi}^{(i)}\right).$$

Expanding $\mathcal{F}$ and its derivative about $\xi_1 = 0$ via Taylor series, inserting the result into the above, and using the fact that $\mathsf{D}_{\xi_l}^{(1D)}$ is degree p, after some algebra, results in

$$\begin{aligned}\mathbf{error}(\boldsymbol{\xi}^{(i)}) &= \sum_{j=1}^{N} \mathsf{D}_{\xi_1}^{(1D)}(i,j) \sum_{k=0}^{\infty} \frac{\partial^k \mathcal{F}}{\partial \xi_1^k}(\xi_1 = 0) \frac{\left(\boldsymbol{\xi}^{(j)}\right)^k}{k!} - \sum_{k=0}^{\infty} \frac{\partial^{k+1} \mathcal{F}}{\partial \xi_1^{k+1}}(\xi_1 = 0) \frac{\left(\boldsymbol{\xi}^{(i)}\right)^k}{k!} \\ &= \sum_{k=p}^{\infty} \frac{\partial^{k+1} \mathcal{F}}{\partial \xi_1^{k+1}}(\xi_1 = 0) \left(\sum_{j=1}^{N} \mathsf{D}_{\xi_1}^{(1D)}(i,j) \frac{\left(\boldsymbol{\xi}^{(j)}\right)^{k+1}}{(k+1)!} - \frac{\left(\boldsymbol{\xi}^{(i)}\right)^k}{k!} \right).\end{aligned} \tag{C2}$$

To obtain an error estimate from (C2), it is necessary to introduce the element size, h, and expand the partials in terms of the physical coordinate x_1. This is accomplished by take take advantage of the Faá di Bruno formula [29]

$$\frac{\partial^k \mathcal{F}\left(x_1\left(\xi_1\right)\right)}{\partial \xi_1^k} = \sum_{m=1}^{k} \frac{\partial^m \mathcal{F}}{\partial x_1^m} \mathcal{B}_{k,m}\left(\frac{\partial x_1}{\partial \xi_1}, \ldots, \frac{\partial^{k-m+1} x_1}{\partial \xi_1^{k-m+1}}\right).$$

The Bell polynomials, $\mathcal{B}_{k,m}$, are given by

$$\mathcal{B}_{k,m}\left(\frac{\partial x_1}{\partial \xi_1},\ldots,\frac{\partial^{k-m+1}x_1}{\partial \xi_1^{k-m+1}}\right) \equiv$$
$$\sum \frac{k!}{j_1!j_2!\ldots j_{k-m+1}!}\left(\frac{\partial x_1}{\partial \xi_1}\frac{1}{1!}\right)^{j_1}\left(\frac{\partial^2 x1}{\partial \xi_1^2}\frac{1}{2!}\right)^{j_2}\cdots\left(\frac{\partial^{k-m+1}x_1}{\partial \xi_1^{k-m+1}}\frac{1}{(k-m+1)!}\right)^{j_{k-m+1}},$$

where the sum is over all positive solutions to

$$\sum_{i=1}^{k-m+1} j_i = m, \qquad \sum_{i=1}^{k-m+1} i j_i = k.$$

By (C1) and the definition of the Bell polynomials, (C2) reduces to

$$\mathbf{error}(\boldsymbol{\xi}^{(i)}) = \sum_{k=p}^{\infty}\frac{\partial^{k+1}\mathcal{F}}{\partial x_1^{k+1}}\left(\xi_1=0\right)\left(\frac{h}{2}\right)^{k+1}\left(\sum_{j=1}^{n}\mathsf{D}_{\xi_1}^{(1D)}(i,j)\frac{\left(\boldsymbol{\xi}^{(j)}\right)^{k+1}}{(k+1)!}-\frac{\left(\boldsymbol{\xi}^{(i)}\right)^{k}}{k!}\right).$$

The leading truncation error is of order $\mathcal{O}(h^{p+1})$, which is a natural result since the PDE itself is scaled by the Jacobian $\mathcal{J}\propto\mathcal{O}(h)$. Extrapolating, for problems in d dimensions, a degree p differentiation operator has the following error properties:

$$\mathsf{D}_{\xi_1}\boldsymbol{f} = \frac{\partial \mathcal{F}}{\partial \xi_1}\left(\boldsymbol{\xi}\right)+\mathcal{O}\left(h^{p+1}\right).$$

Using a similar analysis, it can be concluded that the degree r interpolation operators that for general R (the ones used in the main paper are exact) have error properties

$$\mathsf{R}_{\alpha_l}\boldsymbol{f} = \mathcal{F}\left(\boldsymbol{\xi}_{\hat{\Gamma}^{\alpha_l}}\right)+\mathcal{O}\left(h^{r+1}\right), \qquad \mathsf{R}_{\beta_l}\boldsymbol{f} = \mathcal{F}\left(\boldsymbol{\xi}_{\hat{\Gamma}^{\beta_l}}\right)+\mathcal{O}\left(h^{r+1}\right)$$

where $\boldsymbol{\xi}_{\hat{\Gamma}^{\alpha_l}}$ and $\boldsymbol{\xi}_{\hat{\Gamma}^{\beta_l}}$ are the face nodes on the α_l and β_l surfaces, respectively. From the above discussion, it is now possible to relate polynomial exactness to order and these relations are used in developing error estimates for the nonlinear approximations.

In addition, it is necessary to understand the scaling effect on order of the metric Jacobian and the metric terms; these can be characterized as

$$\mathcal{J}\propto\mathcal{O}\left(h^d\right), \qquad \mathcal{J}_\kappa\frac{\partial \xi_l}{\partial x_m}\propto\mathcal{O}\left(h^{d-1}\right). \tag{C3}$$

Remark 7. *One way of seeing how the scaling in the Jacobian and the metric terms arises in a proper mesh refinement sequence, is to break the curvilinear coordinate transformation into two steps. In the first, there is an affine transformation from the child element to the parent element (this is where the scaling shows up); the second transformation is a curvilinear transformation from the parent element to physical space.*

Appendix D

Proof of Theorem 8

It is shown how to construct the first estimate, as the second follows in a similar manner. Using the decomposition of the surface matrix gives

$$\begin{aligned}\boldsymbol{v}_\kappa^{\mathrm{T}}\left\{\left(\overline{\mathsf{E}}_{\xi_l}^{\kappa}\overline{[\mathcal{A}]}_\kappa\right)\circ\mathsf{F}_{x_m}^{[i]}\left(\boldsymbol{q}_\kappa,\boldsymbol{q}_\kappa\right)\overline{\mathbf{1}}_\kappa\right\}&=\boldsymbol{v}_\kappa^{\mathrm{T}}\left\{\left(\left(\overline{\mathsf{R}}_{\beta_l}^{\kappa}\right)^{\mathrm{T}}\overline{\mathsf{P}}_{\perp\xi_l}^{\kappa}\overline{\mathsf{R}}_{\beta_l}^{\kappa}\overline{[\mathcal{A}]}_\kappa\right)\circ\mathsf{F}_{x_m}^{[i]}\left(\boldsymbol{q}_\kappa,\boldsymbol{q}_\kappa\right)\overline{\mathbf{1}}_\kappa\right\}\\&-\boldsymbol{v}_\kappa^{\mathrm{T}}\left\{\left(\left(\overline{\mathsf{R}}_{\alpha_l}^{\kappa}\right)^{\mathrm{T}}\overline{\mathsf{P}}_{\perp\xi_l}^{\kappa}\overline{\mathsf{R}}_{\alpha_l}^{\kappa}\overline{[\mathcal{A}]}_\kappa\right)\circ\mathsf{F}_{x_m}^{[i]}\left(\boldsymbol{q}_\kappa,\boldsymbol{q}_\kappa\right)\overline{\mathbf{1}}_\kappa\right\}.\end{aligned}\tag{D1}$$

Concentrating on the first term in the right-hand side of (D1)

$$\begin{aligned}&\boldsymbol{v}_\kappa^{\mathrm{T}}\left\{\left(\left(\overline{\mathsf{R}}_{\beta_l}^{\kappa}\right)^{\mathrm{T}}\overline{\mathsf{P}}_{\perp\xi_l}^{\kappa}\overline{\mathsf{R}}_{\beta_l}^{\kappa}\overline{[\mathcal{A}]}_\kappa\right)\circ\mathsf{F}_{x_m}^{[i]}\left(\boldsymbol{q}_\kappa,\boldsymbol{q}_\kappa\right)\overline{\mathbf{1}}_\kappa\right\}=\\&=\sum_{a=1}^{N_\kappa}\sum_{b=1}^{N_\kappa}\boldsymbol{v}_\kappa(a)\left(\left(\overline{\mathsf{R}}_{\beta_l}^{\kappa}\right)^{\mathrm{T}}\overline{\mathsf{P}}_{\perp\xi_l}^{\kappa}\overline{\mathsf{R}}_{\beta_l}^{\kappa}\overline{[\mathcal{A}]}_\kappa\right)(a,b)\boldsymbol{f}_{x_m}^{sc}\left(\boldsymbol{q}_\kappa^{(a)},\boldsymbol{q}_\kappa^{(b)}\right)(i)\\&=\sum_{a=1}^{N_\kappa}\sum_{c=1}^{N_{\hat{\Gamma}^{\beta_l}}}\boldsymbol{v}_\kappa(a)\left(\left(\overline{\mathsf{R}}_{\beta_l}^{\kappa}\right)^{\mathrm{T}}\overline{\mathsf{P}}_{\perp\xi_l}^{\kappa}\right)(a,c)\sum_{b=1}^{N_\kappa}\overline{\mathsf{R}}_{\alpha_l}^{\kappa}(c,b)\overline{[\mathcal{A}]}_\kappa(b,b)\boldsymbol{f}_{x_m}^{sc}\left(\boldsymbol{q}_\kappa^{(a)},\boldsymbol{q}_\kappa^{(b)}\right),\end{aligned}$$

with $N_{\hat{\Gamma}^{\beta_l}}$ the number of nodes on face $\hat{\Gamma}^{\beta_l}$.

The interpolation operator is of degree r, and therefore, of order $r+1$, thus,

$$\begin{aligned}&\boldsymbol{v}_\kappa^{\mathrm{T}}\left\{\left(\left(\overline{\mathsf{R}}_{\beta_l}^{\kappa}\right)^{\mathrm{T}}\overline{\mathsf{P}}_{\perp\xi_l}^{\kappa}\overline{\mathsf{R}}_{\beta_l}^{\kappa}\overline{[\mathcal{A}]}_\kappa\right)\circ\mathsf{F}_{x_m}^{[i]}\left(\boldsymbol{q}_\kappa,\boldsymbol{q}_\kappa\right)\overline{\mathbf{1}}_\kappa\right\}=\\&\sum_{a=1}^{N_\kappa}\sum_{c=1}^{N_{\hat{\Gamma}^{\beta_l}}}\boldsymbol{v}_\kappa(a)\left(\left(\overline{\mathsf{R}}_{\alpha_l}^{\kappa}\right)^{\mathrm{T}}\overline{\mathsf{P}}_{\perp\xi_l}^{\kappa}\right)(a,c)\mathcal{A}(\boldsymbol{\xi}^{(c)})\boldsymbol{f}_{x_m}^{sc}\left(\boldsymbol{q}_\kappa^{(a)},\boldsymbol{\mathcal{Q}}\left(\boldsymbol{\xi}^{(c)}\right)\right)+\mathcal{O}\left(h^{r+1}\right),\end{aligned}$$

where $\mathcal{A}\left(\boldsymbol{\xi}^{c}\right)$ and $\boldsymbol{\mathcal{Q}}\left(\boldsymbol{\xi}^{(c)}\right)$ are $\mathcal{A}$ and $\boldsymbol{\mathcal{Q}}$ evaluated at the c^{th} node on surface $\hat{\Gamma}^{\beta_l}$ of element κ. Continuing,

$$\begin{aligned}&\boldsymbol{v}_\kappa^{\mathrm{T}}\left\{\left(\left(\overline{\mathsf{R}}_{\beta_l}^{\kappa}\right)^{\mathrm{T}}\overline{\mathsf{P}}_{\perp\xi_l}^{\kappa}\overline{\mathsf{R}}_{\beta_l}^{\kappa}\overline{[\mathcal{A}]}_\kappa\right)\circ\mathsf{F}_{x_m}^{[i]}\left(\boldsymbol{q}_\kappa,\boldsymbol{q}_\kappa\right)\overline{\mathbf{1}}_\kappa\right\}=\\&\sum_{c=1}^{\hat{\Gamma}^{\beta_l}}\sum_{d=1}^{\hat{\Gamma}^{\beta_l}}\overline{\mathsf{P}}_{\perp\xi_l}^{\kappa}(d,c)\left(\mathcal{A}\right)\left(\boldsymbol{\xi}^{(c)}\right)\sum_{a=1}^{N_\kappa}\overline{\mathsf{R}}_{\beta_l}(d,a)\boldsymbol{v}_\kappa(a)\boldsymbol{f}_{x_m}^{sc}\left(\boldsymbol{q}_\kappa^{(a)},\boldsymbol{\mathcal{Q}}\left(\boldsymbol{\xi}^{(c)}\right)\right)+\mathcal{O}\left(h^{r+1}\right).\end{aligned}$$

By the accuracy of the interpolation operator (i.e., in the general case $\overline{\mathsf{R}}$ is assumed to be of degree r and therefore order $r+1$), noting that $\overline{\mathsf{P}}_{\perp\xi_l}^{\kappa}$ is a diagonal matrix, and using the fact that

$\boldsymbol{f}^{sc}_{x_m}\left(\boldsymbol{q}^{(j)}_\kappa, \boldsymbol{q}^{(j)}_\kappa\right) = \boldsymbol{\mathcal{F}}_{x_m}\left(\boldsymbol{q}^{(j)}_\kappa\right)$, i.e., the j^{th} entry in $\boldsymbol{\mathcal{F}}_{x_m}$ evaluated at $\boldsymbol{q}^{(j)}_\kappa$,

$$\boldsymbol{v}^{\mathrm{T}}_\kappa \left\{ \left(\left(\overline{\mathsf{R}}^\kappa_{\beta_l}\right)^{\mathrm{T}} \overline{\mathsf{P}}^\kappa_{\perp\xi_l} \overline{\mathsf{R}}^\kappa_{\beta_l} \overline{[\mathcal{A}]}_\kappa \right) \circ \mathsf{F}^{[i]}_{x_m}\left(\boldsymbol{q}_\kappa, \boldsymbol{q}_\kappa\right) \overline{\mathbf{1}}_\kappa \right\} =$$
$$\sum_{c=1}^{N_{\hat{\Gamma}^{\beta_l}}} \overline{\mathsf{P}}_{\perp\xi_l}(c,c) \boldsymbol{v}_\kappa(c) \mathcal{A}\left(\boldsymbol{\xi}^{(c)}\right) \left(\boldsymbol{\mathcal{F}}_{x_m}\left(\boldsymbol{\mathcal{Q}}\left(\boldsymbol{\xi}^{(c)}\right)\right)\right)(i) + \mathcal{O}\left(h^{r+1}\right).$$

Noting that $\overline{\mathsf{P}}_{\perp\xi_l}$ is a degree p_{P} approximation to the L^2 inner product over planes orthogonal to ξ_l,

$$\boldsymbol{v}^{\mathrm{T}}_\kappa \left\{ \left(\left(\overline{\mathsf{R}}^\kappa_{\beta_l}\right)^{\mathrm{T}} \overline{\mathsf{P}}^\kappa_{\perp\xi_l} \overline{\mathsf{R}}^\kappa_{\beta_l} \overline{[\mathcal{A}]}_\kappa \right) \circ \mathsf{F}^{[i]}_{x_m}\left(\boldsymbol{q}_\kappa, \boldsymbol{q}_\kappa\right) \overline{\mathbf{1}}_\kappa \right\} = \oint_{\hat{\Gamma}^{\beta_l}_\kappa} \mathcal{VA}(\boldsymbol{\mathcal{F}}_{x_m})(i) n_{\xi_l} \mathrm{d}\hat{\Gamma} + \max\left[\mathcal{O}\left(h^{p_{\mathsf{P}}+1}\right), \mathcal{O}\left(h^{r+1}\right)\right].$$

Similarly,

$$\boldsymbol{v}^{\mathrm{T}}_\kappa \left\{ \left(\left(\overline{\mathsf{R}}^\kappa_{\alpha_l}\right)^{\mathrm{T}} \overline{\mathsf{P}}^\kappa_{\perp\xi_l} \overline{\mathsf{R}}^\kappa_{\alpha_l} \overline{[\mathcal{A}]}_\kappa \right) \circ \mathsf{F}^{[i]}_{x_m}\left(\boldsymbol{q}_\kappa, \boldsymbol{q}_\kappa\right) \overline{\mathbf{1}}_\kappa \right\} = \oint_{\hat{\Gamma}^{\alpha_l}_\kappa} \mathcal{VA}(\boldsymbol{\mathcal{F}}_{x_m})(i) n_{\xi_l} \mathrm{d}\hat{\Gamma} + \max\left[\mathcal{O}\left(h^{p_{\mathsf{P}}+1}\right), \mathcal{O}\left(h^{r+1}\right)\right].$$

Therefore, via the additive property of integrals, the first equality in (D1) is obtained.

Appendix E

Elementwise conservation

The nonlinear hyperbolic nature of the Euler equations means that in finite, time nonsmooth solutions can result despite being closed with smooth data. To allow for nonsmooth solutions, it is necessary to consider the weak form of the conservation law

$$\begin{aligned}&\int_{t=0}^{T}\int_{\hat{\Omega}_\kappa}\left(\boldsymbol{\mathcal{Q}}\frac{\partial\mathcal{V}}{\partial t}\mathcal{J}_\kappa+\sum_{l,m=1}^{3}\mathcal{J}_\kappa\frac{\partial\xi_l}{\partial x_m}\boldsymbol{\mathcal{F}}_{x_m}\frac{\partial\mathcal{V}}{\partial\xi_l}\right)\mathrm{d}\hat{\Omega}\mathrm{d}t-\int_{\hat{\Omega}_\kappa}\mathcal{V}\boldsymbol{\mathcal{Q}}\mathcal{J}_\kappa|_{t=0}^{T}\,\mathrm{d}\hat{\Omega}\\&-\int_{t=0}^{T}\oint_{\hat{\Gamma}_\kappa}\mathcal{V}\sum_{l,m=1}^{3}\mathcal{J}_\kappa\frac{\partial\xi_l}{\partial x_m}\boldsymbol{\mathcal{F}}_{x_m}n_{\xi_l}\mathrm{d}\hat{\Gamma}\mathrm{d}t=\mathbf{0},\\&t>0,\kappa=1,2,\ldots,K,\end{aligned}\tag{E1}$$

for all smooth test functions $\mathcal{V}$ with compact support.

The weak form supports a restricted class of discontinuous solutions which satisfy the jump conditions [33]

$$v[[\boldsymbol{\mathcal{Q}}]]=[[\boldsymbol{\mathcal{F}}_n]],$$

where v is the speed of the discontinuity, $\boldsymbol{\mathcal{F}}_n$ is the flux normal to the discontinuity, and $[[\boldsymbol{\mathcal{V}}]]$ is the jump in $\boldsymbol{\mathcal{V}}$ across the discontinuity. The interest is in numerically approximating this restricted set of discontinuous solutions satisfying the above jump conditions. Thus, the class of schemes that are of interest are those that are a consistent approximation to (E1) for nonsmooth solutions almost everywhere (consistent for smooth solutions everywhere); this is an essential property for demonstrating that if the numerical solution converges then it converges to a solution satisfying the weak form almost everywhere [34].

In this paper, a method of lines approach is used and the focus is on the analysis of the semidiscrete equations; thus, rather than use (E1), conservation is discussed in the context of the following:

$$\int_{\hat{\Omega}_\kappa}\mathcal{V}\frac{\partial\boldsymbol{\mathcal{Q}}}{\partial t}\mathcal{J}_\kappa\mathrm{d}\hat{\Omega}-\int_{\hat{\Omega}_\kappa}\sum_{l,m=1}^{3}\mathcal{J}_\kappa\frac{\partial\xi_l}{\partial x_m}\boldsymbol{\mathcal{F}}_{x_m}\frac{\partial\mathcal{V}}{\partial\xi_l}\mathrm{d}\hat{\Omega}+\oint_{\hat{\Gamma}_\kappa}\mathcal{V}\sum_{l,m=1}^{3}\mathcal{J}_\kappa\frac{\partial\xi_l}{\partial x_m}\boldsymbol{\mathcal{F}}_{x_m}n_{\xi_l}\mathrm{d}\hat{\Gamma}=\mathbf{0}.\tag{E2}$$

Conservation of the fully discrete scheme can always be achieved with an appropriate choice of time integration scheme, e.g., Euler implicit or explicit.

At its core, the analysis that is used relies on a semidiscrete version of the Lax-Wendroff Thrm. [34]. To use this theorem, it is necessary to express the scheme in telescoping flux form, which in one dimension, at node j over a control volume $\left[x_{j-\frac{1}{2}},x_{j+\frac{1}{2}}\right]$ is given as

$$\frac{\mathrm{d}q_j}{\mathrm{d}t}=-\frac{\left(f_{j+\frac{1}{2}}-f_{j-\frac{1}{2}}\right)}{\Delta x},$$

where f is a general flux function at the boundaries of the control volume. The importance of this form can be seen by viewing it as a finite-volume discretization and the link to the integral form is immediate, recalling that the integral and weak forms are equivalent. The Lax-Wendroff Thrm. [34] proceeds instead by multiplying by a continuous test function and using summation-by-parts. Assuming that the general flux function is reasonably well-behaved, one can show that the limit solution is a solution to the weak form almost everywhere [34,35]. It is clear then that an essential feature of the analysis is to demonstrate that the scheme can be algebraically manipulated into a form that is a consistent approximation to the weak form (E2).

For the purpose of analysis, a general form of the semidiscrete equations for the κ^{th} element is introduced,

$$\mathsf{J}_\kappa \frac{\mathrm{d}\boldsymbol{q}_\kappa}{\mathrm{d}t} + \sum_{l,m=1}^{3} \left(\mathsf{D}^\kappa_{\xi_l} \left[\mathcal{J} \frac{\partial \xi_l}{\partial x_m} \right]_\kappa + \left[\mathcal{J} \frac{\partial \xi_l}{\partial x_m} \right]_\kappa \mathsf{D}^\kappa_{\xi_l} \right) \circ \mathsf{F}_{x_m}\left(\boldsymbol{q}_\kappa, \boldsymbol{q}_\kappa\right) \mathbf{1}_\kappa = \\ \left(\mathsf{P}^\kappa\right)^{-1} \left\{ \sum_{l,m=1}^{3} \left(\mathsf{E}^\kappa_{\xi_l} \left[\mathcal{J} \frac{\partial \xi_l}{\partial x_m} \right]_\kappa \right) \circ \mathsf{F}_{x_m}\left(\boldsymbol{q}_\kappa, \boldsymbol{q}_\kappa\right) \mathbf{1}_\kappa + \sum_{f=1}^{6} \sum_{m=1}^{3} \mathsf{E}^{f\text{to}\kappa} \left(\left[\mathcal{J} \frac{\partial \xi_f}{\partial x_m} \right] \right) \circ \mathsf{F}_{x_m}\left(\boldsymbol{q}_\kappa, \boldsymbol{q}_f\right) \mathbf{1}_f \right\}, \tag{E3}$$

where $\mathsf{E}^{f\text{to}\kappa}\left(\left[\mathcal{J}\frac{\partial \xi_f}{\partial x_m}\right]\right)$ are the coupling matrices acting on the six faces, (f) with orthogonal coordinate direction ξ_f, of the hexahedral element in the three Cartesian directions (m), and $\boldsymbol{q}_f$ is the solution from the element touching face f. In the simple example in the paper, these are the matrices $-\mathsf{E}^{\text{LtoH}}\left(\left[\mathcal{J}\frac{\partial \xi_1}{\partial x_m}\right]\right)$ and $\mathsf{E}^{\text{HtoL}}\left(\left[\mathcal{J}\frac{\partial \xi_1}{\partial x_m}\right]\right)$ (note that the n_{ξ_l} component of the unit normal has been absorbed into the definition of $\mathsf{E}^{f\text{to}\kappa}\left(\left[\mathcal{J}\frac{\partial \xi_f}{\partial x_m}\right]\right)$).

Moreover, for the conservation proofs it is convenient to introduce the scalar version of the semidiscrete equations for the κ^{th} element is introduced,

$$\overline{\mathsf{J}}_\kappa \frac{\mathrm{d}\boldsymbol{q}^{[i]}_\kappa}{\mathrm{d}t} + \sum_{l,m=1}^{3} \left(\overline{\mathsf{D}}^\kappa_{\xi_l} \overline{\left[\mathcal{J} \frac{\partial \xi_l}{\partial x_m} \right]}_\kappa + \overline{\left[\mathcal{J} \frac{\partial \xi_l}{\partial x_m} \right]}_\kappa \overline{\mathsf{D}}^\kappa_{\xi_l} \right) \circ \mathsf{F}^{[i]}_{x_m}\left(\boldsymbol{q}_\kappa, \boldsymbol{q}_\kappa\right) \overline{\mathbf{1}}_\kappa = \\ \left(\overline{\mathsf{P}}^\kappa\right)^{-1} \left\{ \sum_{l,m=1}^{3} \left(\overline{\mathsf{E}}^\kappa_{\xi_l} \overline{\left[\mathcal{J} \frac{\partial \xi_l}{\partial x_m} \right]}_\kappa \right) \circ \mathsf{F}^{[i]}_{x_m}\left(\boldsymbol{q}_\kappa, \boldsymbol{q}_\kappa\right) \overline{\mathbf{1}}_\kappa + \sum_{f=1}^{6} \sum_{m=1}^{3} \overline{\mathsf{E}}^{\text{fto}\kappa} \left(\overline{\left[\mathcal{J} \frac{\partial \xi_f}{\partial x_m} \right]} \right) \circ \mathsf{F}^{[i]}_{x_m}\left(\boldsymbol{q}_\kappa, \boldsymbol{q}_f\right) \overline{\mathbf{1}}_f \right\}, \tag{E4}$$

In this paper, elementwise conservation is proven by demonstrating that the scheme has a telescoping flux form at the element level. Recently, Shi and Shu [48] have presented an extension of the Lax-Wendroff Thrm. to consider elementwise conservation for general multidimensional discretizations. We rely on the proofs in that paper and therefore need only show that the semidiscrete equations satisfy the following:

- Telescoping form: That the scheme can be algebraically manipulated into a general telescoping flux form at the element level given as

$$\frac{\mathrm{d}\bar{\boldsymbol{q}}_\kappa}{\mathrm{d}t} + \sum_{f=1}^{6} \boldsymbol{g}^\kappa_f = 0, \tag{E5}$$

where $\bar{\boldsymbol{q}}_\kappa$ is a generalized locally conserved quantity and $\boldsymbol{g}_f^\kappa$ is a generalized flux on the f face of the κ^{th} hexahedral element. In order to telescope, the fluxes must be uniquely defined at each surface. Thus, for the two element example, $\boldsymbol{g}_{\text{L}} = -\boldsymbol{g}_{\text{H}}$.

- Consistency: For a constant flow $\boldsymbol{\mathcal{Q}} = \boldsymbol{\mathcal{Q}}_c$,

$$\begin{aligned} \bar{\boldsymbol{q}}_\kappa &= \left(\int_{\hat{\Omega}_\kappa} \mathcal{J}_\kappa \mathrm{d}\hat{\Omega} + \mathcal{O}\left(h\right) \right) \boldsymbol{\mathcal{Q}}_c, \\ \boldsymbol{g}_f^\kappa &= \left(\sum_{m=1}^{3} \oint_{\hat{\Gamma}_\kappa^f} \mathcal{J}_\kappa \frac{\partial \xi_l}{\partial x_m} n_{\xi_l} \mathrm{d}\hat{\Gamma} + \mathcal{O}\left(h\right) \right) \boldsymbol{\mathcal{F}}_{x_m}\left(\boldsymbol{\mathcal{Q}}_c\right) \end{aligned} \tag{E6}$$

  where $\hat{\Gamma}_\kappa^f$ is the f^{th} face of element κ, and where in contrast to Shi and Shu [48], error terms have been added to account for the curvilinear coordinate transformation (this results because, in general, the curvilinear coordinate transformation bumps terms in the discretization outside of the polynomial space that can be resolved by the discrete integrals); this addition has no impact on the proofs presented in [48].

- Boundedness: the generalized conserved quantity and fluxes are bounded in terms of the L^∞ norm of the numerical solution:

$$\begin{aligned} &|\bar{\boldsymbol{q}}_\kappa(i) - \bar{\boldsymbol{v}}_\kappa(i)| \leq C h^d \|\boldsymbol{q}_h - \boldsymbol{v}_h\|_{L^\infty(B_\kappa)}, \\ &\left|(\boldsymbol{g}_f^\kappa\left(\boldsymbol{q}_h\right))(i) - (\boldsymbol{g}_f^\kappa\left(\boldsymbol{v}_h\right))(i)\right| \leq C h^{d-1} \|\boldsymbol{q}_\kappa - \boldsymbol{v}_\kappa\|_{L^\infty(B_\kappa)}, \end{aligned} \tag{E7}$$

  where $\boldsymbol{q}_h$ and $\boldsymbol{v}_h$ are numerical solutions over the entire mesh and C is some positive constant. Moreover, $B_\kappa \equiv \left\{\boldsymbol{x} \in \mathbb{R}^d : |\boldsymbol{x} - \boldsymbol{x}_c| < ch\right\}$, $\boldsymbol{x}_c$ is the element center, and c (> 1) is independent of the mesh size. Note that the h^d and h^{d-1} scaling originate from the metric Jacobian and metric terms, respectively.

- Global conservation:

$$\sum_{\kappa=1}^{K} \bar{\boldsymbol{q}}_\kappa(i) = \int_\Omega \mathcal{Q}(i) \mathrm{d}\Omega + \mathcal{O}\left(h\right), \qquad i = 1, \ldots, 5, \tag{E8}$$

  where again, a discretization error has been introduced for the above stated reasons and again this has no impact on the proofs in Shi and Shu [48].

Now, a theorem is presented that delineates the conditions that need to be satisfied by the semidiscrete equations so that elementwise conservation is obtained.

Theorem 10. *If the coupling matrices, for example* $\mathsf{E}^{\text{HtoL}}\left(\left[\mathcal{J}\frac{\partial \xi_1}{\partial x_m}\right]\right)$*, in the SATs on either side of a given interface are the negative transpose of each other, e.g.,*

$$\mathsf{E}^{\text{HtoL}}\left(\left[\mathcal{J}\frac{\partial \xi_1}{\partial x_m}\right]\right) = -\left(\mathsf{E}^{\text{LtoH}}\left(\left[\mathcal{J}\frac{\partial \xi_1}{\partial x_m}\right]\right)\right)^{\text{T}},$$

then the semidiscrete form (E3) *can be algebraically manipulated into the general elementwise telescoping form* (E5) *where*

$$\bar{\boldsymbol{q}}_\kappa(i) \equiv \overline{\mathbf{1}}_\kappa^{\mathrm{T}} \overline{\mathsf{P}\mathsf{J}}_\kappa \boldsymbol{q}_\kappa^{[i]}$$
$$\boldsymbol{g}_f^\kappa(i) \equiv \sum_{m=1}^{3} \overline{\mathsf{E}}^{\mathrm{fto}\kappa} \left(\overline{\left[\mathcal{J} \frac{\partial \xi_f}{\partial x_m} \right]} \right) \circ \mathsf{F}_{x_m}^{[i]} \left(\boldsymbol{q}_\kappa, \boldsymbol{q}_f \right) \overline{\mathbf{1}}_f,$$
$$i = 1, \ldots, 5.$$

The scheme is elementwise conservative if, in addition, for a constant state $\boldsymbol{\mathcal{Q}}_c$ *the coupling terms satisfy*

$$\overline{\mathbf{1}}_\kappa^{\mathrm{T}} \overline{\mathsf{E}}^{\mathrm{fto}\kappa} \left(\overline{\left[\mathcal{J} \frac{\partial \xi_f}{\partial x_m} \right]} \right) \circ \circ \mathsf{F}_{x_m}^{[i]} \left(\boldsymbol{q}_\kappa, \boldsymbol{q}_f \right) \overline{\mathbf{1}}_f = \left(\oint_{\hat{\Gamma}_\kappa^f} \mathcal{J}_\kappa \frac{\partial \xi_l}{\partial x_m} n_{\xi_l} \mathrm{d}\hat{\Gamma} + \mathcal{O}\left(h\right) \right) \boldsymbol{\mathcal{F}}_{x_m}(i) \left(\boldsymbol{\mathcal{Q}}_c \right), \tag{E9}$$
$$i = 1, \ldots, 5.$$

Proof. The proof is given in Appendix E.1. □

E.1 Proof of Theorem 10

In the subsections that follow, the various requirements for elementwise conservation given in Section E are proven under the assumptions in Thrm. 10.

E.1.1 Consistency

Coupling terms are assumed to satisfy the consistency conditions. The remaining task is to prove the generalized conservative quantity satisfies the consistency condition. However, this is immediate since $\overline{\mathsf{P}}^\kappa$ is at least a degree $2p-1$ approximation to the L^2 inner product, that is for scalar functions $\mathcal{V}$ and $\mathcal{U}$

$$\boldsymbol{v}_\kappa^{\mathrm{T}} \overline{\mathsf{P}}^\kappa \boldsymbol{u}_\kappa = \int_{\hat{\Omega}_\kappa} \mathcal{V}\mathcal{U} \mathrm{d}\hat{\Omega} + \mathcal{O}\left(h^{2p}\right).$$

For a constant state $\boldsymbol{\mathcal{Q}}_c$, $\boldsymbol{q}_\kappa^{[i]} = \overline{\mathbf{1}}_\kappa \boldsymbol{\mathcal{Q}}_c(i)$ thus,

$$\bar{\boldsymbol{q}}_\kappa(i) = \overline{\mathbf{1}}_\kappa^{\mathrm{T}} \overline{\mathsf{P}}^\kappa \overline{\mathsf{J}}_\kappa \overline{\mathbf{1}}_\kappa \boldsymbol{\mathcal{Q}}_c(i) = \left(\int_{\hat{\Omega}_\kappa} \mathcal{J}_\kappa \mathrm{d}\hat{\Omega} + \mathcal{O}\left(h^{2p}\right) \right) \boldsymbol{\mathcal{Q}}_c(i).$$

E.1.2 Telescoping flux form

To obtain the telescoping flux form, the semidiscrete form of each of the scalar conservation laws is discretely integrated over each element. This is accomplished by multiplying the scalar semidiscrete forms obtained from (E4) by $\overline{\mathbf{1}}_\kappa^{\mathrm{T}} \overline{\mathsf{P}}^\kappa$, which gives

$$\overline{\mathbf{1}}_\kappa^{\mathrm{T}} \overline{\mathsf{P}}^\kappa \overline{\mathsf{J}}_\kappa \frac{\mathrm{d}\boldsymbol{q}_\kappa^{[i]}}{\mathrm{d}t} + \overline{\mathbf{1}}_\kappa^{\mathrm{T}} \sum_{l,m=1}^{3} \left(\overline{\mathsf{Q}}_{\xi_l}^\kappa \overline{\left[\mathcal{J} \frac{\partial \xi_l}{\partial x_m} \right]}_\kappa + \overline{\left[\mathcal{J} \frac{\partial \xi_l}{\partial x_m} \right]}_\kappa \overline{\mathsf{Q}}_{\xi_l}^\kappa \right) \circ \mathsf{F}_{x_m}^{[i]} \left(\boldsymbol{q}_\kappa, \boldsymbol{q}_\kappa \right) \overline{\mathbf{1}}_\kappa =$$
$$\overline{\mathbf{1}}_\kappa^{\mathrm{T}} \sum_{l,m=1}^{3} \overline{\mathsf{E}}_{\xi_l}^\kappa \overline{\left[\mathcal{J} \frac{\partial \xi_l}{\partial x_m} \right]}_\kappa \circ \mathsf{F}_{x_m}^{[i]} \left(\boldsymbol{q}_\kappa, \boldsymbol{q}_\kappa \right) \overline{\mathbf{1}}_\kappa - \overline{\mathbf{1}}_\kappa^{\mathrm{T}} \boldsymbol{C}\boldsymbol{T}. \tag{E10}$$

where $\boldsymbol{CT}$ are the coupling terms. By the symmetry of $\mathsf{F}^{[i]}_{x_m}(\boldsymbol{q}_\kappa, \boldsymbol{q}_\kappa)$, $\overline{\mathsf{E}}^\kappa_{\xi_l}$, and $\overline{\left[\mathcal{J}\frac{\partial \xi_l}{\partial x_m}\right]}_\kappa$, (E10) reduces to

$$\overline{\mathbf{1}}^{\mathrm{T}}_\kappa \overline{\mathsf{P}}^\kappa \bar{\mathsf{J}}_\kappa \frac{\mathrm{d}\boldsymbol{q}^{[i]}_\kappa}{\mathrm{d}t} + \overline{\mathbf{1}}^{\mathrm{T}}_\kappa \sum_{l,m=1}^{3} \left(\overline{\mathsf{S}}^\kappa_{\xi_l} \overline{\left[\mathcal{J}\frac{\partial \xi_l}{\partial x_m}\right]}_\kappa + \overline{\left[\mathcal{J}\frac{\partial \xi_l}{\partial x_m}\right]}_\kappa \overline{\mathsf{S}}^\kappa_{\xi_l} \right) \circ \mathsf{F}^{[i]}_{x_m}(\boldsymbol{q}_\kappa, \boldsymbol{q}_\kappa)\, \overline{\mathbf{1}}_\kappa = - \overline{\mathbf{1}}^{\mathrm{T}}_\kappa \boldsymbol{CT},$$

The matrix $\left(\left(\overline{\mathsf{S}}^\kappa_{\xi_l} \overline{\left[\mathcal{J}\frac{\partial \xi_l}{\partial x_m}\right]}_\kappa + \overline{\left[\mathcal{J}\frac{\partial \xi_l}{\partial x_m}\right]}_\kappa \overline{\mathsf{S}}^\kappa_{\xi_l} \right) \circ \mathsf{F}^{[i]}_{x_m}(\boldsymbol{q}_\kappa, \boldsymbol{q}_\kappa) \right)$ is skew-symmetric and therefore, when contracted from the left and right by the same vector, its contribution is zero. Rearrangement and explicitly writing out the coupling terms, yields

$$\overline{\mathbf{1}}^{\mathrm{T}}_\kappa \overline{\mathsf{P}}^\kappa \bar{\mathsf{J}}_\kappa \frac{\mathrm{d}\boldsymbol{q}^{[i]}_\kappa}{\mathrm{d}t} + \overline{\mathbf{1}}^{\mathrm{T}}_\kappa \sum_{f=1}^{6} \sum_{m=1}^{3} \overline{\mathsf{E}}^{\mathrm{fto}\kappa} \left(\overline{\left[\mathcal{J}\frac{\partial \xi_f}{\partial x_m}\right]} \right) \circ \mathsf{F}^{[i]}_{x_m}(\boldsymbol{q}_\kappa, \boldsymbol{q}_f)\, \overline{\mathbf{1}}_f = 0, \tag{E11}$$

which is in the form of (E5) with

$$\begin{aligned}
&\bar{\boldsymbol{q}}_\kappa(i) \equiv \overline{\mathbf{1}}^{\mathrm{T}}_\kappa \overline{\mathsf{P}}^\kappa \bar{\mathsf{J}}_\kappa \boldsymbol{q}^{[i]}_\kappa, \\
&\boldsymbol{g}^\kappa_f \equiv \overline{\mathbf{1}}^{\mathrm{T}}_\kappa \sum_{m=1}^{3} \overline{\mathsf{E}}^{\mathrm{fto}\kappa} \left(\overline{\left[\mathcal{J}\frac{\partial \xi_f}{\partial x_m}\right]} \right) \circ \mathsf{F}^{[i]}_{x_m}(\boldsymbol{q}_\kappa, \boldsymbol{q}_f)\, \overline{\mathbf{1}}_f, \\
&i = 1, \ldots, 5.
\end{aligned}$$

What remains to be shown is that the flux at the element boundaries is unique, or equivalently that the contributions from two abutting elements; this can be readily demonstrated by considering the coupling terms on the simple two element example and using the SBP preserving property of the interpolation operators.

E.1.3 Boundedness

The boundedness estimate on the generalized conserved quantity can be shown as follows:

$$\begin{aligned}
|\bar{\boldsymbol{q}}_\kappa(i) - \bar{\boldsymbol{v}}_\kappa(i)| &= \left| \overline{\mathbf{1}}^{\mathrm{T}}_\kappa \overline{\mathsf{P}}^\kappa \bar{\mathsf{J}}_\kappa \left(\boldsymbol{q}^{[i]}_\kappa - \boldsymbol{v}^{[i]}_\kappa \right) \right| \\
&= \left| \sum_{j=1}^{N_\kappa} \overline{\mathsf{P}}^\kappa(j,j) \bar{\mathsf{J}}_\kappa(j,j) \left(\boldsymbol{q}^{[i]}_\kappa(j) - \boldsymbol{v}^{[i]}_\kappa(j) \right) \right| \\
&\leq h^d \sum_{j=1}^{N_\kappa} \overline{\mathsf{P}}^\kappa(j,j) \left| \boldsymbol{q}^{[i]}_\kappa(j) - \boldsymbol{v}^{[i]}_\kappa(j) \right| \\
&\leq C h^d \max \left(\left| \boldsymbol{q}^{[i]}_\kappa(j) - \boldsymbol{v}^{[i]}_\kappa(j) \right| \right) \\
&= C h^d \| \boldsymbol{q}^{[i]}_\kappa - \boldsymbol{v}^{[i]}_\kappa \|_{L^\infty} \leq C h^d \| \boldsymbol{q}_h - \boldsymbol{v}_h \|_{L^\infty(B_\kappa)},
\end{aligned}$$

where the scaling comes from the fact that $\mathcal{J}_\kappa \propto h^d$.

The generalized flux is constructed from linear combinations of the two-point flux function, for which the Ishmael-Roe flux has been shown to be continuously differentiable with respect to its arguments (see Crean *et al.* [13]) and therefore the generalized flux is bounded in the L^∞ norm, where the scaling in the inequalities comes from the fact that $\mathcal{J}_\kappa \frac{\partial \xi_l}{\partial x_m} \propto h^{d-1}$.

E.1.4 Global conservation

The matrix norm is an L^2 discrete inner product and naturally leads to global conservation; thus,

$$\begin{aligned}\sum_{\kappa=1}^{k} \bar{\boldsymbol{q}}_\kappa(i) &= \sum_{\kappa=1}^{K} \overline{\mathbf{1}}_\kappa^{\mathrm{T}} \overline{\mathsf{P}}^\kappa \overline{\mathsf{J}}_\kappa \boldsymbol{q}_\kappa^{[i]} \\ &= \sum_{\kappa=1}^{K} \int_{\hat{\Omega}_\kappa} \boldsymbol{\mathcal{Q}}(i) \mathcal{J}_\kappa \mathrm{d}\hat{\Omega} + \mathcal{O}\left(h^{2p}\right) \\ &= \int_{\Omega} \boldsymbol{\mathcal{Q}}(i) \mathrm{d}\Omega + \mathcal{O}\left(h^{2p}\right).\end{aligned}$$

Appendix F

Proof of Theorem. 2

For simplicity, the proof given here is in terms of the Thomas and Lombard [58] approximate metrics; the proof for the symmetric metrics of Vinokur and Yee [59], follows identically.

The Thomas Lombard approximate metrics as well as what they approximate are given below.

$$\overline{\left[\mathcal{J}\frac{\partial \xi_1}{\partial x_1}\right]}_\kappa = \overline{\mathsf{D}}_{\xi_3}\,\mathrm{diag}(\boldsymbol{x}_3)\overline{\mathsf{D}}_{\xi_2}\boldsymbol{x}_2 - \overline{\mathsf{D}}_{\xi_2}\,\mathrm{diag}(\boldsymbol{x}_3)\overline{\mathsf{D}}_{\xi_3}\boldsymbol{x}_2$$
$$\approx \left(\frac{\partial x_3}{\partial \xi_3}\frac{\partial x_2}{\partial \xi 2} - \frac{\partial x_3}{\partial \xi_2}\frac{\partial x_2}{\partial \xi_3}\right)(\boldsymbol{\xi}) = \left(\frac{\partial}{\partial \xi_3}\left(x_3\frac{\partial x_2}{\partial \xi_2}\right) - \frac{\partial}{\partial \xi_2}\left(x_3\frac{\partial x_2}{\partial \xi_3}\right)\right)(\boldsymbol{\xi}),$$

$$\overline{\left[\mathcal{J}\frac{\partial \xi_1}{\partial x_2}\right]}_\kappa = \overline{\mathsf{D}}_{\xi_3}\,\mathrm{diag}(\boldsymbol{x}_1)\overline{\mathsf{D}}_{\xi_2}\boldsymbol{x}_3 - \overline{\mathsf{D}}_{\xi_2}\,\mathrm{diag}(\boldsymbol{x}_1)\overline{\mathsf{D}}_{\xi_3}\boldsymbol{x}_3$$
$$\approx \left(\frac{\partial x_1}{\partial \xi_3}\frac{\partial x_3}{\partial \xi_2} - \frac{\partial x_1}{\partial \xi_2}\frac{\partial x_3}{\partial \xi_3}\right)_{C_\kappa} = \left(\frac{\partial}{\partial \xi_3}\left(x_1\frac{\partial x_3}{\partial \xi_2}\right) - \frac{\partial}{\partial \xi_2}\left(x_1\frac{\partial x_3}{\partial \xi_3}\right)\right)(\boldsymbol{\xi}),$$

$$\overline{\left[\mathcal{J}\frac{\partial \xi_1}{\partial x_3}\right]}_\kappa = \overline{\mathsf{D}}_{\xi_3}\,\mathrm{diag}(\boldsymbol{x}_2)\overline{\mathsf{D}}_{\xi_2}\boldsymbol{x}_1 - \overline{\mathsf{D}}_{\xi_2}\,\mathrm{diag}(\boldsymbol{x}_2)\overline{\mathsf{D}}_{\xi_3}\boldsymbol{x}_1$$
$$\approx \left(\frac{\partial x_2}{\partial \xi_3}\frac{\partial x_1}{\partial \xi_2} - \frac{\partial x_2}{\partial \xi_2}\frac{\partial x_1}{\partial \xi_3}\right)(\boldsymbol{\xi}) = \left(\frac{\partial}{\partial \xi_3}\left(x_2\frac{\partial x_1}{\partial \xi_2}\right) - \frac{\partial}{\partial \xi_2}\left(x_2\frac{\partial x_1}{\partial \xi_3}\right)\right)(\boldsymbol{\xi}),$$

$$\overline{\left[\mathcal{J}\frac{\partial \xi_2}{\partial x_1}\right]}_\kappa = \overline{\mathsf{D}}_{\xi_1}\,\mathrm{diag}(\boldsymbol{x}_3)\overline{\mathsf{D}}_{\xi_3}\boldsymbol{x}_2 - \overline{\mathsf{D}}_{\xi_3}\,\mathrm{diag}(\boldsymbol{x}_3)\overline{\mathsf{D}}_{\xi_1}\boldsymbol{x}_2$$
$$\approx \left(\frac{\partial x_3}{\partial \xi_1}\frac{\partial x_2}{\partial \xi_3} - \frac{\partial x_3}{\partial \xi_3}\frac{\partial x_2}{\partial \xi_1}\right)(\boldsymbol{\xi}) = \left(\frac{\partial}{\partial \xi_1}\left(x_3\frac{\partial x_2}{\partial \xi_3}\right) - \frac{\partial}{\partial \xi_3}\left(x_3\frac{\partial x_2}{\partial \xi_1}\right)\right)(\boldsymbol{\xi}),$$

$$\overline{\left[\mathcal{J}\frac{\partial \xi_2}{\partial x_2}\right]}_\kappa = \overline{\mathsf{D}}_{\xi_1}\,\mathrm{diag}(\boldsymbol{x}_1)\overline{\mathsf{D}}_{\xi_3}\boldsymbol{x}_3 - \overline{\mathsf{D}}_{\xi_3}\,\mathrm{diag}(\boldsymbol{x}_1)\overline{\mathsf{D}}_{\xi_1}\boldsymbol{x}_3$$
$$\approx \left(\frac{\partial x_1}{\partial \xi_1}\frac{\partial x_3}{\partial \xi_3} - \frac{\partial x_1}{\partial \xi_3}\frac{\partial x_3}{\partial \xi_1}\right)(\boldsymbol{\xi}) = \left(\frac{\partial}{\partial \xi_1}\left(x_1\frac{\partial x_3}{\partial \xi_3}\right) - \frac{\partial}{\partial \xi_3}\left(x_1\frac{\partial x_3}{\partial \xi_1}\right)\right)(\boldsymbol{\xi}),$$

$$\overline{\left[\mathcal{J}\frac{\partial \xi_2}{\partial x_3}\right]}_\kappa = \overline{\mathsf{D}}_{\xi_1}\,\mathrm{diag}(\boldsymbol{x}_2)\overline{\mathsf{D}}_{\xi_3}\boldsymbol{x}_1 - \overline{\mathsf{D}}_{\xi_3}\,\mathrm{diag}(\boldsymbol{x}_2)\overline{\mathsf{D}}_{\xi_1}\boldsymbol{x}_1$$
$$\approx \left(\frac{\partial x_2}{\partial \xi_1}\frac{\partial x_1}{\partial \xi_3} - \frac{\partial x_2}{\partial \xi_3}\frac{\partial x_1}{\partial \xi_1}\right)(\boldsymbol{\xi}) = \left(\frac{\partial}{\partial \xi_1}\left(x_2\frac{\partial x_1}{\partial \xi_3}\right) - \frac{\partial}{\partial \xi_3}\left(x_2\frac{\partial x_1}{\partial \xi_1}\right)\right)(\boldsymbol{\xi}),$$

$$\overline{\left[\mathcal{J}\frac{\partial \xi_3}{\partial x_1}\right]}_\kappa = \overline{\mathsf{D}}_{\xi_2}\,\mathrm{diag}(\boldsymbol{x}_3)\overline{\mathsf{D}}_{\xi_1}\boldsymbol{x}_2 - \overline{\mathsf{D}}_{\xi_1}\,\mathrm{diag}(\boldsymbol{x}_3)\overline{\mathsf{D}}_{\xi_2}\boldsymbol{x}_2$$
$$\approx \left(\frac{\partial x_3}{\partial \xi_2}\frac{\partial x_2}{\partial \xi_1} - \frac{\partial x_3}{\partial \xi_1}\frac{\partial x_2}{\partial x_2}\right)(\boldsymbol{\xi}) = \left(\frac{\partial}{\partial \xi_2}\left(x_3\frac{\partial x_2}{\partial \xi_1}\right) - \frac{\partial}{\partial \xi_1}\left(x_3\frac{\partial x_2}{\partial \xi_2}\right)\right)(\boldsymbol{\xi}),$$

$$\overline{\left[\mathcal{J}\frac{\partial \xi_3}{\partial x_2}\right]}_\kappa = \mathsf{D}_{\xi_2}\,\mathrm{diag}(\boldsymbol{x}_1)\mathsf{D}_{\xi_1}\boldsymbol{x}_2 - \mathsf{D}_{\xi_1}\,\mathrm{diag}(\boldsymbol{x}_1)\mathsf{D}_{\xi_2}\boldsymbol{x}_2$$
$$\approx \left(\frac{\partial x_1}{\partial \xi_2}\frac{\partial x_2}{\partial \xi_1} - \frac{\partial x_1}{\partial \xi_1}\frac{\partial x_2}{\partial x_2}\right)(\boldsymbol{\xi}) = \left(\frac{\partial}{\partial \xi_2}\left(x_1\frac{\partial x_2}{\partial \xi_1}\right) - \frac{\partial}{\partial \xi_1}\left(x_1\frac{\partial x_2}{\partial \xi_2}\right)\right)(\boldsymbol{\xi}),$$

$$\overline{\left[\mathcal{J}\frac{\partial \xi_3}{\partial x_3}\right]}_\kappa = \mathsf{D}_{\xi_2}\,\mathrm{diag}(\boldsymbol{x}_2)\mathsf{D}_{\xi_1}\boldsymbol{x}_1 - \mathsf{D}_{\xi_1}\,\mathrm{diag}(\boldsymbol{x}_2)\mathsf{D}_{\xi_2}\boldsymbol{x}_1$$
$$\approx \left(\frac{\partial x_2}{\partial \xi_2}\frac{\partial x_1}{\partial \xi_1} - \frac{\partial x_2}{\partial \xi_1}\frac{\partial x_1}{\partial x_2}\right)(\boldsymbol{\xi}) = \left(\frac{\partial}{\partial \xi_2}\left(x_2\frac{\partial x_1}{\partial \xi_1}\right) - \frac{\partial}{\partial \xi_1}\left(x_2\frac{\partial x_1}{\partial \xi_2}\right)\right)(\boldsymbol{\xi}).$$

In order for the condition $\mathbf{1}_\kappa^{\mathrm{T}}\boldsymbol{c}_m^\kappa = 0$ to be met, the coupling terms need to match the analytical terms in the integration of the GCL conditions for example

$$\overline{\mathbf{1}}_\kappa^{\mathrm{T}}\overline{\mathsf{E}}^{\mathrm{fto}\kappa}\left(\overline{\left[\mathcal{J}\frac{\partial \xi_f}{\partial x_m}\right]}\right)\overline{\mathbf{1}}_f = \oint_{\hat{\Gamma}^f}\mathcal{J}_\kappa\frac{\partial \xi_f}{\partial x_m}n_{\xi_f}\mathrm{d}\hat{\Gamma}.$$

Consider the κ^{th} element as having at least one nonconforming interface but a conforming interface on the face perpendicular to where ξ_1 is maximum, abutting a fully conforming element (this face will be denoted face 2). The contribution of the coupling elements to the discrete GCL for $m = 1, 2, 3$, listed in that order, are

$$\overline{\mathbf{1}}_\kappa^{\mathrm{T}}\overline{\mathsf{E}}^{2\mathrm{to}\kappa}\left(\overline{\left[\mathcal{J}\frac{\partial \xi_1}{\partial x_1}\right]}\right) = \overline{\mathbf{1}}_\kappa^{\mathrm{T}}\overline{\mathsf{R}}_{\beta_1}^{\mathrm{T}}\overline{\mathsf{P}}_{\perp\xi_1}\overline{\mathsf{R}}_{\alpha_1}\overline{\left[\mathcal{J}\frac{\partial \xi_1}{\partial x_1}\right]}, \qquad \overline{\mathbf{1}}_\kappa^{\mathrm{T}}\overline{\mathsf{E}}^{2\mathrm{to}\kappa}\left(\overline{\left[\mathcal{J}\frac{\partial \xi_1}{\partial x_2}\right]}\right) = \overline{\mathbf{1}}_\kappa^{\mathrm{T}}\overline{\mathsf{R}}_{\beta_1}^{\mathrm{T}}\overline{\mathsf{P}}_{\perp\xi_1}\overline{\mathsf{R}}_{\alpha_1}\overline{\left[\mathcal{J}\frac{\partial \xi_1}{\partial x_2}\right]},$$
$$\overline{\mathbf{1}}_\kappa^{\mathrm{T}}\overline{\mathsf{E}}^{2\mathrm{to}\kappa}\left(\overline{\left[\mathcal{J}\frac{\partial \xi_1}{\partial x_3}\right]}\right) = \overline{\mathbf{1}}_\kappa^{\mathrm{T}}\overline{\mathsf{R}}_{\beta_1}^{\mathrm{T}}\overline{\mathsf{P}}_{\perp\xi_1}\overline{\mathsf{R}}_{\alpha_1}\overline{\left[\mathcal{J}\frac{\partial \xi_1}{\partial x_3}\right]},$$

where the metric terms, for example $\overline{\left[\mathcal{J}\frac{\partial \xi_1}{\partial x_1}\right]}$, are those computed in the fully conforming element using the Thomas and Lombard [58] approach. What needs to be shown is that each term is exact,

i.e.,

$$\begin{aligned}
\overline{\mathbf{1}}_\kappa^{\mathrm{T}}\overline{\mathsf{E}}^{2\mathrm{to}\kappa}\left(\overline{\left[\mathcal{J}\frac{\partial\xi_1}{\partial x_1}\right]}\right) &= \oint_{\hat{\Gamma}_2}\mathcal{J}\frac{\partial\xi_1}{\partial x_1}\mathrm{d}\hat{\Gamma} = \oint_{\hat{\Gamma}_2}\left(\frac{\partial x_3}{\partial\xi_3}\frac{\partial x_2}{\partial\xi_2}-\frac{\partial x_3}{\partial\xi_2}\frac{\partial x_2}{\partial\xi_3}\right)\mathrm{d}\hat{\Gamma}\\
&= \oint_{\Gamma_1}\left(\frac{\partial}{\partial\xi_3}\left(x_3\frac{\partial x_2}{\partial\xi_2}\right)-\frac{\partial}{\partial\xi_2}\left(x_3\frac{\partial x_2}{\partial\xi_3}\right)\right)\mathrm{d}\hat{\Gamma}\\
&= \int_{\xi_2=-1}^{1}\left(x_3\frac{\partial x_2}{\partial\xi_2}\Big|_{\xi_3=-1}^{1}\right)\mathrm{d}\xi_2-\int_{\xi_3=-1}^{1}\left(x_3\frac{\partial x_2}{\partial\xi_3}\Big|_{\xi_2=-1}^{1}\right)\mathrm{d}\xi_3,\\
\overline{\mathbf{1}}_\kappa^{\mathrm{T}}\overline{\mathsf{E}}^{2\mathrm{to}\kappa}\left(\overline{\left[\mathcal{J}\frac{\partial\xi_1}{\partial x_2}\right]}\right) &= \oint_{\hat{\Gamma}_2}\mathcal{J}\frac{\partial\xi_1}{\partial x_2}\mathrm{d}\hat{\Gamma} = \oint_{\hat{\Gamma}_2}\left(\frac{\partial}{\partial\xi_3}\left(x_1\frac{\partial x_3}{\partial\xi_2}\right)-\frac{\partial}{\partial\xi_2}\left(x_1\frac{\partial x_3}{\partial\xi_3}\right)\right)\mathrm{d}\hat{\Gamma}\\
&= \int_{\xi_2=-1}^{1}\left(x_1\frac{\partial x_3}{\partial\xi_2}\Big|_{\xi_3=-1}^{1}\right)\mathrm{d}\xi_2-\int_{\xi_3=-1}^{1}\left(x_1\frac{\partial x_3}{\partial\xi_3}\Big|_{\xi_2=-1}^{1}\right)\mathrm{d}\xi_3,\\
\overline{\mathbf{1}}_\kappa^{\mathrm{T}}\overline{\mathsf{E}}^{2\mathrm{to}\kappa}\left(\overline{\left[\mathcal{J}\frac{\partial\xi_1}{\partial x_3}\right]}\right) &= \oint_{\hat{\Gamma}_2}\mathcal{J}\frac{\partial\xi_1}{\partial x_3}\mathrm{d}\hat{\Gamma} = \oint_{\hat{\Gamma}_2}\left(\frac{\partial}{\partial\xi_3}\left(x_2\frac{\partial x_1}{\partial\xi_2}\right)-\frac{\partial}{\partial\xi_2}\left(x_2\frac{\partial x_1}{\partial\xi_3}\right)\right)\mathrm{d}\hat{\Gamma}\\
&= \int_{\xi_2=-1}^{1}\left(x_2\frac{\partial x_1}{\partial\xi_2}\Big|_{\xi_3=-1}^{1}\right)\mathrm{d}\xi_2-\int_{\xi_3=-1}^{1}\left(x_2\frac{\partial x_1}{\partial\xi_3}\Big|_{\xi_2=-1}^{1}\right)\mathrm{d}\xi_3.
\end{aligned}$$

Inserting the Thomas Lombard approximation in the first coupling term

$$\begin{aligned}
&\overline{\mathbf{1}}_\kappa^{\mathrm{T}}\overline{\mathsf{E}}^{2\mathrm{to}\kappa}\left(\overline{\left[\mathcal{J}\frac{\partial\xi_1}{\partial x_1}\right]}\right) = \overline{\mathbf{1}}_\kappa^{\mathrm{T}}\overline{\mathsf{R}}_{\beta_1}^{\mathrm{T}}\overline{\mathsf{P}}_{\perp\xi_1}\overline{\mathsf{R}}_{\alpha_1}\left(\overline{\mathsf{D}}_{\xi_3}\,\mathrm{diag}(\boldsymbol{x}_3)\overline{\mathsf{D}}_{\xi_2}\boldsymbol{x}_2-\overline{\mathsf{D}}_{\xi_2}\,\mathrm{diag}(\boldsymbol{x}_3)\overline{\mathsf{D}}_{\xi_3}\boldsymbol{x}_2\right)\\
&= \overline{\mathbf{1}}_\kappa^{\mathrm{T}}\left\{\left(\boldsymbol{e}_{N_1}\boldsymbol{e}_{1_1}^{\mathrm{T}}\otimes\mathsf{P}_\xi^{(1D)}\otimes\mathsf{Q}_\xi^{(1D)}\right)\mathrm{diag}(\boldsymbol{x}_3)\overline{\mathsf{D}}_{\xi_2}\boldsymbol{x}_2-\left(\boldsymbol{e}_{N_1}\boldsymbol{e}_{1_1}^{\mathrm{T}}\otimes\mathsf{Q}_\xi^{(1D)}\otimes\mathsf{P}_\xi^{(1D)}\right)\mathrm{diag}(\boldsymbol{x}_3)\overline{\mathsf{D}}_{\xi_3}\boldsymbol{x}_2\right\}\\
&= \Big\{\mathbf{1}^{\mathrm{T}}\left(\boldsymbol{e}_{N_1}\boldsymbol{e}_{1_1}^{\mathrm{T}}\otimes\mathbf{1}^{\mathrm{T}}\mathsf{P}_\xi^{(1D)}\otimes\mathbf{1}^{\mathrm{T}}\mathsf{Q}_\xi^{(1D)}\right)\mathrm{diag}(\boldsymbol{x}_3)\overline{\mathsf{D}}_{\xi_2}\boldsymbol{x}_2\\
&-\left(\mathbf{1}^{\mathrm{T}}\boldsymbol{e}_{N_1}\boldsymbol{e}_{1_1}^{\mathrm{T}}\otimes\mathbf{1}^{\mathrm{T}}\mathsf{Q}_\xi^{(1D)}\otimes\mathbf{1}^{\mathrm{T}}\mathsf{P}_\xi^{(1D)}\right)\mathrm{diag}(\boldsymbol{x}_3)\overline{\mathsf{D}}_{\xi_3}\boldsymbol{x}_2\Big\}\\
&= \Big\{\mathbf{1}^{\mathrm{T}}\left(\boldsymbol{e}_{N_1}\boldsymbol{e}_{1_1}^{\mathrm{T}}\otimes\mathbf{1}^{\mathrm{T}}\mathsf{P}_\xi^{(1D)}\otimes\mathbf{1}^{\mathrm{T}}\mathsf{E}_\xi^{(1D)}\right)\mathrm{diag}(\boldsymbol{x}_3)\overline{\mathsf{D}}_{\xi_2}\boldsymbol{x}_2\\
&-\left(\mathbf{1}^{\mathrm{T}}\boldsymbol{e}_{N_1}\boldsymbol{e}_{1_1}^{\mathrm{T}}\otimes\mathbf{1}^{\mathrm{T}}\mathsf{E}_\xi^{(1D)}\otimes\mathbf{1}^{\mathrm{T}}\mathsf{P}_\xi^{(1D)}\right)\mathrm{diag}(\boldsymbol{x}_3)\overline{\mathsf{D}}_{\xi_3}\boldsymbol{x}_2\Big\}
\end{aligned}$$

From the last equality, it can be concluded that

$$\overline{\mathbf{1}}_\kappa^{\mathrm{T}}\overline{\mathsf{E}}^{2\mathrm{to}\kappa}\left(\overline{\left[\mathcal{J}\frac{\partial\xi_1}{\partial x_1}\right]}\right) = \oint_{\Gamma_1}\left(\frac{\partial}{\partial\xi_3}\left(x_3\frac{\partial x_2}{\partial\xi_2}\right)-\frac{\partial}{\partial\xi_2}\left(x_3\frac{\partial x_2}{\partial\xi_3}\right)\right)\mathrm{d}\hat{\Gamma},$$

because the projection operators pick off the functions at the boundary and the E matrices are at least degree $2p-1$, which is the degree of the terms that they are integrating if the curvilinear coordinate transformation is constructed from degree p tensor products. The remaining coupling terms are shown to exactly equal the required surface/line integrals.

REPORT DOCUMENTATION PAGE

Form Approved
OMB No. 0704–0188

1. REPORT DATE *(DD-MM-YYYY)*	2. REPORT TYPE	3. DATES COVERED *(From - To)*
01-03-2020	Technical Memorandum	07/2018-03/2020

4. TITLE AND SUBTITLE
Entropy Stable Nonconforming Discretizations with the Summation-By-Parts Property for Curvilinear Coordinates.

5a. CONTRACT NUMBER

5b. GRANT NUMBER

5c. PROGRAM ELEMENT NUMBER

6. AUTHOR(S)
David C. Del Rey Fernández, Mark H. Carpenter, Lisandro Dalcin, Lucas Fredrich, Diego Rojas, Andrew R. Winters, Gregor J. Gassner, Stefano Zampini, Matteo Parsani

5d. PROJECT NUMBER

5e. TASK NUMBER

5f. WORK UNIT NUMBER
794072.02.07.02.03

7. PERFORMING ORGANIZATION NAME(S) AND ADDRESS(ES)
NASA NASA Langley Research Center
Hampton, Virginia 23681-2199

8. PERFORMING ORGANIZATION REPORT NUMBER
L–21068

9. SPONSORING/MONITORING AGENCY NAME(S) AND ADDRESS(ES)
National Aeronautics and Space Administration
Washington, DC 20546-0001

10. SPONSOR/MONITOR'S ACRONYM(S)
NASA

11. SPONSOR/MONITOR'S REPORT NUMBER(S)
NASA-TM–2020–220574

12. DISTRIBUTION/AVAILABILITY STATEMENT
Subject Category 02
Availability: NASA STI Program (757) 864-9658

13. SUPPLEMENTARY NOTES

14. ABSTRACT
The entropy conservative/stable algorithm of Friedrich *et al.* (2018) for hyperbolic conservation laws on nonconforming p-refined/coarsened Cartesian grids, is extended to curvilinear grids for the compressible Euler equations. The primary focus is on constructing appropriate coupling procedures across the curvilinear nonconforming interfaces. A simple and flexible approach is proposed that uses interpolation operators from one element to the other. On the element faces, the analytic metrics are used to construct coupling terms, while metric terms in the volume are approximated to satisfy a discretization of the geometric conservation laws. The resulting scheme is entropy conservative/stable, elementwise conservative, and freestream preserving. The accuracy and stability properties of the resulting numerical algorithm are shown to be comparable to those of the original conforming scheme ($\sim p+1$ convergence) in the context of the isentropic Euler vortex and the inviscid Taylor–Green vortex problems on manufactured high order grids.

15. SUBJECT TERMS
Entropy stability, high-order, Discontinuous Galerkin, Robustness, Monomial Equations, Compressible Euler, Summation-By-Parts, Simultaneous-Approximation-Term, Unstructured Grids

16. SECURITY CLASSIFICATION OF:			17. LIMITATION OF ABSTRACT	18. NUMBER OF PAGES	19a. NAME OF RESPONSIBLE PERSON
a. REPORT	b. ABSTRACT	c. THIS PAGE			STI Help Desk (email: help@sti.nasa.gov)
U	U	U	UU	66	19b. TELEPHONE NUMBER *(Include area code)* (757) 864-9658